Evaluation of Shock Response Spectrum Similarity and Repeatability in the Qualification Testing of Space Components

著者	Oluwatobi Adebolu Ibukun
year	2021-06
その他のタイトル	宇宙機器の認定試験における衝撃応答スペクトラムの相似性と再現性の評価
学位授与年度	令和3年度
学位授与番号	17104甲工第524号
URL	http://hdl.handle.net/10228/00008416

Evaluation of Shock Response Spectrum Similarity and Repeatability in the Qualification Testing of Space Components

by

ADEBOLU Ibukun Oluwatobi
(17595906)

Submitted to
The Department of Applied Science for Integrated System Engineering
Graduate School of Engineering
Kyushu Institute of Technology, Kitakyushu, Japan
In Partial Fulfilment of the Requirements for the Award of
Doctor of Philosophy (Ph.D.) in Applied Science for Integrated Systems Engineering

SUPERVISED BY

Prof. Mengu Cho
Dr. Hirokazu Masui

June 2021

CERTIFICATION

Evaluation of Shock Response Spectrum Similarity and Repeatability in the Qualification Testing of Space Components

Examination Committee:

Prof. Mengu Cho

Prof. Yasuhiro Akahoshi

Prof Minoru Iwata

Prof. Hiroshi Sakai

ACKNOWLEDGMENT

First, I would like to thank my Supervisors, Prof. Mengu Cho and Dr. Hirokazu Masui, for their insights and guidance throughout my graduate studies. I appreciate them for believing in me and allowing me to work on several projects in the Laboratory of Lean Satellite Enterprises and In-orbit Experiments.

I appreciate Mr. Isamu Inoue for teaching me the ropes in small satellites' shock and vibration testing. I thank Mr. Tom Irvine, who made his Vibration analysis suite (*Vibrationdata*) open and free of charge.

I thank the entire faculty and staff of the Laboratory of Lean Satellite Enterprises and In-orbit Experiments for their insightful contributions that shaped this thesis's outcome.

I am indebted to the Japan Student Services Organization (JASSO) for several scholarship grants I received. I am also indebted to the Rotary Yoneyama Memorial Foundation for granting me a scholarship. I thank the Rotary Club International members, District 2700, especially my *Sewa* club, Yahata-Chuo Rotary Club.

I thank the members of the Nigeria Union, Kyushu, and the community of African students at the Kyushu Institute of Technology for giving me a home away from home. I also appreciate my spiritual family, the Kitakyushu Agape House, for their support throughout my studies.

My special thanks and appreciation go to my parents, siblings, fiancée, and friends, too numerous to mention, for their love, emotional, and financial support that got me going in my difficult and trying times. I appreciate the almighty God, for life and breath, and without whom I am nothing.

ABSTRACT

The shock loading on satellite components during any of the separation events (of rocket boosters, rocket stages, and the payload fairing) leading to the eventual separation of a satellite at its destination orbit may be detrimental to satellite components. Generally, the shock response spectrum (SRS) describes the shock severity level in a Qualification Testing (QT). In QT, a component is subjected to an extreme (simulated) environmental condition, such as shock, as a means of guaranteeing its performance when used in an environment of similar severity. Shock simulation by a mechanical impact is one of several shock qualification test methods.

The problem in QT, especially when using a mechanical impact simulator, is that the shock tests show a huge variability from test to test and generating repeatable SRS profiles that satisfy the target shock level involves a lot of trial-and-error (up to 85 have been reported in the literature). Moreover, fully characterizing a mechanical impact involves understanding the interaction of several parameters, such as the impact velocity, impact angle, and absorber materials between impacting bodies. To reduce the number of trial-and-error and facilitate rapid testing, testing facilities match a target SRS to a database shock and retrieve its associated testing conditions. This process relies on the similarity between the target SRS and the database SRS.

The purpose of this research is to investigate the SRS variation in tests simulated using an air gun shock testing machine and reduce the trial and error before satisfying a QT requirement. In particular, this research contributes a new similarity metric, the weighted RMSE, that can be used by commercial testing facilities to retrieve an SRS similar to a target SRS from a database of previous shock tests. In an SRS database retrieval task, the weighted RMSE outperformed other known SRS similarity measures in that it not only

retrieves the SRS most similar to the target SRS, but also an SRS that satisfies the requirement that at least 50% of the measured SRS shall exceed the target SRS. Moreover, the SRS response of impact shocks using the air gun shock machine were characterized experimentally. This research shows that with careful data acquisition, at a given driving pressure, the knee frequency of the measured SRS is influenced by the mass and material of the projectile. The heavier, metallic projectile tends to excite a higher knee frequency, than the lighter, non-metallic projectile.

TABLE OF CONTENTS

TABLE OF FIGURES

1. Introduction

This chapter introduces the concept of qualification testing of satellite components in the context of the shock environment. It presents background information about the shock environment during a rocket launch, the various qualification testing approaches, and the problem with qualification testing by metal-metal impact using an air-gun shock machine.

1.1 Background

Small satellite components may experience a range of static and dynamic loading conditions during a rocket launch, including quasi-static accelerations, sinusoidal vibrations, random vibrations, and shock[1]. Component failure may be induced by catastrophic vibration and shock-loading if the satellite's design (or its components) is not robust enough to support the loading environments adequately. A shock is a dynamic load whose duration is short relative to the excited system's natural frequency [2]. Small electronic components in a satellite's functional subsystems may fail when resonating in response to an input shock. The purpose of qualification testing (QT) is to verify a system's performance in a representative environment by testing the load-bearing components to design loads above the predicted flight conditions [1].

The need for QT has increased globally as the number of rocket launches increase. The small satellite industry's explosive growth has facilitated increased access to space for new space industry players. Small launch vehicles are rapidly expanding to meet the launch demand for small satellites. In total, there were 103 rocket (orbital) launches in 2019[3]. Figure 1-1 shows the launch vehicles that were active in 2019.

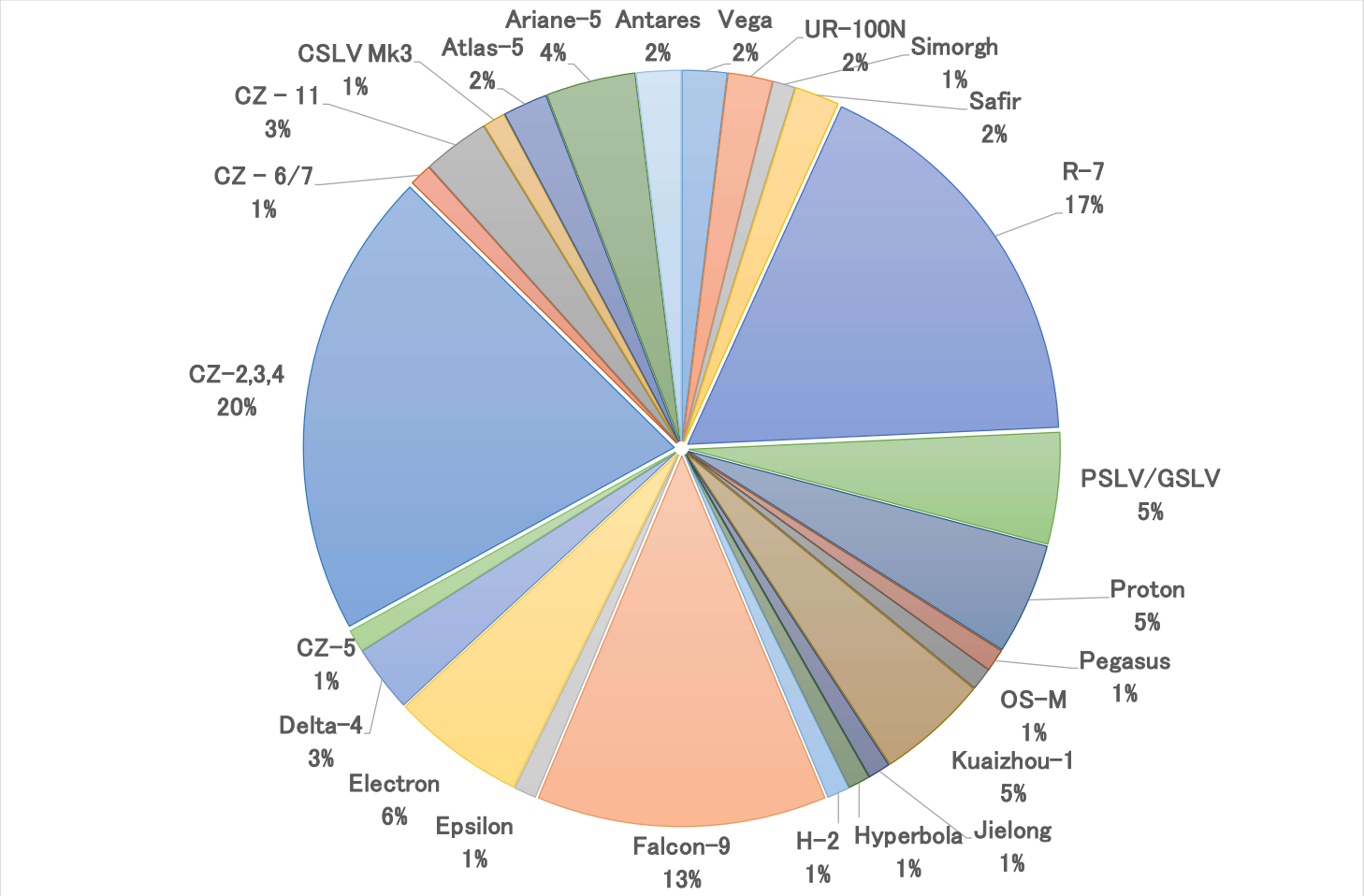

Figure 1-1 Summary of orbital launches in 2019[3]

There are three major shock events during a rocket launch. The first shock loading occurs during the separation of the solid rocket boosters (SRB). Shock loading also occurs in separating the different rocket stages and the payload fairing. The spacecraft is separated from the last rocket stage by a separation mechanism on reaching the target orbit. Figure 1-2 shows a typical launch sequence for an H-II launch vehicle[4] from lift-off to payload delivery to its destination orbit.

Satellites may be separated from a rocket body using a range of explosive (pyrotechnic) and non-explosive separation mechanisms. Pyrotechnic products are fast-acting. When used with auxiliary separation elements like springs, they provide the torque to initiate a spin and the compression to effect a separation [5]. Non-pyrotechnic small satellite separation adapters are also commercially available. Figure 1-3 shows a *lightband*™ adapter manufactured by RUAG Space. The separation adapters are available in various configurations, and it is possible to choose a configuration that delivers a predetermined separation velocity [6].

The structural response to shocks induced during pyrotechnic separation (pyroshock) is characterized by very high accelerations (> 1000 g), very high frequencies (~10 kHz), and the release of very high strain energy[7,8]. According to the pyroshock test criteria [8], a pyroshock may be near-field, mid-field, or far-field. Table 1-1 summarizes the definitions for the acceleration and frequency content of the three levels of pyroshock.

Davie and Bateman[7] identified six QT methods depending on the level of pyroshock: shock simulation on an electrodynamic shaker, the use of live ordnance with system structure, the use of live ordnance with mock structure, the use of live ordnance with a resonant plate fixture, a mechanical impact with mock structure, and a mechanical impact with a resonant fixture [4]. The simulation of near field pyroshock typically involves

using the actual pyrotechnic devices. Pyrotechnic products include linear-shaped charges, explosive bolts, nuts, and clamps. Near field pyroshock may also be simulated by laser excitation. Lee *et. al.*[9] demonstrated the use of Q switched laser for near field pyroshock simulation. The shock response in a near-field pyroshock excitation using an actual pyrotechnic device shows significant variation from test-to-test [10]. A metal-metal impact (with a mock structure or resonant plate) may generate a near-field pyroshock response when little material deformation is allowed at the impact point [11].

Table 1-1 Pyroshock classification

	Near-field	Mid-field	Far-field
Dominant spectral content (Hz)	>10,000 Hz	3 – 10 kHz	<3 kHz
Peak acceleration	>10,000 g	1,000 – 10,000 g	<1000 g

Typically, fair-field shock simulation involves using an electrodynamic shaker[12]. The response to an input shock simulated on an electrodynamic shaker is easy to predict. However, frequency control beyond 3 kHz is challenging because of the shaker's displacement and frequency limits. Bateman and Davie [13] demonstrated the use of a tunable resonant fixture for mid and far-field shock simulation on satellite components. Some impact shock machines may also produce mid and far-field pyroshock [7].

At the Kyushu Institute of Technology's (Kyutech) Center for Nanosatellite Testing, the annual demand for QT depends on Japan's H2A piggyback program [14]. In 2015, a metal-metal impact shock test method suitable for nanosatellites was developed at Kyutech in response to this substantial local QT need. [15]. According to [14], the machine could successfully simulate the H2A and DNEPR rockets' shock environment. An air gun shock machine was developed in 2017 in an effort to improve the performance of the previous machine.

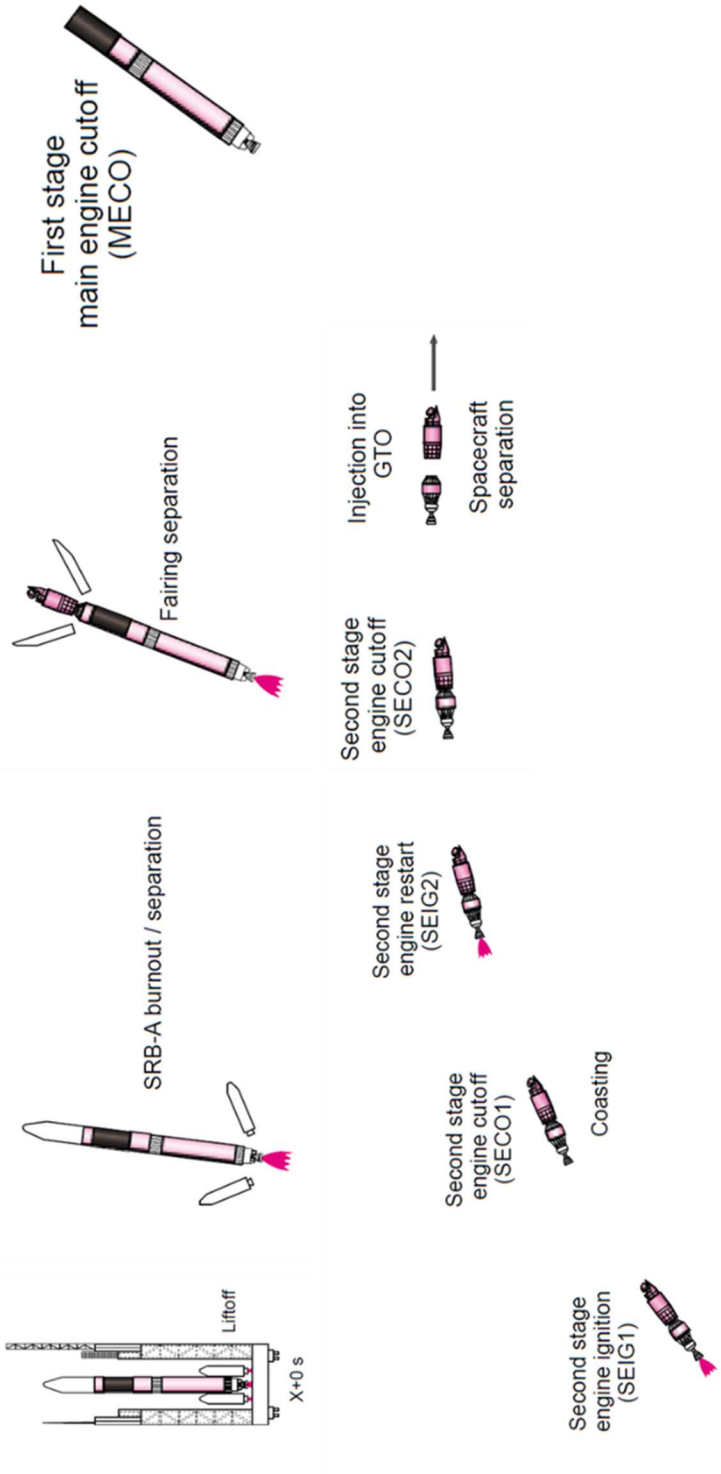

Figure 1-2 A typical launch sequence for a multi-stage H-II rocket launch to GTO[4]

Figure 1-3 RUAG microsatellite separation system PAS 381[6]

1.2 Shock Response Spectrum (SRS)

A system under shock may comprise many subsystems, each having its natural frequency. Suppose each subsystem is modeled mathematically as a single-degree-of-freedom system (s*dof*); the system becomes a series of s*dof* systems. The SRS is the peak acceleration (or velocity or displacement) response to a shock input measured at each s*dof* system, assuming a critical damping factor (typically Q = 10). The natural frequencies are logarithmically-spaced across the entire frequency bandwidth [16]. In a shock test, the input to each *sdof* system is the acceleration response measured on the test article. Figure 1-4 illustrates the formulation of the SRS.

The specifications for a shock test for qualifying a space component are usually in terms of the SRS. The specifications describe the acceleration at a lower frequency limit and the slope of the acceleration ramp between the lower limit of the frequency bandwidth and a knee frequency (k_f). Above the knee frequency, the acceleration has a nearly constant amplitude. The test specification describes the acceleration at k_f and at the upper limit of the frequency bandwidth. Figure 1-5 shows the specifications for recent shock tests at CENT.

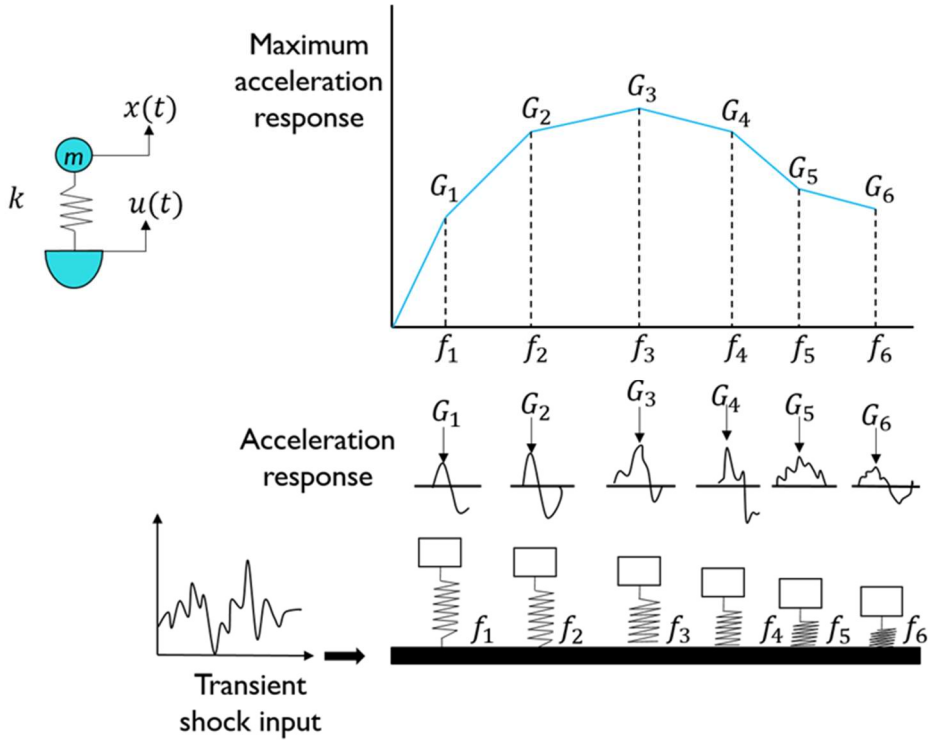

Figure 1-4 Peak response of a series of sdof systems to an acceleration time history input[16]

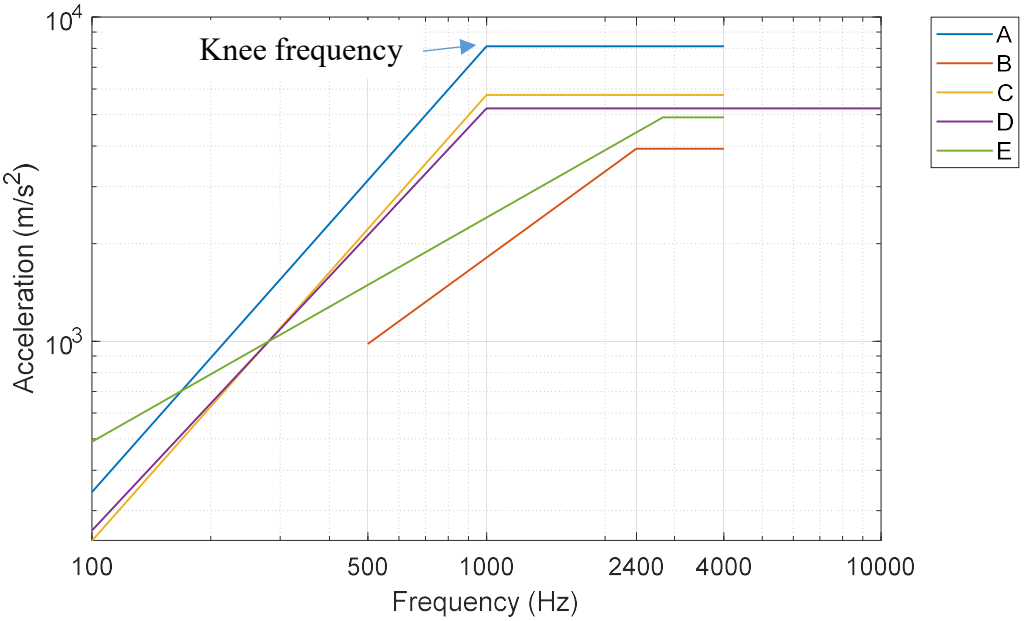

Figure 1-5 Shock specifications for recent tests at CENT

1.3 Qualification testing by mechanical impact

A typical mechanical impact simulation setup comprises a test article (mock or actual component) attached to an interface fixture and a data acquisition system. The impacting material (hammer, projectile, or actuator) excites the fixture, inducing a pyroshock response in the test article attached to the resonating fixture. Placing materials between impacting surfaces or clamping of plate edges alter a mechanical fixture's boundary conditions and may affect the measured shock response in that configuration [17,18]. The measured shock response on the mock or dummy test article should be similar to the measured shock on the actual flight component.

There are four stages in QT using an impact machine. First, a series of fine-tuning tests (with or without a mock structure) determine the initial input parameters (pressure, projectile, materials, impact angle, position, etc.). The second stage involves fixing the initial parameters after assessing the measured response's similarity to the target shock response. The third stage involves repeating the tests on the actual test item with the already fixed input settings. Finally, fine-tuning the shock response on the actual test item may be necessary. Summarily, in QT, the measured response should be similar to the target shock specification and repeatable under controlled conditions.

Figure 1-6 shows an air gun shock machine. The machine generates shock by the quick-release action of a valve [19] that allows propelling a projectile to a shock table base using compressed air stored in a cylinder. The impact excites a test item mounted on the shock table's top, opposite to the impact. Besides adjusting the driving pressure, optionally placing a plate material between the impacting surfaces modifies the shock input. The measured shock on the test item attains a predetermined shock level.

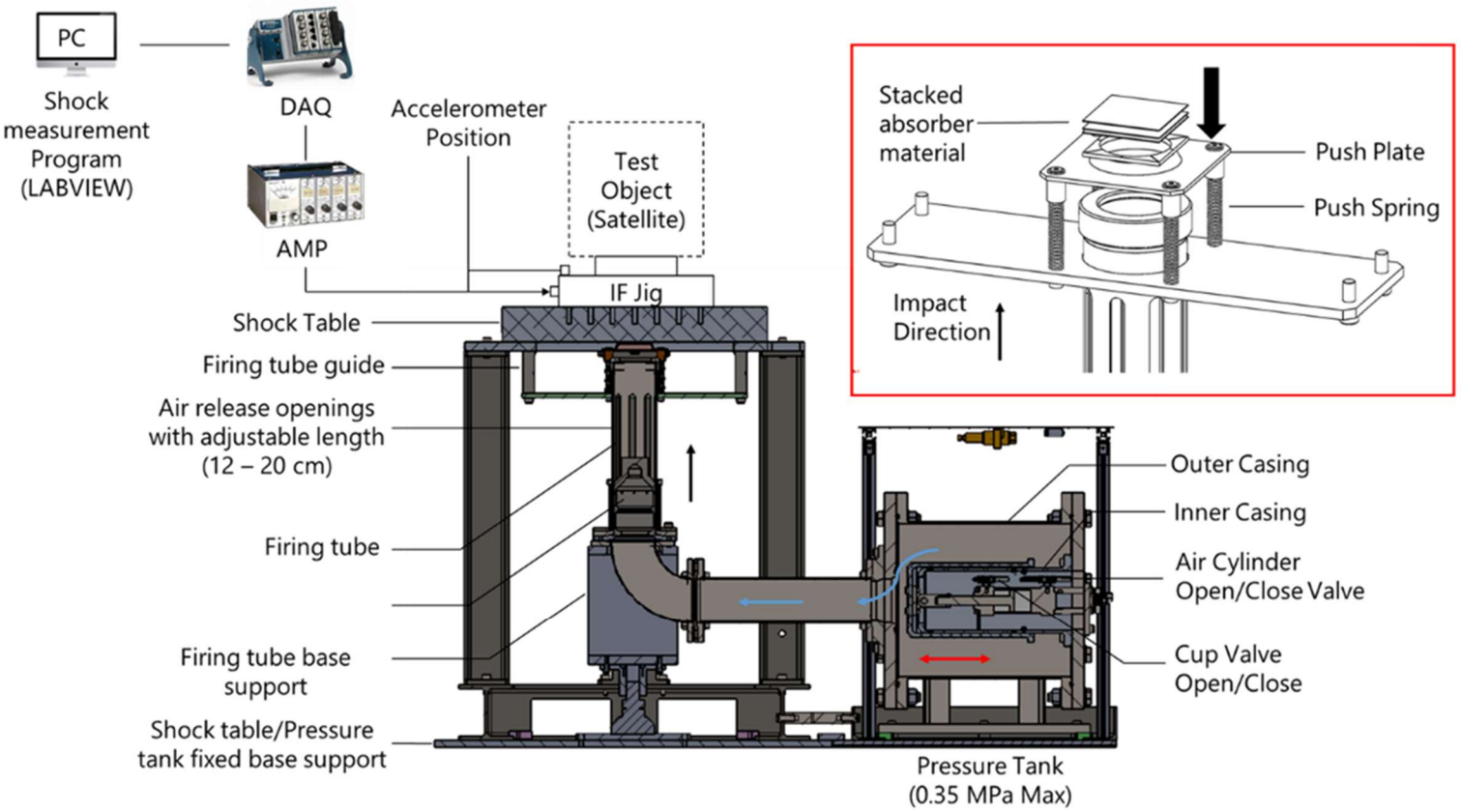

Figure 1-6 Air gun shock machine

1.4 Research Problem

The central problem here is that determining the initial parameters to achieve a target SRS in shock simulation on an air gun shock machine currently involves many trial-and-errors. Moreover, repeated tests using fixed input parameters show high SRS variation, making it challenging to predict the tuning parameters and extending the tuning process unnecessarily.

1.5 Research Objectives

This research aims to minimize the number of trial-and-error and improve the predictability of the initial tuning conditions in the shock simulation using an air gun shock machine. The specific objectives of this research are:

1. To maintain a searchable digital database of previous shock experiments and corresponding tuning parameters
2. To characterize the impact generated in a shock test on an air pressure-based shock testing machine
3. To predict the optimum tuning parameters (pressure, damper /cushion, damper thickness) for a given shock described by a specified SRS

1.6 Thesis overview

Chapter two reviews the impact simulation of mechanical shock and discusses methods of reducing trial-and-error in qualification testing of satellite components. The chapter reviews different types of mechanical impact machines and considers different approaches to predict the shock response in a shock test. The use of artificial neural networks and transfer learning was examined. The chapter concludes by reviewing five different metrics for shock response similarity

estimation. The five metrics are the SRS difference, mean acceleration difference, average SRS ratio, dimensionless SRS coefficients, and the mean square goodness-of-fit method.

Chapter three introduces the concept of case-based reasoning (CBR). CBR solves a problem by retrieving a solution to a similar problem from a database. This chapter proposes a similarity metric for retrieving shock response tuning parameters from an SRS database. First, it evaluates five different quantitative methods reviewed in chapter two for estimating SRS similarity. None of the similarity metrics account for the sign of the deviation between the target SRS and database SRS, making it challenging to satisfy the criteria for a good shock test.

Chapter four covers shock response variation. Shock simulation using the air gun shock machine was discussed in detail. The system design limits the actual tunable parameters to the driving pressure, the material of the absorber between impacting surfaces, the thickness of the absorber material, the material, and the mass of the projectile. Chapter four characterizes the influence of these parameters and also discusses the data acquisition system. The chapter shows that reducing external variations in the measurement system improves SRS repeatability on the shock machine. The shock response (SRS) measured using the machine showed significant variability (± 9 dB on average) below 1,000 Hz. Increasing the sampling rate and using a low-pass filter improved the repeatability of the SRS measurements. The SRS' variation reduced from an average of ± 9 dB to ± 2 dB below 1 kHz and ± 4.5 dB above 1 kHz. The chapter also shows that when a low-pass filter is set at a 10 kHz cutoff frequency, and the sampling rate is increased to 500 kSa/s, reducing the projectile mass will excite a knee frequency lower than 10 kHz. The high frequency response too approaches the target SRS.

Chapter five illustrates the application of the weighted distance in SRS retrieval and shock tuning and discusses policies for determining the initial tuning conditions for a shock test. Chapter five shows that the measured SRS (and retrieved) SRS are significantly higher than the target SRS because the target SRS is a far-field pyroshock, but the equipment simulates a near-field pyroshock.

Chapter six concludes this research and presents recommendations for future work. This research stresses the importance of performing a shock measurement system evaluation before using the machine for shock testing. When the variation in a measurement system exceeds the tolerance in the test specification, the system parameters cannot be predicted with any accuracy. In retrieving tuning parameters for a shock test from an SRS database, the weighted distance outperforms the mean square goodness-of-fit and other metrics.

2. Literature Review

This chapter reviews the existing literature regarding the laboratory simulation of small satellite separation tests. This review includes the shock environment during a rocket launch, a description of the shock response spectrum, and a review of the different laboratory shock simulation methods; the trend in the shock level at the spacecraft-launch vehicle interface, the best practices for pyroshock simulation and data acquisition, and the air gun shock machine central to this study.

2.1 Pyroshock response

The structural response to shocks induced during satellite separation may contain very high accelerations (> 1000 g) and very high frequencies (~10 kHz)[5,7]. Figure 2-1 shows acceleration-time history with a peak acceleration of 2,500 G.

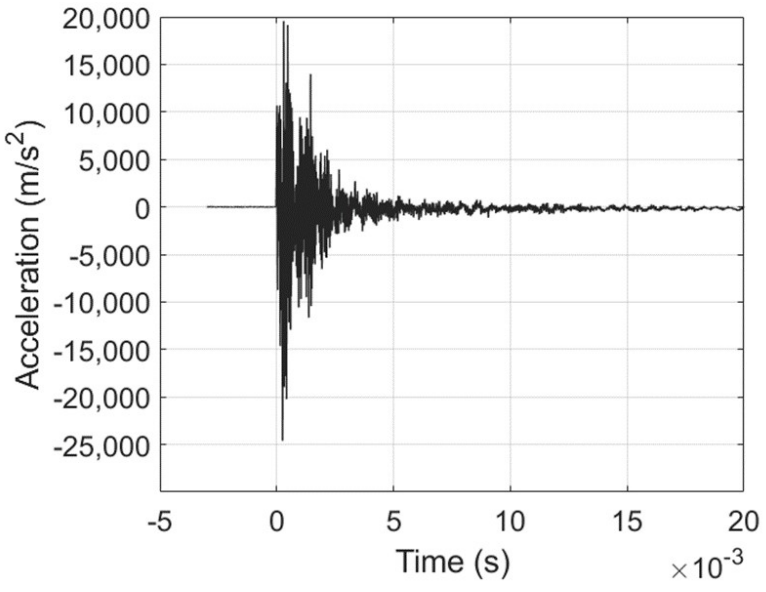

Figure 2-1 A typical pyroshock acceleration time history

A pyroshock does not usually last longer than 30 ms. The main structural components are rarely adversely affected by the induced shock. However, small MEMS devices may resonate at very high frequencies and experience failure[20]. This failure occurs in the form of cracks, dislodging of contaminants, the chattering of switches and relays, and may jeopardize the mission's success [8]. The location of MEMS components that constitute the essential elements for most subsystems within the satellite structure depends on the susceptibility to shock amplification.

Unlike traditional satellites, small satellites have a smaller volume, compact form, and rely on piggyback opportunities or rideshare missions where the small satellites are secondary payloads. The shock environment depends on the adapter selection[21]. The standard adapters at the SC/LV interface are usually interchangeable with smaller low-shock commercial adapters and dispensers. As the satellites become smaller in size, it becomes inevitable to place sensitive components near the separation shock source. Usually, a test article (dummy/mock) of similar build as the flight item or component is dedicated for QT. Under controlled conditions, the measured SRS should be repeatable regardless of the article under test.

Recently, there is a trend towards lightweight, non-explosive, low-shock separation systems. Even when the induced separation shock is low, there is still a risk of component failure. In the simulation of the shock environment during satellite separation, the assumption is that an SRS measurement greater than or equal to a specified target SRS has the same shock severity. The acceptable tolerance limits are usually specified along with the target SRS specification. The test article (satellite/component) undergoes a shock excitation at least twice along three axes [8,20].

Table 2-1 shows the SRS specifications at the spacecraft-launch vehicle (SC/LV) interface for recently active (2019) launch vehicles. *Gunter's space*[3] maintains a database of annual rocket launches. At the SC/LV interface, the slope of the acceleration ramp varies between 7 – 12 dB/octave and k_f has a typical value of 1,000 Hz. The acceleration at the upper-frequency limit (4,000 to 10,000 Hz) varies from 505 g for Epsilon to 4,000 g ($1\ g = 9.81\ m/s^2$) for the Long March rocket. The SRS specifications in Table 2-1 come from many experiments and analyses and represent the maximum expected flight (shock) environment (MEFE). A shock test specification also indicates the test's tolerance limits. The SRS from a shock test must match the MEFE or surpass it within statistical lower and upper tolerance limits to successfully reproduce the shock severity on a small satellite assembly[8].

Table 2-2 shows a list of popular commercial small satellite adapters. Some non-explosive separation adapters may be reset in a matter of hours and used for several tests. Nowadays, the shock test requirements for small satellites have become less severe. The peak acceleration is typically less than 1,000 g. Figure 1-5 shows specifications for five recent tests requested at Kyutech's Center for nanosatellite testing (CENT).

Table 2-1 Shock level at SC/LV interface for recently active launch vehicles

		Year [source]	Slope (dB/octave)	k_f (Hz)	Upper-frequency limit (Hz)	Acceleration (g)
1.	Long March (CZ)	2011 [22]	10.5	1,000	4,000	4,000
2.	Falcon-9	2020 [21]	9.2	1,000	10,000	1,000
3.	Soyuz 2 (R-7)	2018 [23]	10.2	1,000	10,000	700 – 1,000
4.	Electron	2020 [24]	7.2	900	10,000	700
5.	Proton	2009 [25]	12	1,000	10,000	2,000
6.	Kuaizhou-1	2016 [26]	10.7	1,000	10,000	3,000
7.	H-II A	2015 [4]	10.2	1500	3000	4100
8.	Epsilon	2018 [27]	10	1,000	4,000	1,000
			7.8	1,000	4,000	505

Table 2-2. Common Separation Adapters for Small Satellites

	Separation Device	Separation Mechanism	Developer	Shock level	Pyrotechnic	Heritage[1]
1.	Mk II MLB Advanced Light band (8″ – 38″)	Motorized separation	Planetary Systems Corporation	< 300 g's @ 1 kHz	No[2]	>200
2.	QwkSep® 15/24 Low profile Separation system	Low shock Clamp-band opening Device + kick-off springs	Sierra Nevada Corporation	1000 g's (1k – 2kHz, pyro) 100 g's max (10 Hz – 10 kHz, non-pyro)	Optional	>100
3.	PAS381S (15″standard)	Low shock clamp band + separation springs	RUAG	< 100 g's @ 1 kHz	No	> 600[3]
4.	CarboNIX	Spring pusher system	Exolaunch	Zero[4]	No	Yes

2.2 Examples of impact shock machine

The MIPS, THOR, Alcatel Etca, and Maeno-Oguchi machines are all examples of mechanical impact simulators.

2.2.1 The Mechanical Impact Pyroshock Simulator (MIPS)

MIPS is a popular machine used in QT. The MIPS creates shock by the action of a pneumatic actuator on an aluminum plate. The actuator is mounted on a movable bridge, allowing flexibility in the impact location (Figure 2-2). The generated SRS profile is a function of the driving pressure, damping, impact position, impactor head material, and the acceleration measurement position[7,18,29]. Figure 2-3 shows the effects of some parameters on the measured SRS.

[1] Cumulative numbers for a range of products provided by the company (if more than one product is offered).

[2] Planetary Systems Corporation's light band separation devices are compatible with a pyrotechnic pulse[28].

[3] RUAG has a variety of separation devices with a cumulative heritage of over 600 flights (including flights where PAS381S was used).

[4] Exolaunch services claim that the payload (satellite) is separated before shock is generated. *CarboNIX* was demonstrated in a July 2019 Soyuz launch.

According to Dwyer and Moul [18], fine-tuning the MIPS to achieve the required SRS sometimes **required up to 80 trials** involving modifying the force input and plate and test item boundary conditions. The number of trial-and-error involved inspired several characterization experiments. The authors concluded that the test article's weight and the mounting style had the most significant influence on the measured shock response. After successful characterization, the SRS profile generated on the MIPS is **repeatable to within 2 *dB*** of the shock specification. The SRS variation between successive tests under controlled conditions was within 10% in the majority of instances.

2.2.2 Testing Hammer for extra Ordinary Rough environments (THOR)

THOR is a midfield pyroshock simulator that creates shock by hammer impact on a tunable resonant plate [30]. SRS measurements using the THOR were repeatable within 1 dB for three consecutive shocks and showed a slight variation as the number of impacts increased. The author characterized several parameters influencing the SRS measurements, including the hammer mass, anvil material, impact location, hammer material, impact velocity, and boundary conditions on the SRS measurements. Achieving a goal shock on the THOR involved significant tuning tests. IEPE sensors were used for data acquisition.

2.2.3 Alcatel Etca Test Facility

This facility has various pyroshock simulators, including a resonant plate. Single plates, double plates, and more complex configurations are possible. The shock excitation is by detonating explosives, although mechanical impact excitation is also possible. The facility maintains a database of past shock tests. A simple least-squares program retrieves the turning conditions for a new shock test and speeds up the trial-and-error involved. Data acquisition uses various IEPE accelerometers and piezoresistive accelerometers,

analog anti-alias filters, and signal conditioners [31]. The authors define repeatability as consecutive SRS within the test tolerance limits.

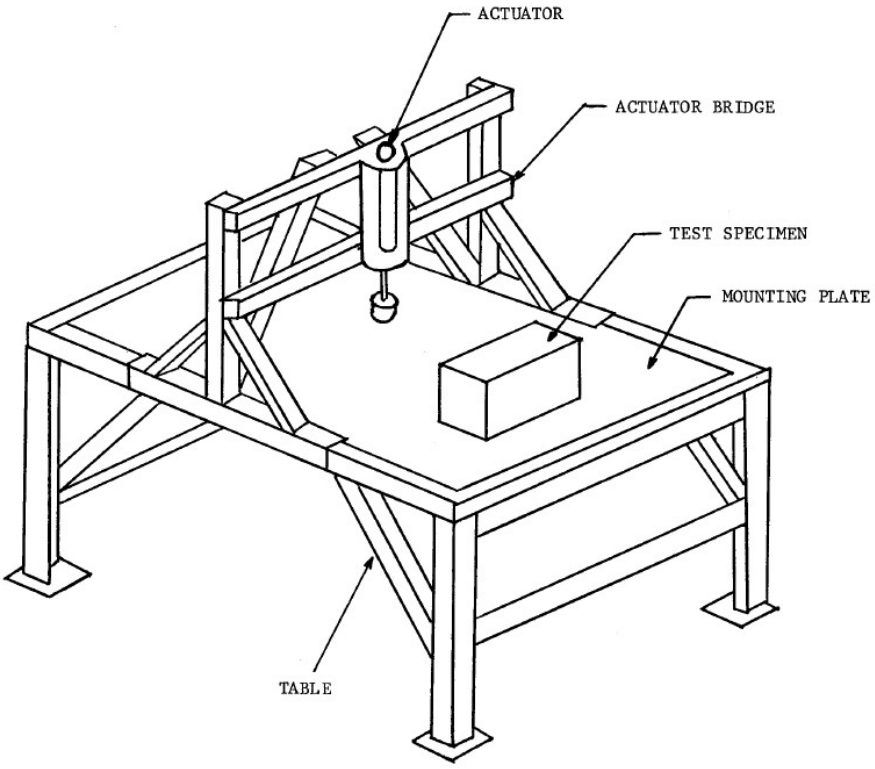

Figure 2-2 General configuration of a MIPS simulator [18]

Variation	Resultant
Paper (cardboard) under striker.....	Damps high frequencies
Steel plate under striker	Increases high frequencies
Clamp table edges to frame	Shifts resonance lower
Support table on wood blocks	Damps high frequencies
Jackstand under impact point	Reduces low frequencies
Component on transition plate	Attenuates all frequencies
Bags of lead shot on table	Damps high frequencies
Lower striker height	Evenly attenuates entire spectrum
Reduce ram pressure	Unevenly attenuates entire spectrum

Figure 2-3 MIPS Characterization[18]

2.2.4 Maeno-Oguchi Impact Simulator

Hatamura [15,19] developed a shock machine that simulates small satellites' separation shock environment using a rectangular plate. The author showed that changing the boundary conditions (frictional coefficient) can control low-frequency SRS measurements.

2.3 Reducing trial-and error: predicting the shock response

Since the measured shock response on a resonant plate depends on the measurement position [32], there is a need for a method to predict the response at any point on the resonant fixture. Shock response prediction can either be by empirical or analytic techniques or a combination of both methods. Empirical techniques involve measuring the SRS accelerations at various positions and finding empirical relationships between the input parameters that influence the measured SRS.

2.3.1 Empirical prediction

Newell [29] attempted to develop an empirical relationship between the various parameters influencing the MIPS's SRS profile using Buckingham-pi analysis, response surface techniques, Levenberg-Marquardt non-linear regression, and TableCurve 3D data fitting. The research concluded that a simple program that retrieved an SRS profile similar to the test specification was more efficient than the other techniques. The Alcatel Etca [31] and the THOR facilities agree that a simple program for SRS similarity estimation improved shock tuning with their test facilities.

2.3.2 Tunable resonant fixtures

Bateman and Davie [13] designed a resonant fixture with a plate and bar geometry for QT of small satellite components. They found that the SRS's knee frequency corresponds to the first bending mode in a free-free (or fixed-fixed) boundary condition in the plate.

In the bar, the knee frequency corresponds to the first longitudinal mode. [13]. After initial characterization efforts, a resonating fixture can reproduce a similar far-field pyroshock response for the same experimental conditions with little trial-and-error[7]. Equations 2.1 calculates the resonant frequency (f) in a resonant bar, length (L), where c is the speed of sound in the material. Equation 2.2 calculates the knee frequency of a plate, thickness (t), and elastic modulus (E), with a free-free boundary condition. The dominant mode is a function of the bending stiffness of the plate (A_n is a constant depending on the nth mode of the plate).

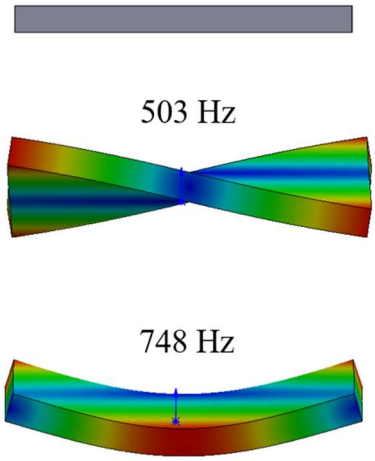

Figure 2-4 Mode shapes in a free-free vibration of a 38 mm thick aluminum plate

Qualification testing by mechanical impact with a resonant fixture can simulate far-field shock simulation with knee frequencies below 10 kHz. However, because the plate has a fixed resonant frequency, every SRS test specification with a different resonant frequency requires a new resonant fixture design. Figure 2-4 shows the first two modes in the modal analysis of a 500 mm square aluminum plate of 38 mm thickness. The plate's first bending mode is at 748 Hz ($A_n = 13.39, 19.79, 24.43 \ldots \quad n = 1, 2, 3, \ldots$). The

values of A_n are determined numerically or by analytically solving the differential equations of plate vibration [33].

$$L = \frac{c}{2f} \tag{2.1}$$

$$L^2 = \frac{A_n}{2\pi f}\sqrt{\frac{Et^2}{12\rho}} \tag{2.2}$$

Equation 2.2 assumes that the plate has a square geometry. The resonant plate may be used with a projectile [34] or explosives [35]. There appears to be a preference for resonant plates with a rectangular geometry [13,30,34,35] regardless of the excitation method. A rectangular plate offers a large surface area for mounting test items and has easy to clamp edges, although circular plates [32] and cylindrical resonant fixture designs [35] also exist. With some modification, Equation 2.2 applies to any thin plate of arbitrary shape undergoing free transverse vibration for various boundary conditions [33].

Table 2-3 compares the drop table, MIPS simulator, and tunable resonant fixture as examples of mechanical impact shock simulators. Besides changing the impact force (pressure or velocity), various materials, such as felt [34], papers [18], metals, and natural rubber [36], between the impacting surfaces, can raise or lower the SRS about specific frequencies. The measured shock response along the direction of impact depends on the test article and resonant fixture's geometry and boundary conditions.

Measuring the SRS accelerations in the lateral directions involves changing from a planar impact to impacting the resonant plate's edge or using a mounting fixture to change the test item's orientation. In other instances, the planar impact is strong enough to cause a significant response in the lateral directions. Consequently, the SRS accelerations in a

single impact measured using a tri-axial accelerometer may satisfy the shock specification in the X, Y and Z axes simultaneously. Typically, the measured response is higher in the impact direction than in the lateral directions [31].

Table 2-3. Comparison of various Mechanical impact shock simulators

		Drop-Table	Resonant Plate (MIPS)	Tunable bar/beam
1.	**Acceleration pulse**	Single-sided pulses with significant velocity change as compared to a typical pyrotechnic pulse with zero net velocity change.	This method can simulate a complex acceleration time-history similar to the time-history measurements in a pyroshock environment	It matches the dominant fixture response frequency (first bending mode in plates and first longitudinal mode in bars) to the target SRS's knee frequency.
2.	**Simultaneous measurement**	It requires a configuration change to measure the shock generated in the lateral axes.	A simultaneous measurement may be possible but may require several trial-and-error trials.	Simultaneous measurement of the response across three axes may be possible,
3.	**Test configuration**	Separate configuration per axis	It involves much trial-and-error. A separate configuration may be required to satisfy the test requirements.	It does not require significant configuration changes for different test items. However, since shock transmission is axial, a separate configuration may be required per axis.
4.	**Response**	A function of the drop height and "programming" materials between the impacting surfaces	A function of geometry, material, impact mass, speed, impact duration, impact location, external clamps	The attached test item does not significantly influence the response of a thick resonant fixture.
5.	**Over/under testing**	Possible over-test at low frequencies (except when the fundamental frequency is higher than the frequencies where over-test occurs)	Considerable over-test is possible, especially in the high frequencies of the near-field shock environment.	The absence of significant frequency content above the knee frequency may cause the response to be lower in this range
6.	**Repeatability**	It is easy to create simple pulses repeatedly	It requires a proper characterization of the machine. Once understood, generated shocks are repeatable	This method allows reasonable control and repeatability of the SRS, especially below the knee frequency
7.	**Modeling**	It is easy to model the simple pulse shapes mathematically	Empirical and analytic models are possible	A modal survey (or frequency analysis) may be required to determine the dominant vibration modes of the tunable bar/beam

2.3.3 Finite element analysis

Analytic techniques for predicting shock response include finite element modeling (FEM/FEA)[37], statistical energy analysis (SEA)[38], numerical modeling[39,40], and other methods [41]. Empirical methods cannot be extrapolated to another dataset [42]. A finite element program determines the plate's mode shapes and natural frequencies in characterizing a resonant plate to determine the appropriate position for mounting a test item for a future test. It uses any of the implicit or explicit integration techniques, such as the Newmark integration. After determining the natural frequencies, the modal participation extraction shows which modes dominate the SRS [32,42]. This process is as time-consuming as an actual experiment. The results are unique for each test item, and several configurations must be explored to determine the most suitable impact and test article mounting position.

Recent research interest in rubber waveform generators focused on determining parameters suitable for predicting a shock pulse's shape and duration using genetic algorithms [43]. Instead of modeling the shock response, the authors modeled the input to the *sdof* systems as a simple half-sine pulse. Previous research already showed that placing rubber of predefined shape between impact surfaces could simulate half-sine shock pulses [17]. The prediction relied on constitutive models that account for rubber's hyperplastic and viscoelastic properties. This kind of analysis is limited to acceleration shock inputs with a simple pulse.

2.3.4 Pyroshock data validation

Bateman *et al.* [44] have attributed common errors in pyroshock data acquisition to aliasing and inadequate slew rate of the signal conditioner. The authors insist that unisolated piezoelectric (PE) accelerometers must not be used in pyroshock data

acquisition because they are susceptible to zero-shift. The sensing element in the accelerometer also experiences resonance, making the SRS measurements about the resonant frequency of the accelerometer unreliable and unrepeatable[11]. The resonant response of the accelerometer's sensing element may cause saturation and DC offsets in the signal conditioner, making the data unusable [45]. The telltale sign of aliasing is a velocity time history that slopes (upward) or downward. The study also stated the importance of anti-alias filters and higher sampling rates. The authors stated the recommended practices for valid data acquisition:

- *Accelerometers.* Only piezoresistive accelerometers should be used for near-field shock measurement. Isolated PE (IEPE) accelerometers may be used for far-field shock.
- *Signal conditioner.* DC to 100 kHz or wider
- *Sampling rate.* 1 MHz or more
- *Analog anti-alias filter cutoff.* 1 octave below Nyquist frequency or lower with at least 60 dB roll-off for 12-bit systems.

2.3.5 Artificial neural networks (ANN)

Zhang et al. [43] recently used finite element modeling, numerical analysis, and a feed-forward back propagation neural network (BPNN) to predict underwater shock loading on a hypothetical structure. The research examined the effects of structural stiffness and damping on shock attenuation, cavitation time, and momentum transfer. At the time of writing this thesis, there are no known publications on artificial neural network for qualification testing are scarce.

2.4 A neural network for tuning?

2.4.1 Artificial neural network approach

Figure 2-5 shows the concept of tuning with a feed-forward back-propagation neural network with a single input layer, single hidden layer (middle) and single output layer. In reality ANNs use multiple interconnected layers and nodes[46]. The challenge in this concept is in determining the values of the weights (w) in the hidden layer. Assuming that random weights are assigned in the hidden layer in the forward-pass of the network, the algorithm computes the error between the final score at the output (y) and an expected score. In the backward pass, the error at y is used to update the weights in the hidden layer. The algorithm iterates, cycling through the input combinations until it reaches convergence. The challenge then becomes how to define the expected value of y from a shock specification.

Figure 2-6 shows the single output node (y) replaced with the input layer in Figure 2-5 and the new input is the frequency and acceleration specifications of the SRS. A neural network can predict multiple outputs as long as the activation function in the final layer is linear. However, when the activation function in the last layer is linear, the network cannot be trained by back propagation since the differential of the error will give a constant value [47].

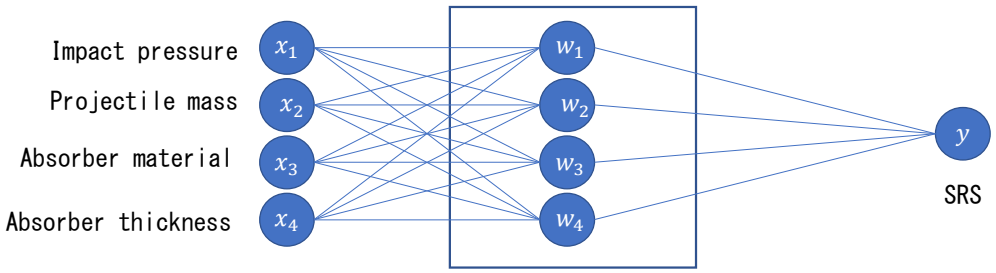

Figure 2-5 Concept of feed forward artificial neural network

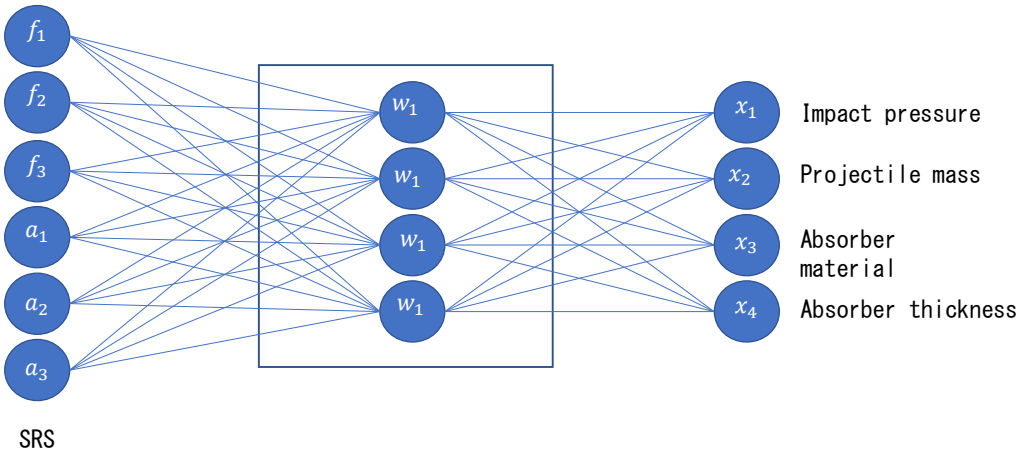

Figure 2-6 ANN with four output nodes

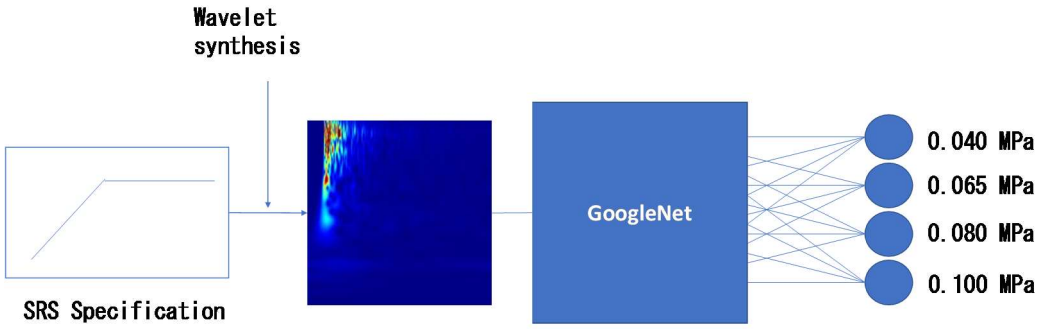

Figure 2-7 Transfer learning concept

2.4.2 Transfer learning approach

In an attempt to bye-pass the tuning phase of qualification testing, we explored the concept of transfer learning. Considering only one output (for example, pressure) in the network in Figure 2-6, a pretrained network can select the class of driving pressure depending on the training data. The SRS can be converted to a scalogram by wavelet synthesis [12]. The scalogram can then be resized for a pretrained network, such as GoogLeNet, and retrained. There are a few demerits of this concept.

- *Insufficient training data.* Machine learning methods require lots of data. It is not feasible to conduct as many experiments as the data needed.
- *Synthesized input.* An acceleration time-history synthesized by wavelet synthesis may have different temporal features when compared to an actual measurement. One of the demerits of the SRS is that it does not have a unique acceleration time history [48].
- *Labeling difficulties.* A convolution neural network is a supervised learning scheme. Significant overlap between two classes (say at 0.04 MPa and 0.08 MPa) mean that the training data cannot be correctly labeled.

2.5 Similarity based tuning

Rapid QT requires a generic approach easily applicable without excessive computation requirements and independent of the test article. Therefore, this research adopted Newell's approach – using a simple program to SRS similarity estimation. Applying the requirements for successive QT helps to structure the nature of the program. The program should be able to retrieve a database SRS that is most similar to the target SRS. Besides, the retrieved SRS shall have at least 50% of its datapoints above the target SRS [8]. There

is a need for a similarity metric that can sort the database SRS according to these requirements and retrieve the tuning parameters of the most similar SRSs.

The tasks required to implement this program are the essential components of a Case-based approximate reasoning system (CBR). CBR is an old machine learning technique used in problem-solving where solutions to previous problems, known as cases, are stored in a database (case-based) and are adapted to fit a new problem by establishing a feature-based similarity between the case base and the new problem [49–51]. This method is suitable for establishing a database for separation shock experiments and the experimental conditions associated with the measured SRS. The tasks involve the following:

1. Setting up a database where each entry is a case (it may be a feature matrix)
2. Definition of a similarity metric
3. Retrieval of similar cases from the database
4. Updating the database

The following section surveys some quantitative similarity measures used in aerospace applications.

2.5.1 Visual Evaluation

The SRS specification with a given lower and upper limit is a type of control chart where acceptable measurement values fall within tolerance limits derived empirically. The data that lies outside the tolerance limits are out-of-control and are therefore of unacceptable quality. Typically, the upper and lower limits for an SRS specification are $\pm 6\ dB$ for natural frequencies below 3 kHz, and $+9/-6\ dB$ when the natural frequency is above 3 kHz[8]. Figure 2-8 shows the SRS from 3 shock measurements for a shock test specification. A visual distinction of 2 SRS is sufficient in some applications to explain

the two shocks' differences. However, a quantitative description of the similarity or difference between two SRS may be necessary for other applications.

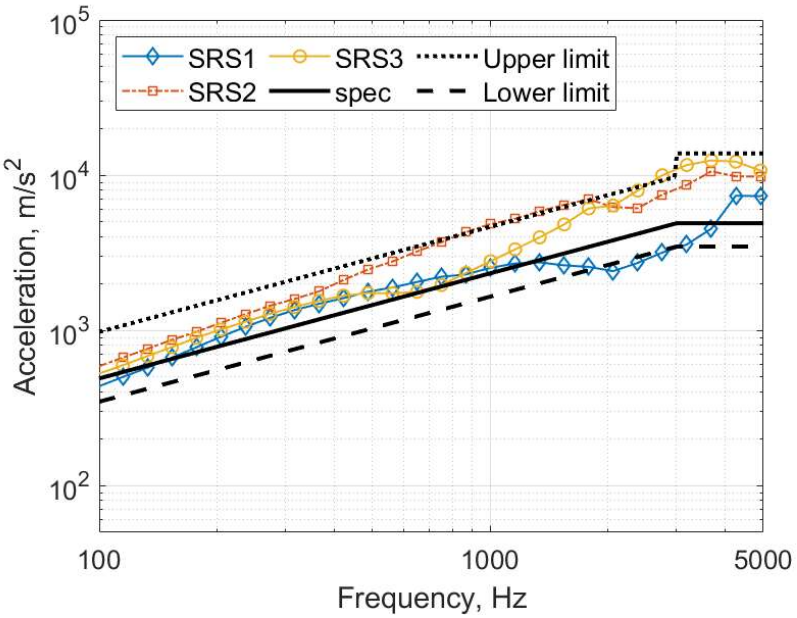

Figure 2-8 Three SRS measurements within NASA recommended lower and upper limits

2.5.2 SRS Difference

The simplest method to evaluate the similarity (or difference) between two SRS is subtracting one from the other. The SRS difference (diff) is the absolute value of the difference in acceleration of the 2 SRS (in dB) at each natural frequency (Equation 2.3). For example, in Figure 2-8, the difference between the upper limit and the SRS specification is 6 dB at all points below 3 kHz and 9 dB otherwise. Park *et al.*[52] used this method to show SRS attenuation for different kinds of absorber materials. Equation 2.3 shows how to calculate the SRS difference.

$$Diff(f) = \left|SRS_{ref}(f) - SRS_{measured}(f)\right| \tag{2.3}$$

2.5.3 Mean Acceleration Difference

Equation (2.4) shows the Mean Acceleration Difference (MAD). The MAD is a ratio of the absolute difference between a reference SRS and a measured (or modeled) SRS for $\boldsymbol{n}$ natural frequencies in the measurement bandwidth. The MAD gives a single scalar value to measure the similarity (or difference) between two SRS. In contrast, the SRS difference method shows a pointwise comparison. When the reference SRS is the same as the measured SRS, the MAD is 0 and tends to positive infinity as the SRS difference becomes more pronounced. Generally, there is an assumption that an SRS is repeatable if the MAD in subsequent measurements under controlled conditions is less than or equal to 10 % [9,53].

$$MAD = \frac{1}{n}\sum_{i=0}^{n-1}\left|\frac{SRS_{ref} - SRS_{measured}}{SRS_{ref}}\right| \tag{2.4}$$

2.5.4 Average SRS ratio

Some applications use the average SRS ratio (ASR) for repeatability analysis [54]. ASR (Equation 2.5) is a ratio of a summed SRS measurements over a bandwidth to the summed reference SRS over the same bandwidth. In Equation 2.5, $\boldsymbol{m}$ is the number of successive measurements or simulation trials.

$$ASR = \frac{1}{m}\sum_{f=1\ kHz}^{10\ kHz}\frac{SRS_{measured}}{SRS_{ref}} \tag{2.5}$$

2.5.5 Dimensionless SRS coefficients

Besides the ASR, recent publications express the similarity between two or more SRS in terms of two dimensionless coefficients [39,40,53,55,56]. The two dimensionless coefficients used frequently are the mean SRS coefficient (E_r), and, the maximum SRS coefficient, M_r. Ding et. al described the SRS coefficients as attenuation rates [40]. The two SRS coefficients are calculated using equations (2.6) and (2.7).

$$E_r = \frac{\sum_{f1}^{fn} SRS_{measured}}{\sum_{f1}^{fn} SRS_{ref}} \tag{2.6}$$

$$M_r = \frac{Max\ (SRS_{measured})}{Max(SRS_{ref})} \tag{2.7}$$

2.5.6 Mean squared goodness-of-fit (RMSE)

Equation (2.8) shows the mean squared goodness-of-fit method. It involves calculating the root-mean-squared-error between a measured SRS and a reference SRS. The RMSE is similar to the SRS difference calculation. Filippi *et al.* [31] compared a target SRS to an SRS database in the least squares sense, adding weights to account for direction and frequency.

$$RMSE = \left(\frac{\sum_{i=1}^{n} 20 \times \left(logSRS_{measured} - logSRS_{ref} \right)^2}{n} \right)^{\frac{1}{2}} \tag{2.8}$$

In the RMSE, a single scalar quantity (in dB) represents the difference between the two SRS. In contrast, the SRS difference can only be shown visually as a pointwise difference between two SRS. n is the number of natural frequencies in the SRS's computation. Table 2-4 summarizes the quantitative measures described in this section.

Table 2-4 Summary of quantitative SRS similarity metrics

Metric	Formula	Best SRS similarity	Worst SRS similarity	Remark
DIFF(f)	$\left\|SRS_{ref}(f) - SRS_{measured}(f)\right\|$	0 dB	Tends to positive infinity	Pointwise calculation; may show attenuation at specific frequencies
MAD	$\frac{1}{n}\sum_{i=0}^{n-1}\left\|\frac{SRS_{ref} - SRS_{measured}}{SRS_{ref}}\right\|$	0	Tends to positive infinity	Single scalar representation of similarity; suitable for repeatability calculations (for minimal differences)
ASR	$\frac{1}{m}\sum_{f=1\,kHz}^{10\,kHz}\frac{SRS_{measured}}{SRS_{ref}}$	1	The SRS profile may be dissimilar for all values	It ignores lower frequencies (< 1 kHz) Suitable for evaluating reproducibility (making the same measurement with different equipment or different personnel)
E_r	$\frac{\sum_{f1}^{fn} SRS_{measured}}{\sum_{f1}^{fn} SRS_{ref}}$	1		May show overall attenuation
M_r	$\frac{Max\,(SRS_{measured})}{Max(SRS_{ref})}$	1		Considers only the peak acceleration value; it may demonstrate attenuation for applications where the peak acceleration is the critical parameter
RMSE	$\left(\frac{\sum_{i=1}^{n} 20 \times \left(logSRS_{measured} - logSRS_{ref}\right)^2}{n}\right)^{\frac{1}{2}}$	0 dB	Tends to positive infinity	Single scalar representation: It cannot distinguish the sign of the deviation from the target SRS.

f: Natural frequency
n: Number of natural frequencies in SRS computation
m: Number of trials in repetitive measurements

3. Retrieving an SRS from a database of shocks: Case-based Rapid Shock Qualification Testing of Spacecraft Components

The purpose of this chapter is to compare the effectiveness of the similarity metrics discussed in section 2.5 for retrieving a similar SRS from a database of previous shock tests as part of a Case-Based Reasoning (CBR) approach for determining the initial tuning parameters in a separation shock simulation. CBR is a problem-solving approach that utilizes accumulated knowledge from previous experience in solving new and similar problems. It is clear from Chapter 3 that successive shock impacts under the same experimental conditions produce similar SRS. The CBR method enables rapid QT by forming an SRS database comprising acceleration measurements and experimental setup parameters for previous shock tests. Determining the setup parameters in a future QT or acceptance testing is a matter of retrieving the SRS that is most similar to the target SRS (and its corresponding setup parameters). A CBR system has four elements: ***case definition, similarity measure, information retrieval, and update scheme.***

3.1 Database Structure and selection criteria

In total, the database comprises SRS measurements from 108 different shock tests. Each database SRS has a test number (TN) and channel number. The channel number assignment is 1, 2, and 3 for the X, Y, and Z-axis. For each measurement, the SRS is computed between 10 Hz and 10,000 Hz at a 1/48 octave spacing and at a damping of 0.05 (Q = 10). There were 480 natural frequencies in total for each measurement. The shock tests included tuning tests using only the interface jig, tuning tests using a dedicated test article (dummy), and acceptance shock tests performed on actual payloads

(components and satellites). The total number of independent measurements (N) in the database is 324. Figure 3-1 shows the database structure. Each new SRS entry is subject to the validity checks described in Chapter 2.

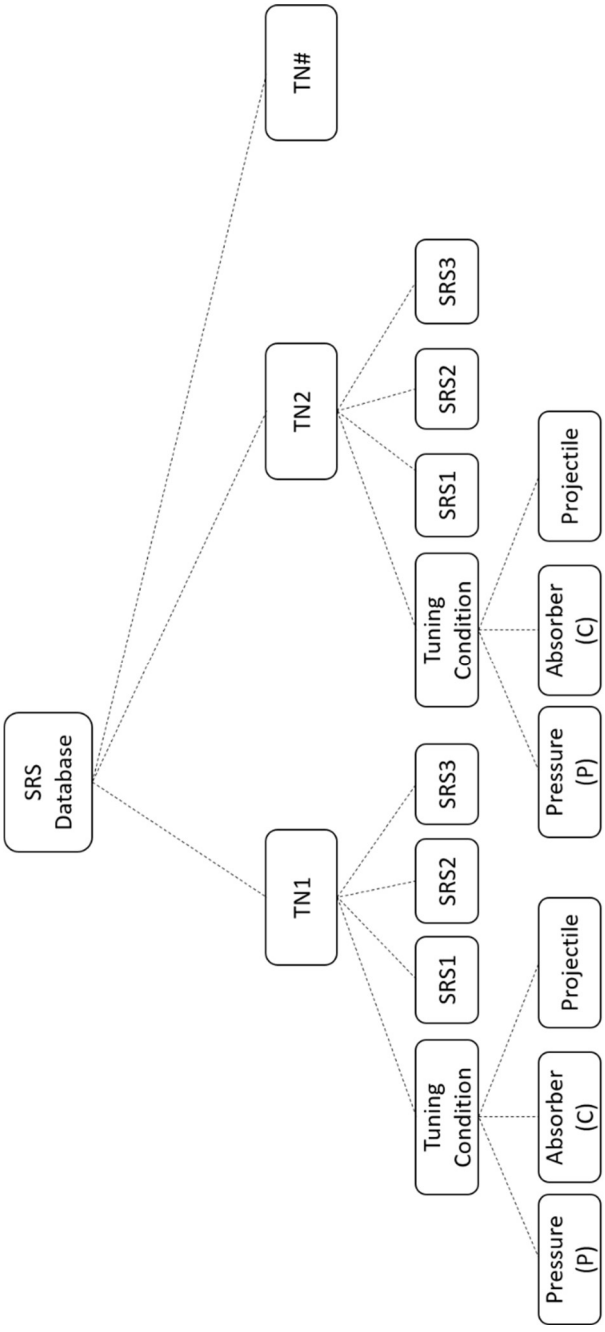

Figure 3-1 SRS Database Structure

Each database entry stores information on the driving pressure, absorber, and the projectile. After setting up the database, the next task was implementing a method to select an SRS similar to the target SRS in a QT from the database based on the NASA criteria. The first criterion is the 95/50 upper limit rule; 95 % of the data points shall exceed the target SRS specification with a 50 % confidence[8,57]. The second criterion is that 100 % of the data points shall exceed the lower limit.

3.2 Establishing a similarity metric

The similarity between a shock response spectrum (SRS) and a target shock specification is essential in evaluating the success of a qualification test of a space component. The similarity function is a metric that minimizes the distance between the target SRS and the database SRS. Here, the use of "similarity" connotes distance between a database SRS and a target SRS. The properties of a similarity function (σ) depend on the kind of application it is used for. Two of the more popular properties are reflexivity ($\sigma|x,x=1$) and symmetry ($\sigma|x,y=\sigma|y,x$). Reflexivity means that the similarity function should have a value of 1 when comparing an SRS to itself. However, the similarity function has a value of zero if two SRS are dissimilar. Symmetry in similarity implies that the value of the similarity function between two SRS, $\boldsymbol{y}$ and $\boldsymbol{x}$, should be the same if either SRS is the reference SRS.

A simple visual evaluation of SRS similarity is insufficient when comparing more than two SRS. There is a need for a quantitative measure of SRS similarity. This section compares the suitability of the five metrics discussed in section 2.5 for an SRS retrieval task.

3.3 Retrieving a similar SRS from the database

First, the SRS accelerations and tuning parameters associated with 108 shock tests (324 channels) were compiled as described in section 3.1. Using the ISO 19683[58] shock level (Table 3-1) as a reference, the three most similar SRS to the target SRS were retrieved using each of the quantitative methods in section 3.2. For each method, the upper natural frequency limit in the SRS retrieval was 5,000 Hz.

Table 3-1 ISO 19683 recommended shock specification

Frequency (f), Hz	100	2600	5000
Acceleration, m/s^2	545	4145	4145

Table 3-2 Comparison of different methods for SRS database retrieval

SRS no	Data above Spec (%)	MAD (%)	ASR	E_R	M_R	RMSE (dB)
101	81	33.3	1.5	1.4	4.0	3.0
73	60	19.3	1.0	1.1	1.9	2.0
14	54	29.1	1.4	1.3	3.8	3.0
100	30	23.0	1.3	1.3	4.2	2.6
71	27	41.9	1.0	0.9	1.4	5.7
79	18	32.2	1.1	1.0	1.9	4.2
76	17	49.3	1.0	0.8	2.2	8.0
110	16	44.0	1.2	1.0	2.7	4.9
323	11	48.3	0.7	0.6	1.3	6.4
218	4	58.4	0.6	0.5	1.2	9.8
203	2	68.8	0.5	0.4	1.0	13.1

Table 3-2 compares the quantitative methods for database SRS retrieval sorted from top to bottom by the percentage positive SRS deviation from the target SRS. These results are calculated using the formulas summarized in Table 2-4. It is clear from Table 3-2 and Figure 3-2 that:

i. The ASR and M_R are not good estimators of SRS similarity for the task of retrieving an SRS similar to a target SRS from a database. Even when both quantities have an approximate value equal to 1, the SRS significantly falls

below the target SRS specification. The reason is that the ASR excludes the SRS's low-frequency portion (<1000 Hz) from the computation.

ii. The M_R considers only the peak SRS magnitude (without considering the frequency at which it occurs). Shock transients typically have instantaneous high magnitude accelerations. Even when the peak amplitude is the same (SRS2), the two SRS profiles may be entirely different. A useful metric should account for all the SRS magnitudes at all the natural frequencies. The M_R has the worst performance of the metrics compared.

iii. Similarly, for the E_R, the SRS magnitudes at the high-frequency portion (> 1000 Hz) are several orders of magnitude higher than in the lower frequencies. Therefore, the sum of the measured SRS magnitudes may exceed the target SRS magnitudes.

iv. The MAD and RMSE have similar results. However, the percentage of data points below the target SRS for some of the retrieved SRS fall below the 50 % threshold.

v. The MAD and RMSE are based on the absolute difference between the SRS magnitudes of the target SRS and the measured SRS. The drawback here is that the absolute difference does not account for the sign of the deviation between the 2 SRS. Two dissimilar SRS can have the same RMSE.

3.4 Improved (weighted) Root-Mean-Square Error (wRMSE)

Section 3.3 showed that the MAD and RMSE could not distinguish the sign of the deviation from the target SRS. This section introduces the weighted RMSE as a way to

select an SRS within a database. Equation 3.1 defines the weighted RMSE for a target SRS specification (subsequently referred to as the weighted distance, Δ_j).

$$\Delta_j = a'_j w_j + (c_j) b, \qquad 0 \leq w_j \leq 1 \tag{3.1}$$

Where

$$a' = RMSE_{norm} = \frac{RMSE}{RMSE_{max} - RMSE_{min}}$$

$$c_j = \frac{RMSE_j}{\sum_{j=1}^{N} RMSE_j} \times 100\%.$$

$$b = 0.01$$

The weighted distance fulfills the following conditions:

i. Prioritize the SRS with more positive deviations from the target SRS if two or more SRS have equal RMSE

ii. If two SRS have an equal-weighted distance, prioritize the SRS with the lower RMSE.

First, the product of the normalized RMSE (a'_j) and weights (w_j) ensure that it is easy to distinguish two SRS within the database with equal RMSE. Reintroducing the positive and negative deviations from the target SRS into the value of the RMSE is critical in selecting $\boldsymbol{w_j}$. Making w_j the percentage of negative deviations from the target SRS maximizes the difference in the RMSE between the two SRS. Within an SRS database, it is possible to have two or more SRS where the product ($a'_j w_j$) is equal. In that case, we need a second term to separate the SRS further, prioritizing the SRS with more positive deviations from the target SRS.

In equation 3.1, the relative RMSE (c_j) gives the magnitude of the RMSE for individual SRS in the database relative to the RMSE sum for the entire database. The

second term in calculating Δ_j is a product of the relative RMSE and a sorting coefficient (b). The sorting coefficient prioritizes selecting an SRS in the database with more positive deviations from the target SRS. If $\boldsymbol{w_j = 0}$, then the weighted distance is determined by c_j. In evaluating the SRS database, $\boldsymbol{\Delta_j \cong 0}$ indicates strong similarity. Similarity decreases as the weighted distance tend to 1. Table 3-3 and Figure 3-3 shows the results of comparing the database SRS described in section 3.3 using Δ_j when $\boldsymbol{b = 10^{-2}}$.

Table 3-3 Weighted distance for 100 Hz – 5000 Hz

SRS TN no	RMSE(dB)	a'_j	w_j	c_j	Δ_j
35-2	4.52	0.138	0	0.131	0.0013
51-2	4.77	0.146	0	0.138	0.0014
101-2	4.99	0.153	0	0.145	0.0014
	Max RMSE(dB)= 34.7				

In Figure 3-3, 100 % of the retrieved SRS data lies above the target SRS, and the SRS with the least RMSE has the least weighted distance. Appendix 7.3 shows there is no significant difference in the percentage of data points above the specification when the octave spacing increases from 1/48 to 1/12.

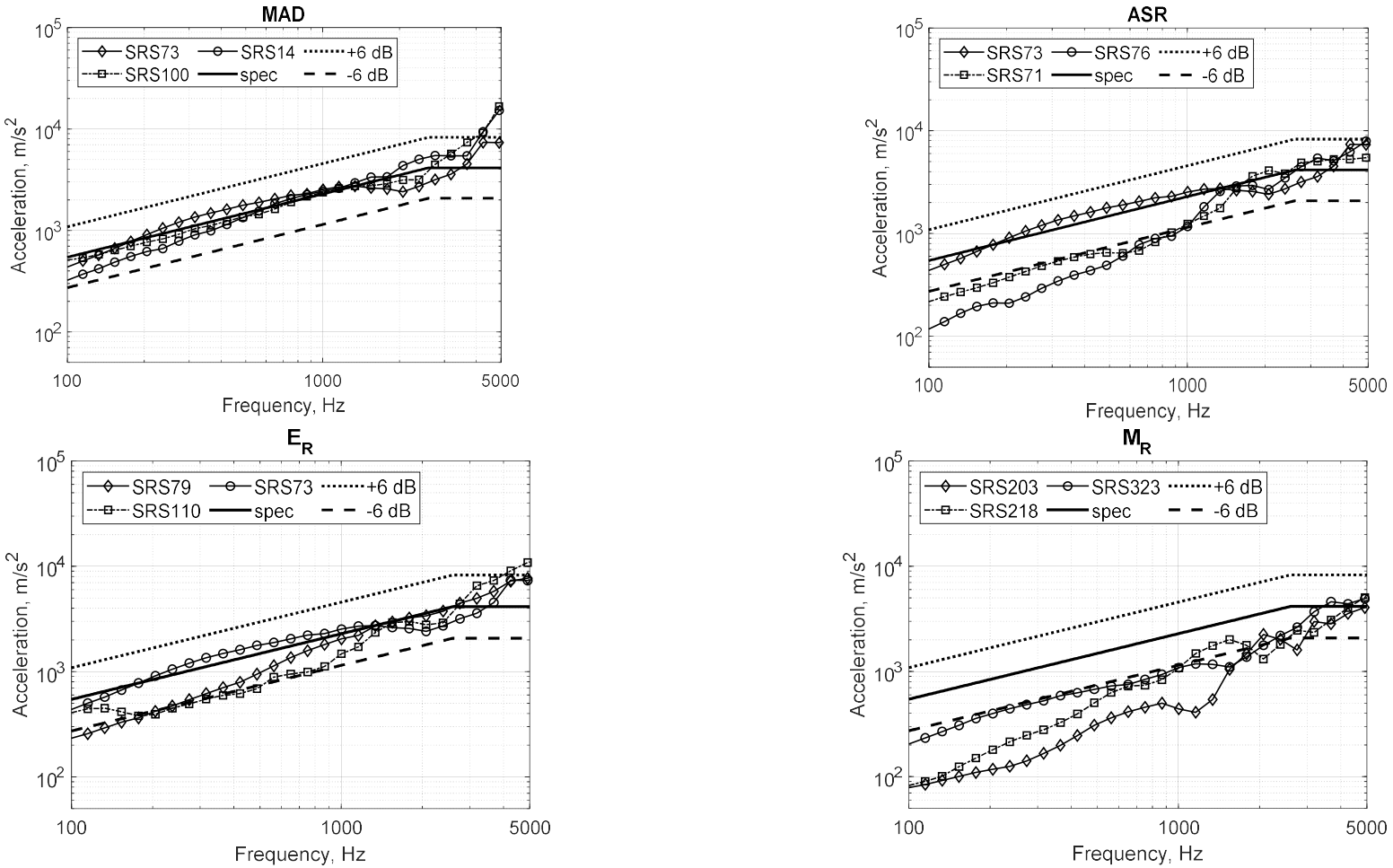

Figure 3-2 a Top three SRS retrieved using different similarity metrics (Database size = 324 channels).

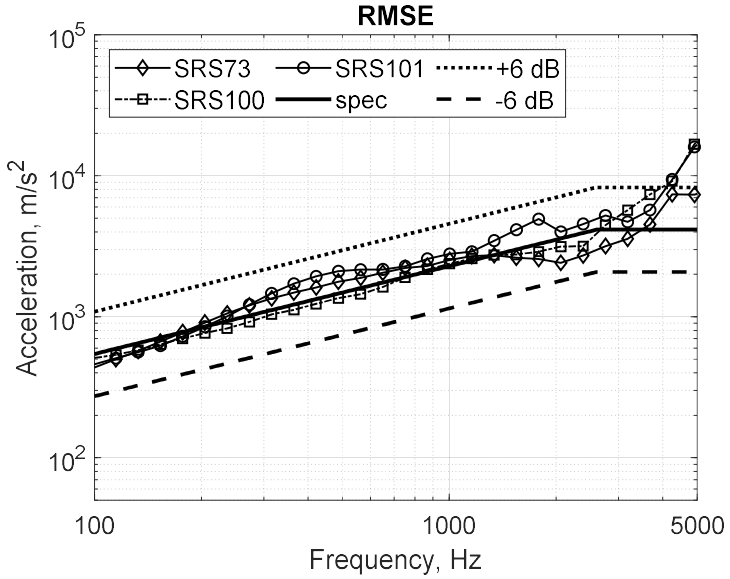

Figure 3-2b Top three SRS retrieved using different similarity metrics

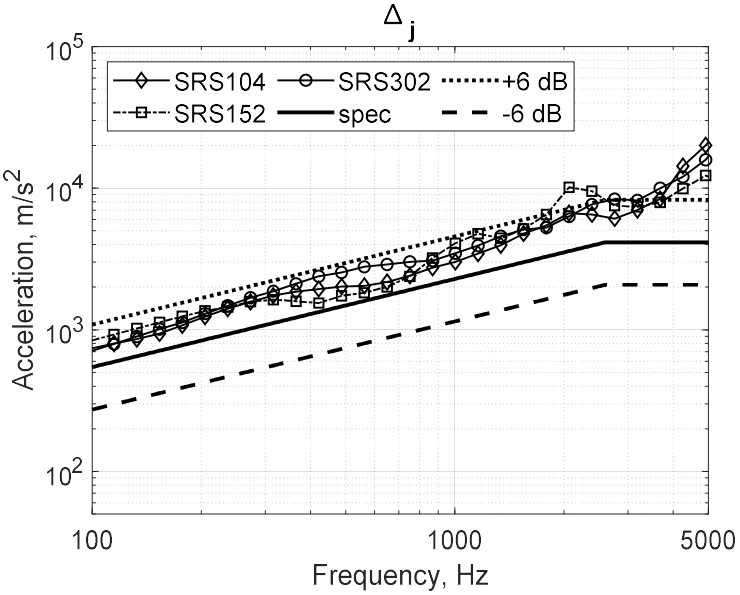

Figure 3-3 Top three SRS retrieved using the weighted distance

4. Characterization of the Shock simulation on an air gun shock machine

This chapter describes the shock testing process on the air gun machine. It investigates shock repeatability and describes experiments to characterize different parameters' influence on the SRS profile generated on the machine. These parameters include the impact velocity (as a function of applied pressure), absorber material (between impacting surfaces), and the projectile mass and material. Understanding the system behavior will help ascertain the possibility of establishing a sequence of actions to achieve the target SRS with minimum trial-and-error.

4.1 Characterizing and tuning a shock machine

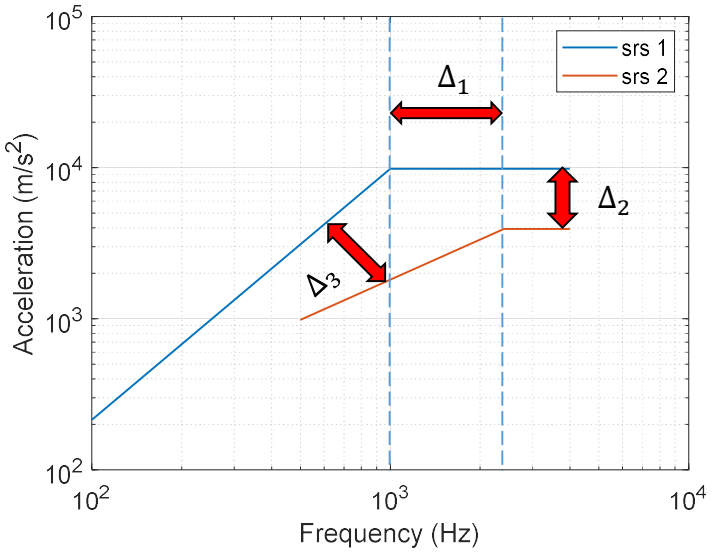

Figure 4-1 Transitioning between SRS specifications in QT

Figure 4-1 shows two shock responses, SRS specifications 1 and 2, having a different knee frequency (1,000 Hz and 2,400 Hz, respectively), different lower frequency limits, and a different slope between the lower frequency limit and the knee frequency. Assuming that srs2 is the target SRS, transitioning from srs1 to srs2 involves making

changes ($\Delta_1 - \Delta_3$) to the knee frequency, acceleration amplitude, and low-frequency slope (acceleration ramp).

The first step in characterizing a shock machine is identifying all the parameters that affect the measured SRS. The second step involves experimenting to see the effect of individual parameter changes on the measured SRS. The subsequent characterization experiments involve combining some of the identified parameters and monitoring the changes in the measured SRS. Characterization helps the machine operator accumulate empirical knowledge about how to manipulate the parameters to achieve a target SRS (Tuning). Therefore, successfully operating the machine relies on operator knowledge.

Figure 4-2 shows the qualification testing process on an air gun shock machine. The process assumes that the actual flight component has a replica item used for tuning purposes. After testing the replica item and fixing the input parameters, the main test item is tested. The machine (Figure 1-6) generates a mechanical shock by impacting a projectile on a hexagonal aluminum shock table. The test article is fixed rigidly to the shock table through an interface (IF) jig. Using a quick-release MO valve[19], compressed air at a preset pressure propels the projectile through a barrel until it impacts the shock table. The projectile's motion is constrained to impact the shock table at $90°$. The projectile may be changed depending on the target shock level. Currently, there are three types of projectile in use: Stainless steel (SUS430), Aluminum (A1050P), and Nylon. A stack of one or more absorbers on the push plate beneath the shock table can modify the projectile impact. The material of the absorbers may be the same or different.

Table 4-1 shows some of the parameters that can be combined to achieve the desired SRS. A manual test log maintains the record of the parameters associated with a shock test. Assuming that the shock tests are repeatable, the test log serves as a reference for

setting the appropriate parameters for a future shock test with a similar SRS. We can assume that the shock table's mass, stiffness, and damping characteristics are equal for test articles with similar mass and geometry. If this assumption holds, the shock response on a mock (or representative) test article can be tailored to an actual test article of similar mass and geometry.

Table 4-1. Shock machine tuning parameters

Items	**Values**
Shock Table mass	220 kg (including the mass of supporting beams)
Dimension (mm)	990 x 770 x 770
Tuning parameters	
Pressure, P	0.35 MPa max
Absorber (C)	Aluminum (A1050P), Stainless steel (SUS430), Natural rubber (NR), Felt
Impact angle	90 degree to impact plane
Absorber thickness (t)*	0.3 mm , 0.5 mm, 1 mm
Test article mass	Up to 50 kg
Projectile	Stainless steel (SUS304), Aluminum (A6061), Nylon (PN)

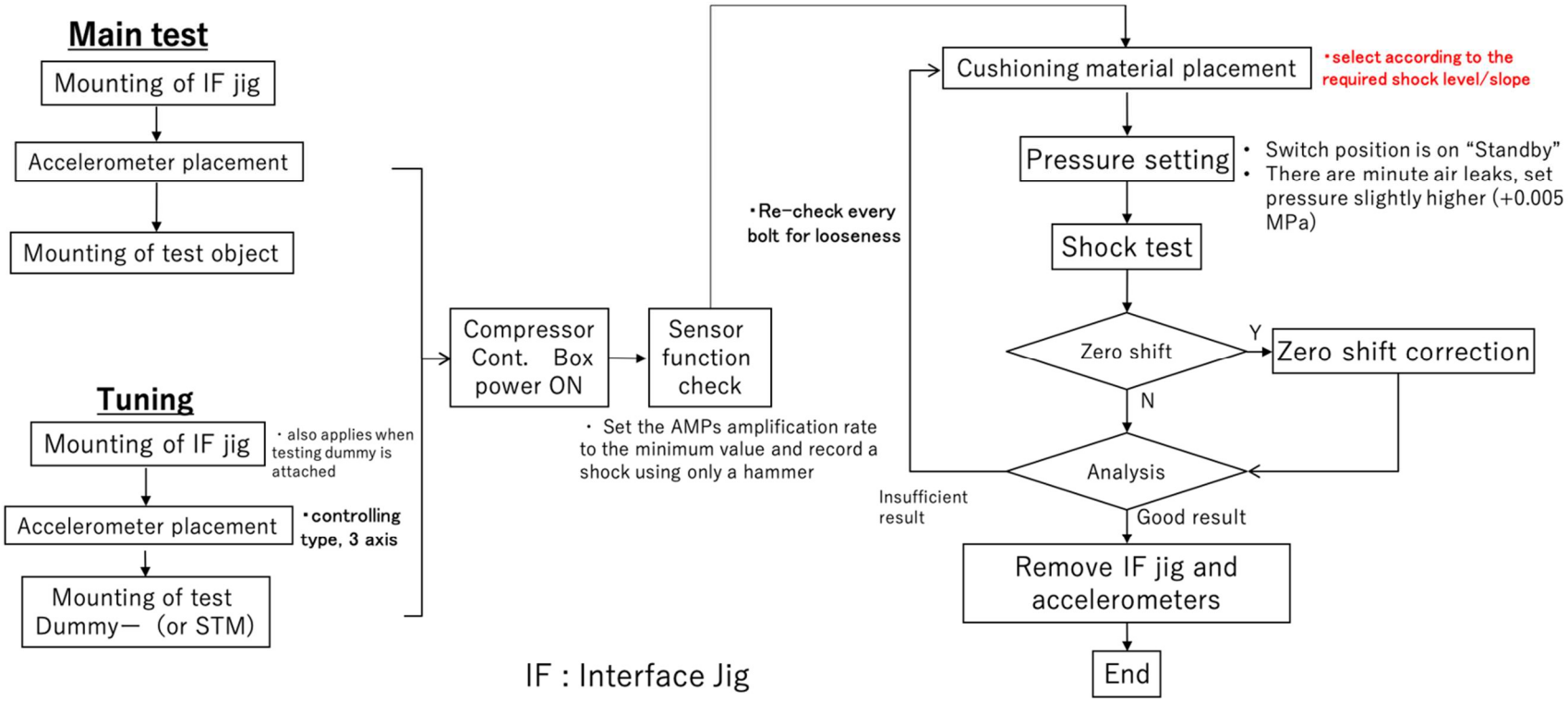

Figure 4-2 Qualification testing on an air-gun shock machine

4.2 The interface (IF) jig

Different IF jigs are available to simulate the SC/LV or component mounting interface. Figure 4-3 shows the IF jigs used in this thesis. The interface (IF) jig is mounted on an 80 mm thick hexagonal shock table. The projectile's impact diameter is 50 mm. We can assume that the shock response measured near the IF jig will be a function of the coupled response of the shock table and the IF jig since the distance from the impact area is less than 2 – 3 times the impact diameter. The size of the test article is also limited by the interface fixture size.

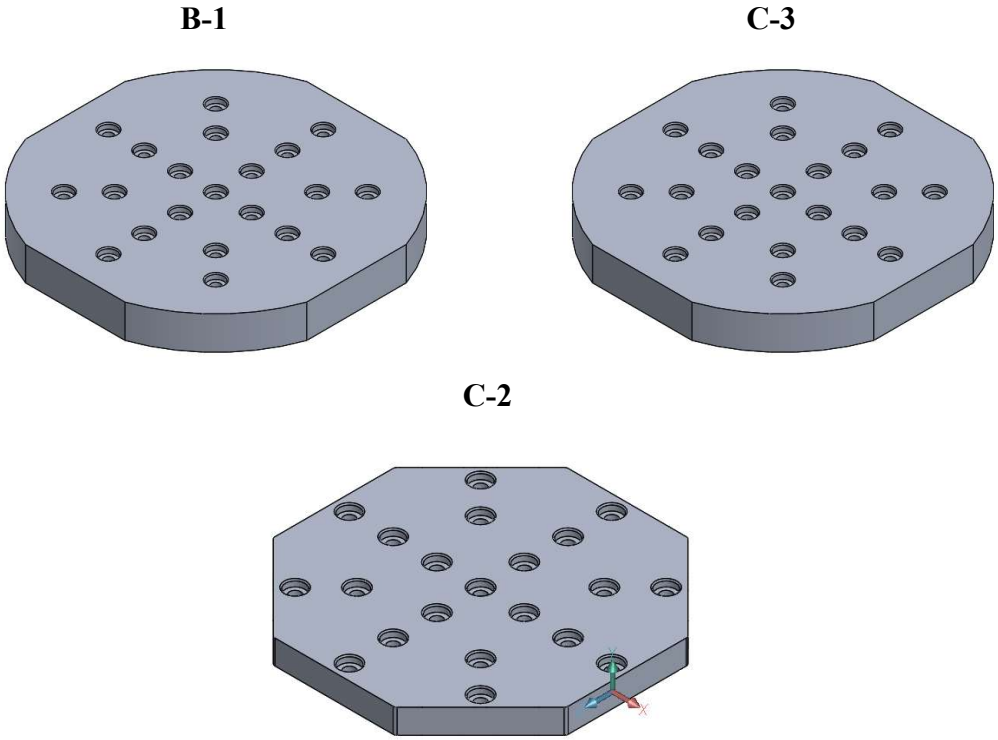

Figure 4-3 Some interface Jigs used on the shock machine

Table 4-2 Data Collection Specification

Items	Specifications
Charge Amplifier (AMP)	SHOWA 4035-52 (large input type)
	Sensitivity: 10～99.9 pC or mV/g
	Range:1, 3.16, 10, 31.6, 100, 316, 1000
	Maximum output: ±10V
DAQ	NI, 9222 module
Sampling rate	500,000 samples/s
Accelerometer	ENDEVCO 2225 (Mounting stud 2981-12)

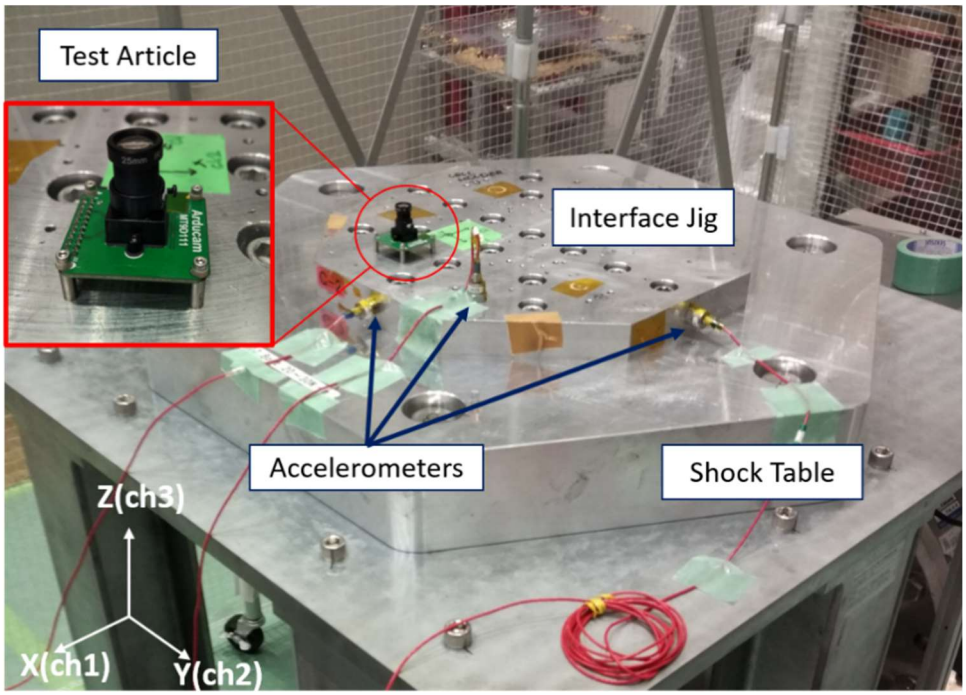

Figure 4-4 COTs component shock test showing the accelerometer positions on an IF jig.

4.3 Data Acquisition

Figure 4-4 shows a typical QT test setup. Piezoelectric accelerometers attached to the IF jig (Endevco 2225) are used to measure the shock response. In actual testing, additional accelerometers are attached near the test article. The accelerometers are connected to a large-input SHOWA 4035-52 charge amplifier. The signal conditioner converts the charge to voltage and may optionally filter high-frequency response from the signal. The data from the signal conditioner passes through a NI 9222 digitizer that samples the signal. The maximum sampling frequency of the NI 9222 module is 500 kSa/s/ch. Typically, the sampling frequency setting is at 100 kS/s. A LabView program analyzes and displays the acceleration data and the SRS in the same interface used for control PC. The analyzed SRS for each channel (axis) ranges from 10 to 10,000 Hz at a 1/48 octave spacing. Table 4-2 summarizes the specifications of the data collection system.

4.4 Preprocessing Data: Removing Zero Shift

Piezoelectric accelerometers typically exhibit zero (baseline) shift. Zero shift is a phenomenon where the measured accelerometer signal does not return to zero after a shock test. A zero shift may be identified in the SRS plot by a constant acceleration response in the low-frequency region instead of a 6 – 12 dB/octave slope(for a pyroshock)[44]. The baseline shift correction is necessary when there is a discrepancy in the positive and negative SRS slope in the low-frequency region.[44,59]. For a valid pyroshock, the velocity-time history should show a net zero velocity. If the velocity-time history exhibits a non-zero-mean, zero shift correction is necessary. Some air gun shock machines generate velocity shocks which characteristically do not have a mean zero velocity. Therefore, in this thesis, the decision to perform zero shift correction does not

depend on the velocity-time history. Figure 3-3 illustrates zero shift correction by wavelet decomposition. Shi and Shigemasa [3] developed the wavelet correction method used in this thesis.

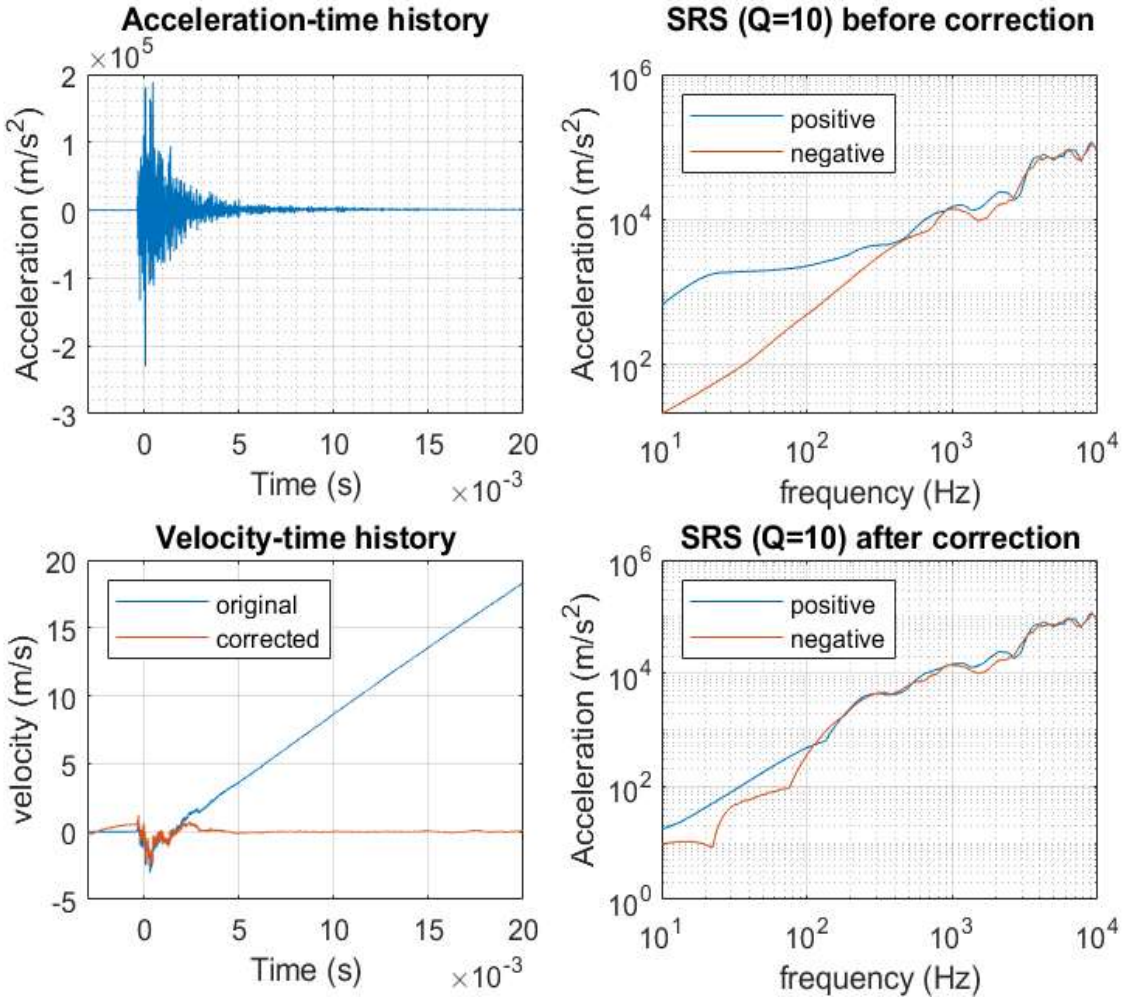

Figure 4-5 Illustration of zero shift correction wavelet decomposition[59]

4.5 Experimentation

Table 4-3 shows the initial sequence of the characterization experiments in this chapter. The experimental setup is shown in

Figure 4-4. The SRS acceleration measurements at different positions on an interface jig are different. The measurements may be affected by various factors such as the impact velocity, mass and material of projectile, nature of absorber between impacting surfaces, impact position, and so on. However, the accelerometers were fixed at the same point along the X, Y, and Z axes of the interface jig for all characterization experiments in this chapter. Moreover, the impact point is the same for all tests.

The measured SRS accelerations were generated using a 2.9 kg aluminum projectile (unless otherwise stated). The B-1 IF jig weighs 22 kg. At least 13 trials were conducted for each of the conditions listed in Table 4-3. Appendix 7.1 shows the formulas for calculating the statistical upper and lower tolerance limits for each characterization test. At least 13 trials are needed to obtain an upper limit that exceeds 95 % (β) of measured SRS values with a confidence of 50% (γ). First, the effect of increasing the driving pressure (velocity) is investigated with no material between the impacting surfaces and no test article mounted on the IF jig. Absorbers of different materials were added between the impacting surfaces in subsequent tests to investigate the effect on the measured SRS. Lastly, a test article was mounted to investigate the influence of the mass loading on the measured SRS.

Table 4-3 Characterization Experiments (B-1)

	Pressure (MPa)	Absorber	Test article mass (kg)	Remark
1.	0.040	None	None	To characterize the effect of increasing the driving pressure
2.	0.065			
3.	0.080			
4.	0.100			
5.	0.150			
6.	0.150	1 mm Natural Rubber	None	To characterize the effect of different absorbers between impacting surfaces
7.	0.150	0.3 mm Aluminum	None	
8.	0.150	0.3 mm Aluminum + 1 mm Natural Rubber	None	
9.	0.150	-	5	To characterize the effect of the mass of the test article

4.6 Increasing the Driving pressure (Velocity)

Equation 4.1 shows the relationship between the driving pressure and the muzzle (projectile exit) velocity of an air gun. The driving pressure (P_o) varies with the impact velocity (barrel exit velocity) under the following assumptions.

i. the pressure chamber has infinite barrel length,

ii. the gas is thermodynamically ideal,

iii. the pressure chamber has a constant diameter, and that there is no loss of energy in the system [60].

$$P_o = \frac{{a_o}^2 m}{AL}\left(\frac{2}{\gamma+1}\right)\left[1 - \frac{1-\left(\frac{\gamma+1}{2}\right)u_o}{\left(1-\left(\frac{\gamma-1}{2}\right)u_o\right)^{\frac{\gamma+1}{\gamma-1}}}\right] \qquad 4.1$$

(where $u_o = \frac{a}{v}$, L = barrel length, A = projectile base area, m = mass of projectile, γ = heat capacity ratio, v = barrel exit velocity, a_o = speed of sound in gas (air), and P_o = driving pressure).

Figure 4-6 shows theoretically that at the same driving pressure and barrel length, the impact velocity of a projectile decreases as the projectile mass increases. It also shows that increasing the driving pressure increases the impact velocity for any projectile mass.

It is easy to understand the projectile's effect on the SRS by examining the relationship between the driving pressure and exit velocity in an air gun shock machine. .Figure 4-7 shows a variation in the measured SRS for15 successive impacts at an driving pressure of 0.04 MPa. The response converges at the higher frequencies. There appears to be a knee frequency at 500 Hz, but the SRS increased again as the frequency approached 10 kHz. Below 500 Hz, there is a significant variation in the measured SRS. Figure 4-8 compares the SRS when the driving pressure is increased from 0.040 to 0.065 MPa. Instead of plotting the 15 SRS measurements which are cumbersome to understand, we can represent the measured SRS with the statistical lower and upper tolerance limits (Appendix 7.1).

Similarly, there is an overlap in the lower frequencies when the driving pressure is increased from 0.040 MPa to 0.080 MPa. Consequently, it is probable that at 0.080 MPa, an SRS similar to 0.040 MPa impact can be produced. The variation in the measured SRS at the same driving pressure is too wide and needs to be controlled.

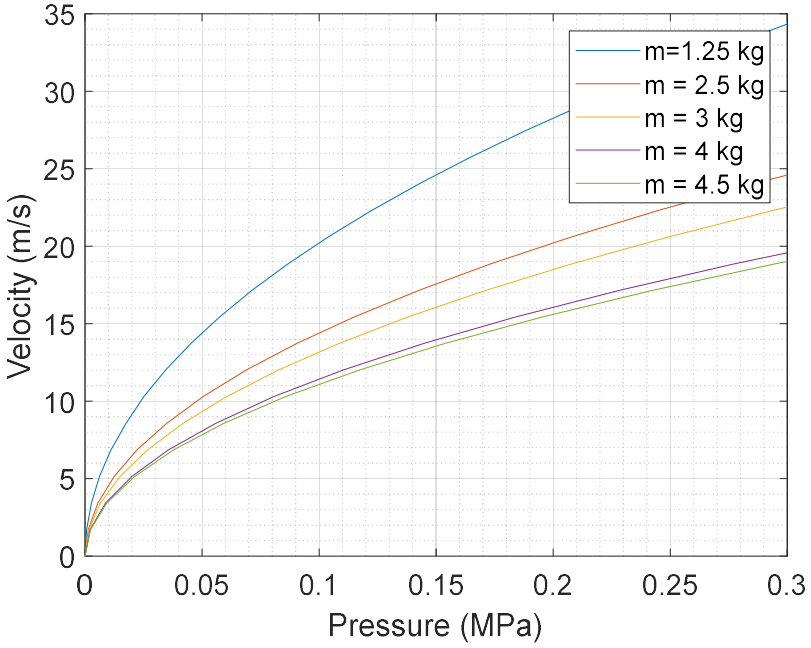

Figure 4-6 Projectile exit velocity as a function of the driving pressure in an air gun barrel

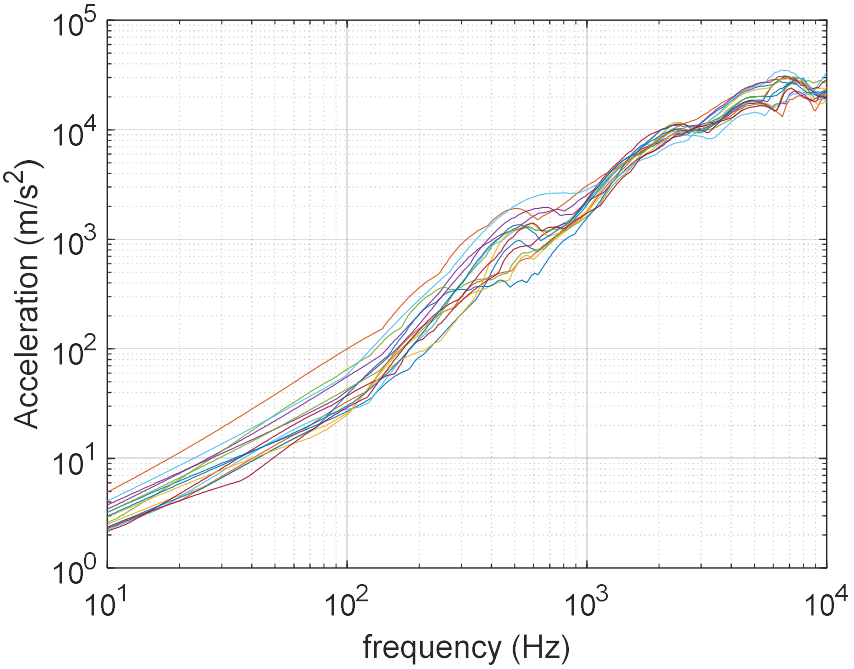

Figure 4-7 Fifteen successive shocks at 0.04 MPa driving pressure (Z-axis)

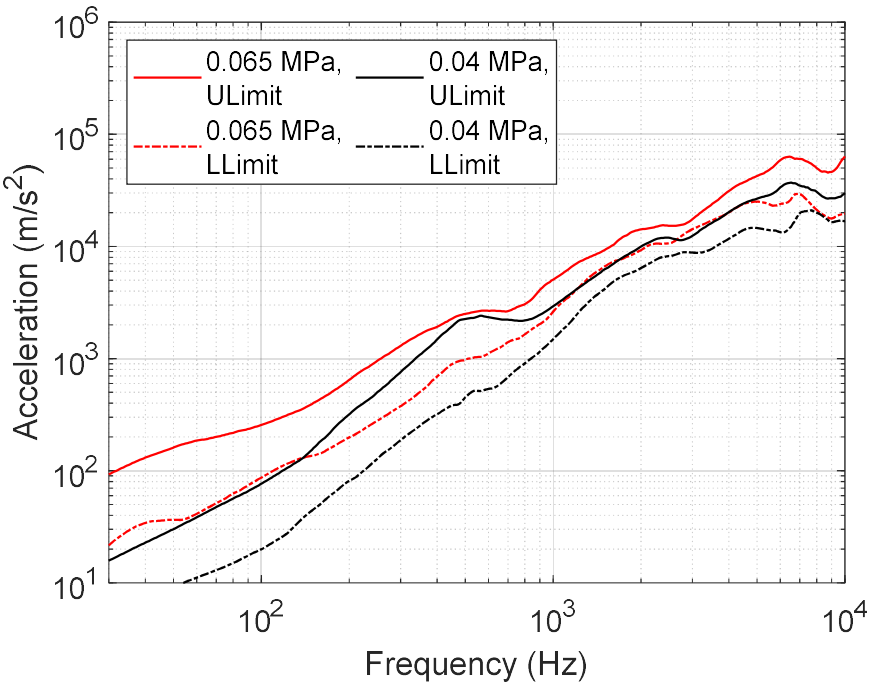

Figure 4-8 Increasing driving pressure shows overlapping upper and lower tolerance limits.

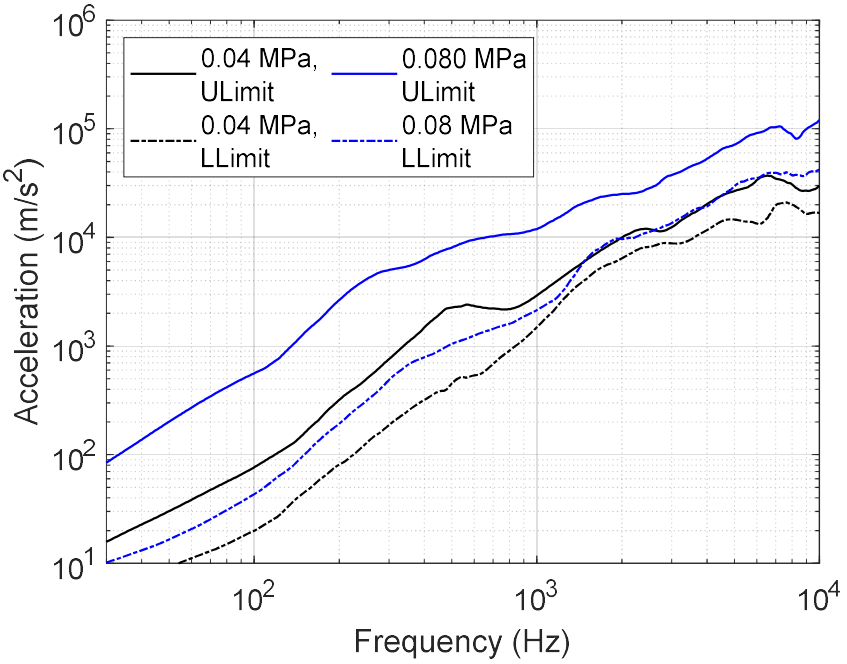

Figure 4-9 Increasing driving pressure to 0.08 MPa

4.7 Investigating SRS variation

In a QT, the SRS must satisfy the shock test SRS specifications at least twice per axis. However, the SRS from successive shocks may have significant variation as shown in Figure 4-7 to Figure 4-9. **An SRS is repeatable if the SRS difference from test to test under controlled conditions is within the test tolerances.** The repeatability must be maintained when the test item (dummy) is swapped for an identical test fixture and when the test item is removed[31]. In other words, the test-to-test variation must be within a controlled tolerance limit.

We can take the shock machine as a system where the output is the final SRS and the inputs to the system are the test personnel, equipment, materials, methods, and environmental conditions. All the system inputs are potential sources of variation in the SRS measurements the total variation in successive measurements under controlled conditions is the sum of the input variations.

Figure 4-11 shows a test article undergoing a shock test. The pod is mounted on an interface fig rigidly fixed to the shock table. The accelerometers measure the SRS accelerations along the X, Y, and Z axes. Fifteen successive measurements were taken using an driving pressure of 0.04 MPa from a 2.9 kg aluminum projectile without the test article. Figure 4-11 shows the SRS measurements for the 15 successive tests along the impact direction (Z-axis). Figure 4-12 and 4-13 show the out-of-plane response measured simultaneously as the response in Figure 4-11. All three measurements show significant variation between successive measurements below 1 kHz.

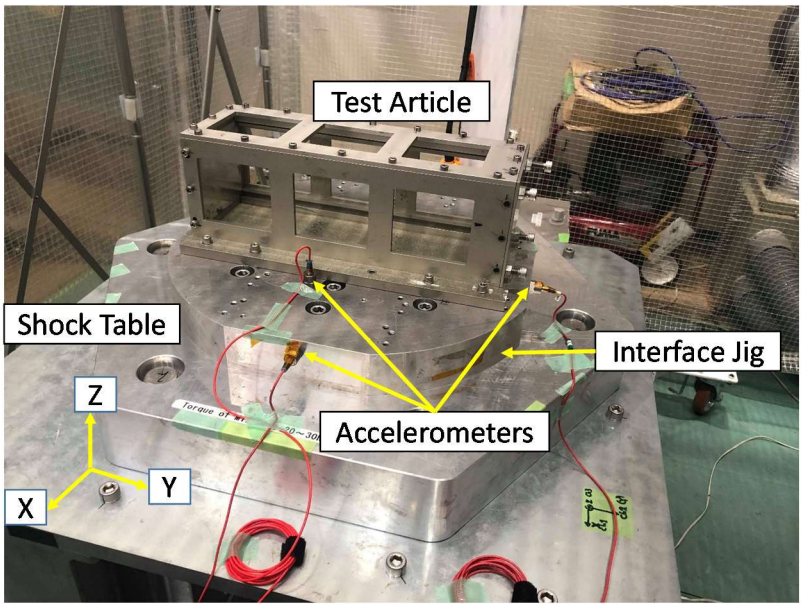

Figure 4-10 Experimental set up for repeatability evaluation

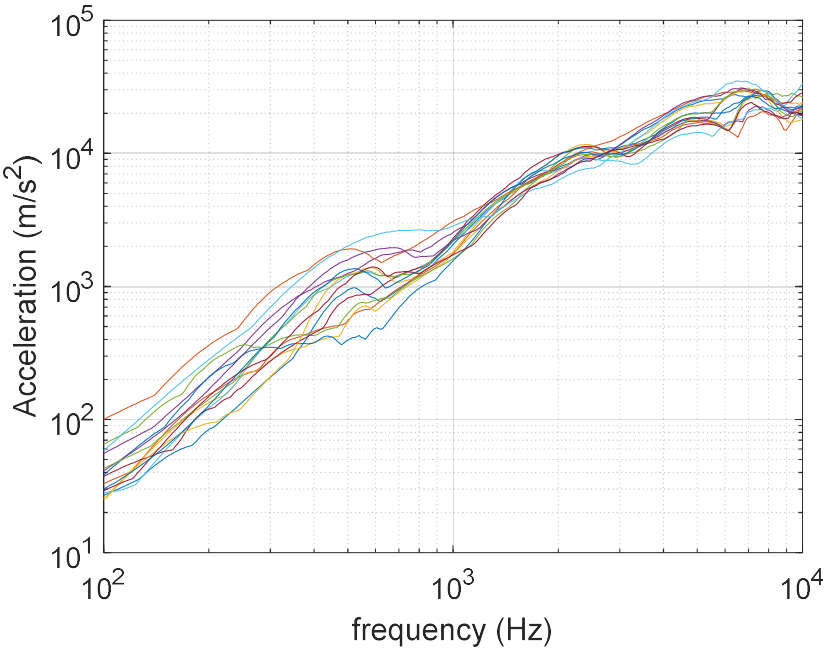

Figure 4-11 SRS of fifteen (successive)in-plane impacts at 0.04 MPa

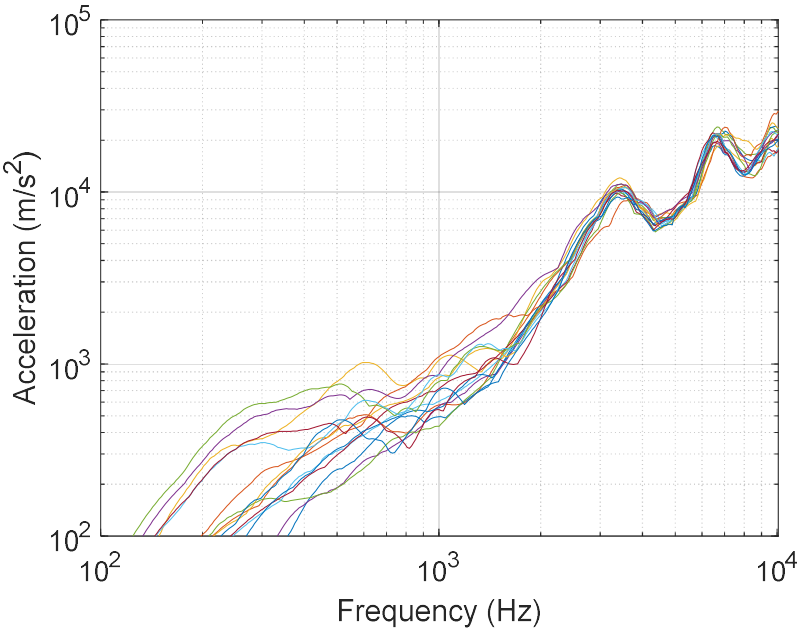

Figure 4-12 X-axis SRS to a 0.04 MPa shock

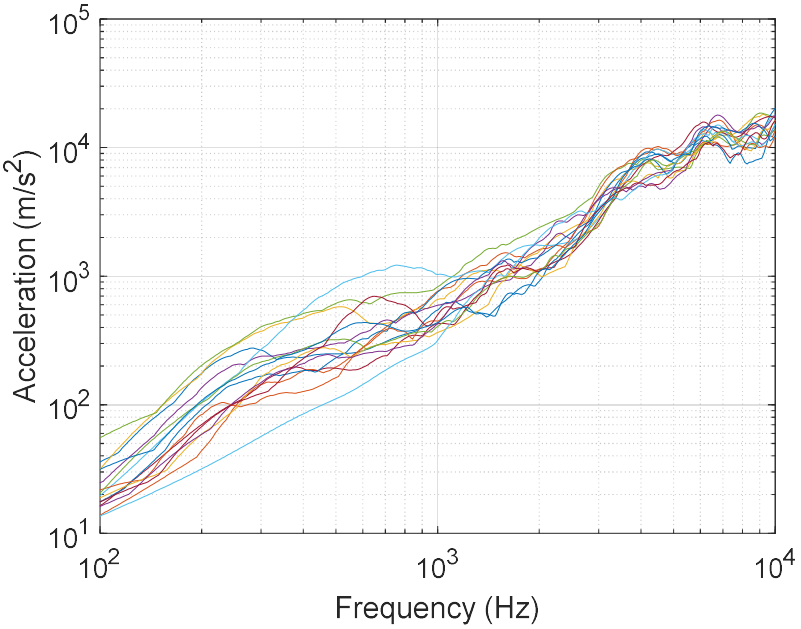

Figure 4-13 Y-axis SRS to a 0.04 MPa impact shock

Figure 4-14 shows the statistical (95/50) upper and lower limits of the X-axis shock shown in Figure 4-12. Appendix 7.1 shows how to determine the statistical upper and lower tolerance limits. **The limits are tighter at the higher frequencies (above 1500 Hz) at ± 3 dB and widen significantly to ± 6 dB below 1000 Hz**. The tolerance limits are wider than ± 6 dB at 500 Hz.

The wider tolerance around 500 Hz could be due to a local system response (Figure 4-14). It has been proven that the dipping of shock spectrum values (SRS dip) occur in structures mounted on non-rigid foundations at the normal modes of the equipment under test [16]. Figure 4-15 shows a modal survey of the shock machine. Four of the dominant normal modes occur at 475 Hz, 488 Hz, 524 Hz and 651 Hz. The dip in the upper limit in Figure 4-14 may be because the spectrum dipped randomly about the dominant modes and this can explain the wide tolerance limit about 500 Hz.

After increasing the driving pressure to 0.15 MPa, the variation at 500 Hz was well within ± 6 dB as the frequency increased from 500 Hz to 10,000 Hz. However, below 500 Hz, the variation widened. Figure 4-16 shows the symmetrical SRS tolerance limits increase from ± 6 dB at 0.04 MPa to ± 8 dB at 0.15 MPa driving pressure between 30 and 300 Hz. An 8 dB tolerance limit is unacceptable because shock test specifications have an even tighter tolerance limit, usually 3 dB or 6 dB. Although increasing the driving pressure solved the SRS's flattening around the lower resonant frequencies, the wider tolerance limits indicate another problem. This finding led to the second hypothesis that the SRS variation could be because the measured data is corrupted.

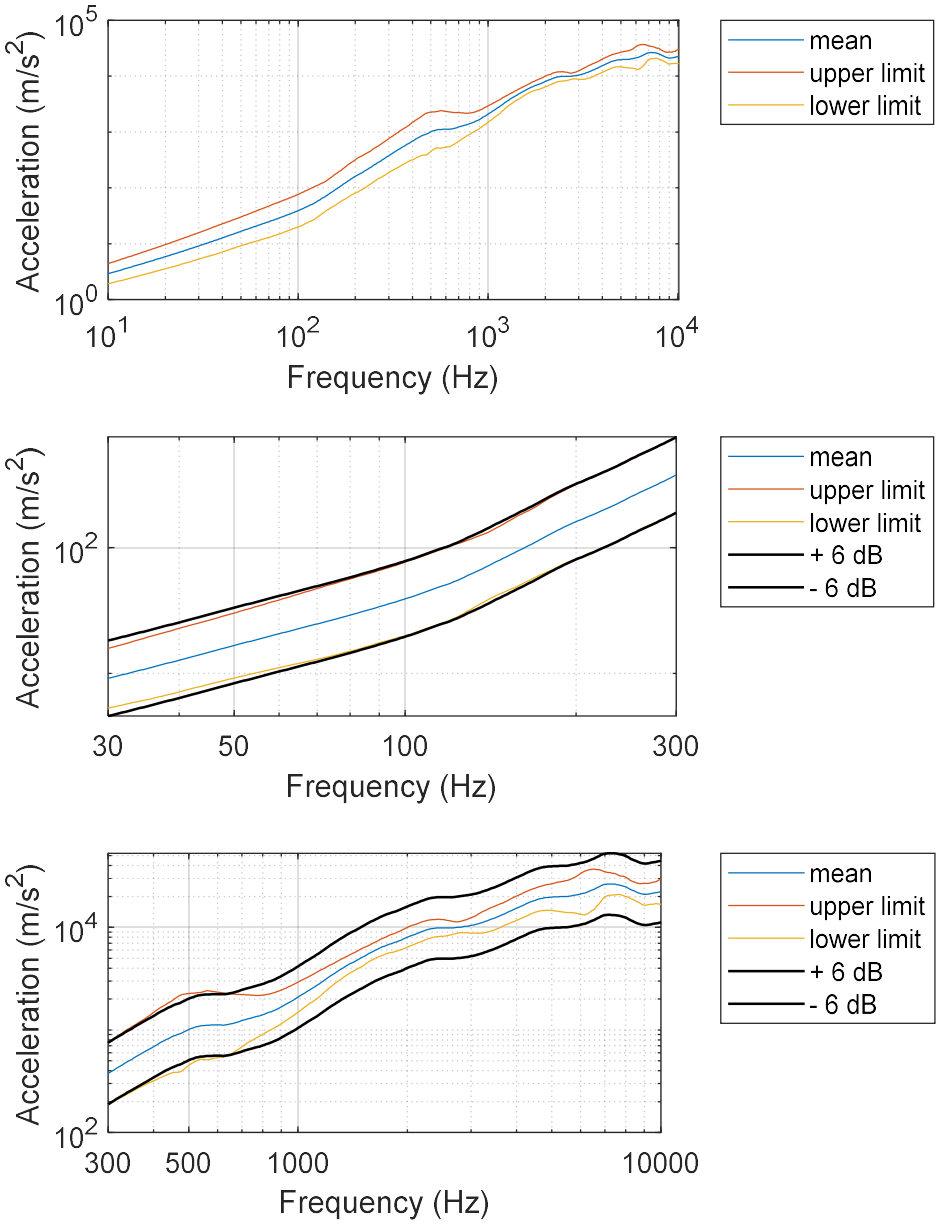

Figure 4-14 SRS Variations for successive shocks at 0.04 MPa (top). The middle figure zooms in on the response between 30 and 300 Hz, and the bottom figure zooms in on the response between 300 Hz and 10,000 Hz to get a sense of the variation in the SRS across the frequency bandwidth. The tolerance limit is wider below 1000 Hz and widest at 500 Hz

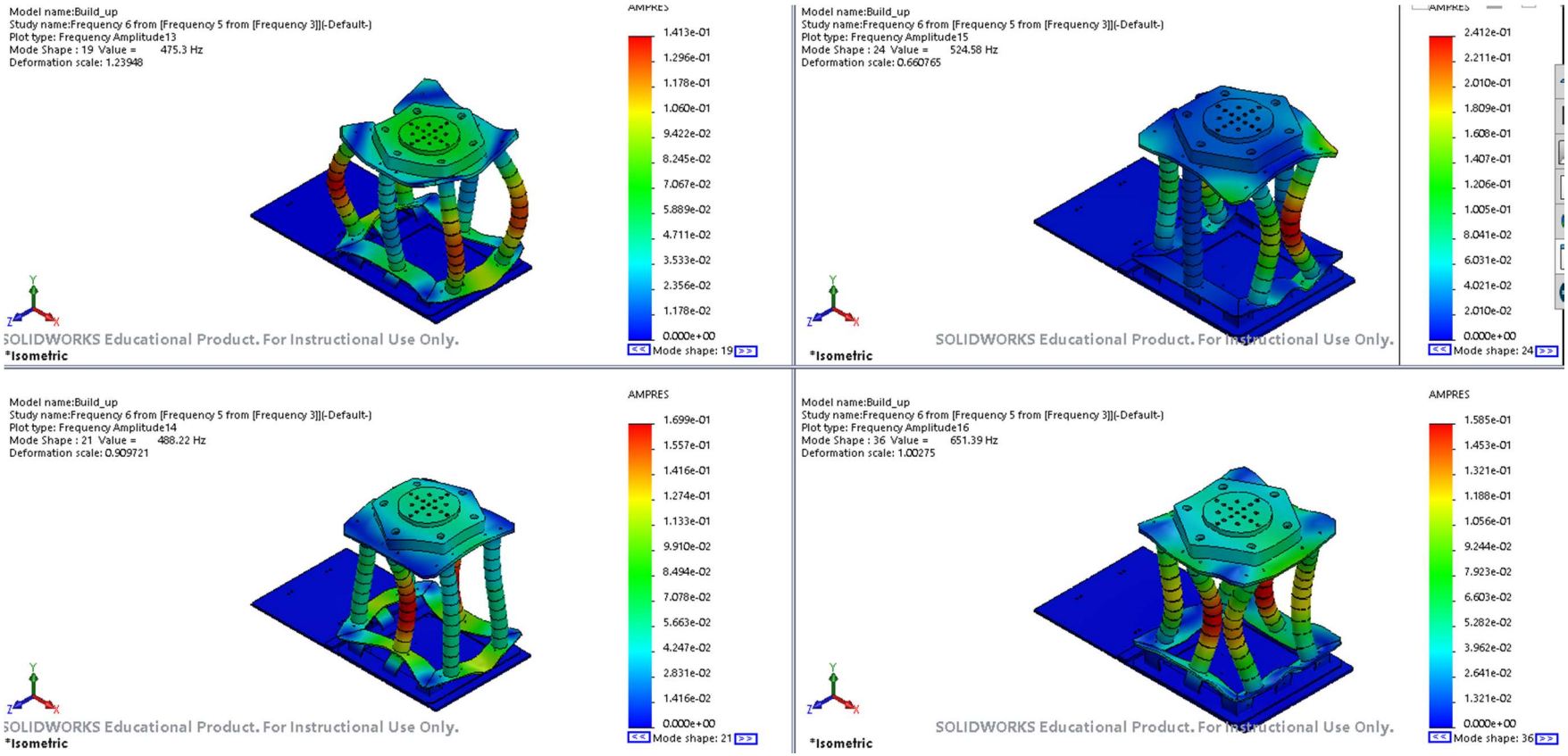

Figure 4-15 Vibration modes of shock machine (table). There were six modes between 475 and 651 Hz. Each of the modes shown above (19,21,24 and 36) have more than 10% effective mass participation

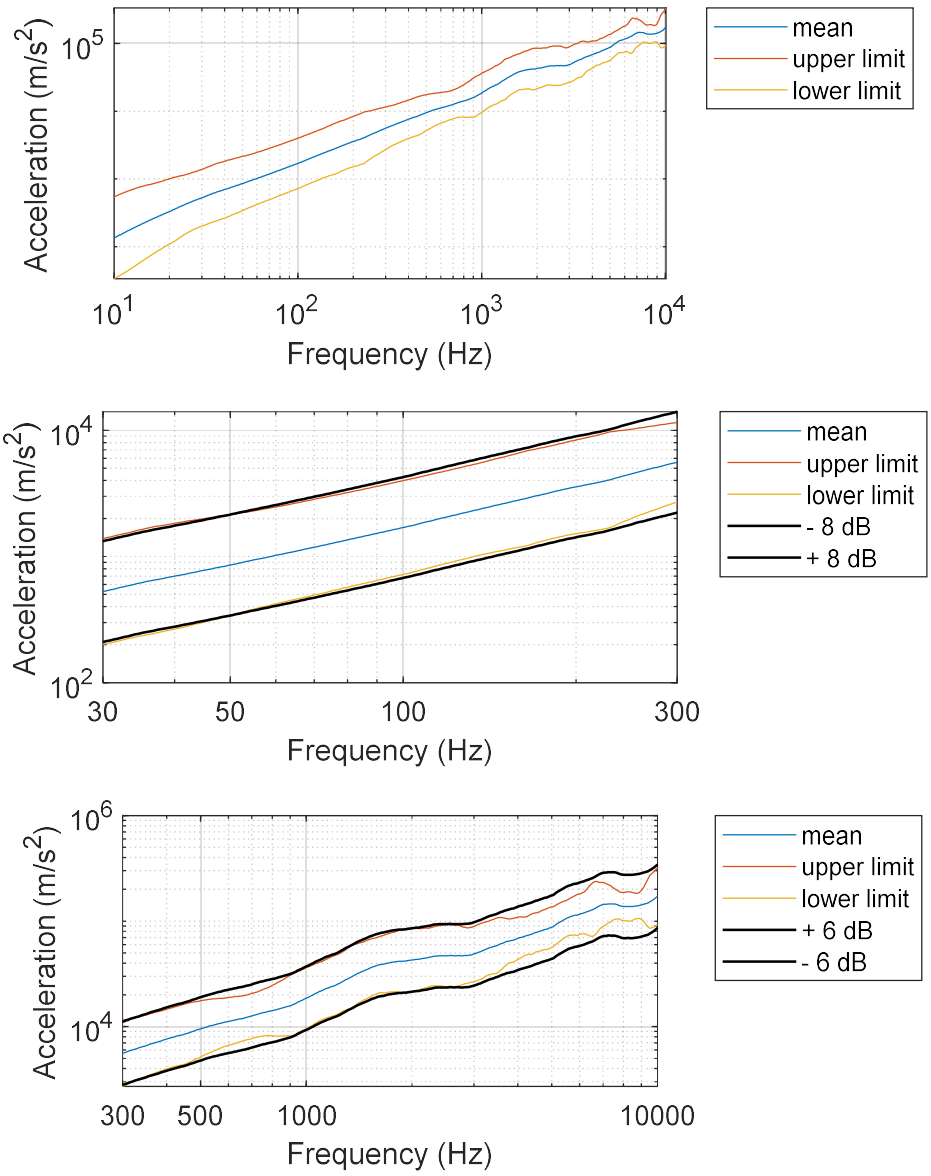

Figure 4-16 SRS variations for successive shocks at 0.15 MPa. Above 300 Hz (bottom plot), the spectrum was well within 6 dB tolerance limits. The middle plot shows that the tolerance limit widens to $\pm$ 8 dB just below 300 Hz.

4.8 Investigating SRS data corruption

Bateman *et al.* [44] identified four sources of data corruption – the accelerometer, inadequate sampling (aliasing), inadequate slew rate of the signal conditioner, and electromagnetic noise. Only piezoelectric accelerometers were available for measurement

during this research. Fortunately, the large input signal conditioner has a built-in 10 kHz low-pass filter (LPF). A method to reduce or prevent aliasing is by using an analog anti-alias filter (AAF) with a sharp roll-off. Another method is to use an AAF with a gradual roll-off while oversampling the data at a sampling rate much higher than twice the highest frequency of interest. This method is the so-called delta-sigma architecture.[61].

An experiment to investigate the effect of the sampling rate showed that the SRS measurements were more repeatable at a higher sampling rate (500 kSa/s) than at 100 kSa/s. Figure 4-17 and Figure 4-18 show the effect of the sampling rate for repeated impacts at 0.07 MPa. Figure 4-17 shows the SRS for five tests sampled at 100 kSa/s. The results show huge variation in the lower frequencies although the SRS results appear to converge above 2,000 Hz. At a sampling speed of 500 kSa/s, the SRS measurements were extremely repeatable in the low frequencies (Figure 4-18). The variation in the SRS above the knee frequency is due to the use of a low-pass filter in some measurements.

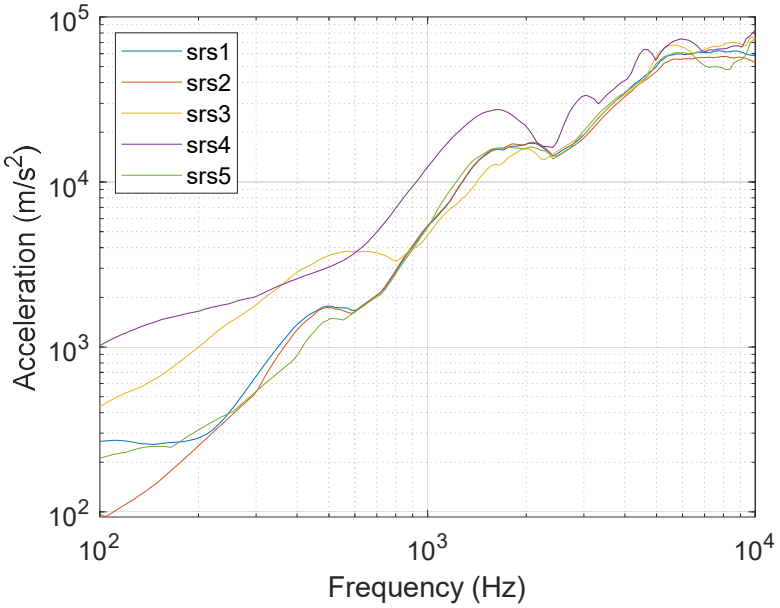

Figure 4-17 Sampling at 100 kSa/s (0.07 MPa, Aluminum projectile) show significant variation below 2,000 Hz although the SRS appear to converge as the frequency approaches 10 kHz.

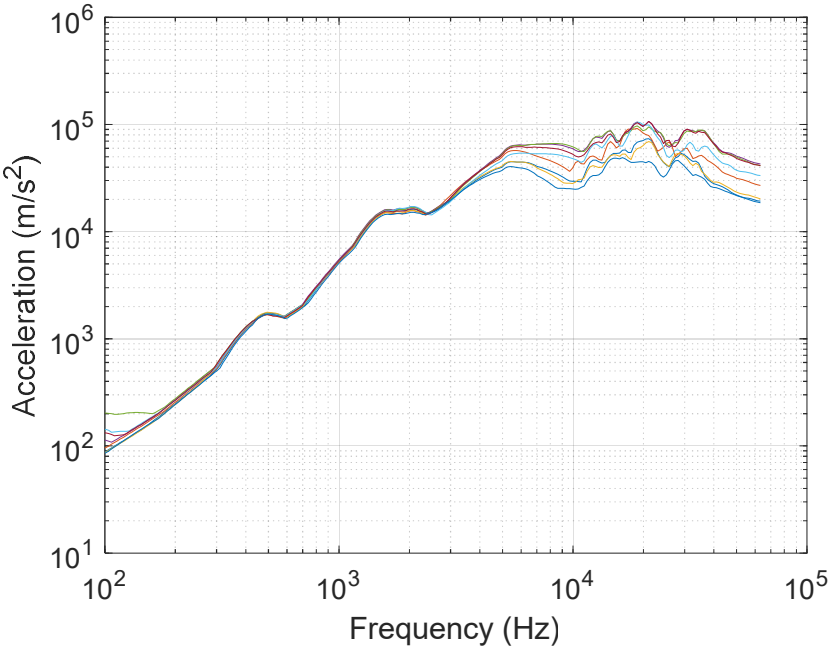

Figure 4-18 Sampling at 500 kSa/s for eight measurements (0.07 MPa, Aluminum Projectile) shows extremely repeatable SRS. The variation in the high frequency region is due to the use of a 10 kHz low-pass filter in some of the measurements.

Figure 4-19 shows the SRS from four successive impacts at 0.05 MPa, using a 2.9 kg aluminum projectile and a 3.5 mm felt material between the impacting surfaces at a maximum sampling rate of 500 kSa/s. The result shows a close tolerance (± 2 dB from 30 Hz to the k_f, 2000 Hz) that widens to ± 4.5 dB above the knee frequency. The wider margin in the upper frequencies is expected. Figure 4-19 suggests that the delta-sigma architecture implemented contributed to reducing the SRS variation, and if this is the case, the nominal data acquisition method may involve the acquisition of corrupted signals that invalidate the SRS acceleration measurements.

Figure 4-20 shows the data validation using a velocity-time history and wideband discrete Fourier transform (DFT). In the work on validation of pyroshock data, Bateman et. al [44] suggested that the velocity time history and the wideband discrete Fourier transform (DFT) can be used to validate acquired pyroshock signal. The velocity-time history of the acquired acceleration signal corrupted by aliasing will show a linear slope, instead of oscillating about the zero velocity. Initially, this behavior was used to describe a signal corrupted by baseline (zero) shift. Figure 4-20 shows that sampling at 500 kSa/s gives a net zero velocity compared to the rising slope of the velocity-time history when sampling at 100 kSa/s.

The wideband DFT shows the effect of the low pass filter [44]. It is recommended for pyroshock data acquisition systems to have at least a 60 dB attenuation (for 12-bit systems) at the Nyquist frequency, and 80 dB or more attenuation for higher resolution systems. The DFT plots (top) in Figure 4-20 show that at the Nyquist frequency, the power attenuation was barely -40 dB when sampling at 100 kSa/s and more than 80 dB when sampling at 500 kSa/s.

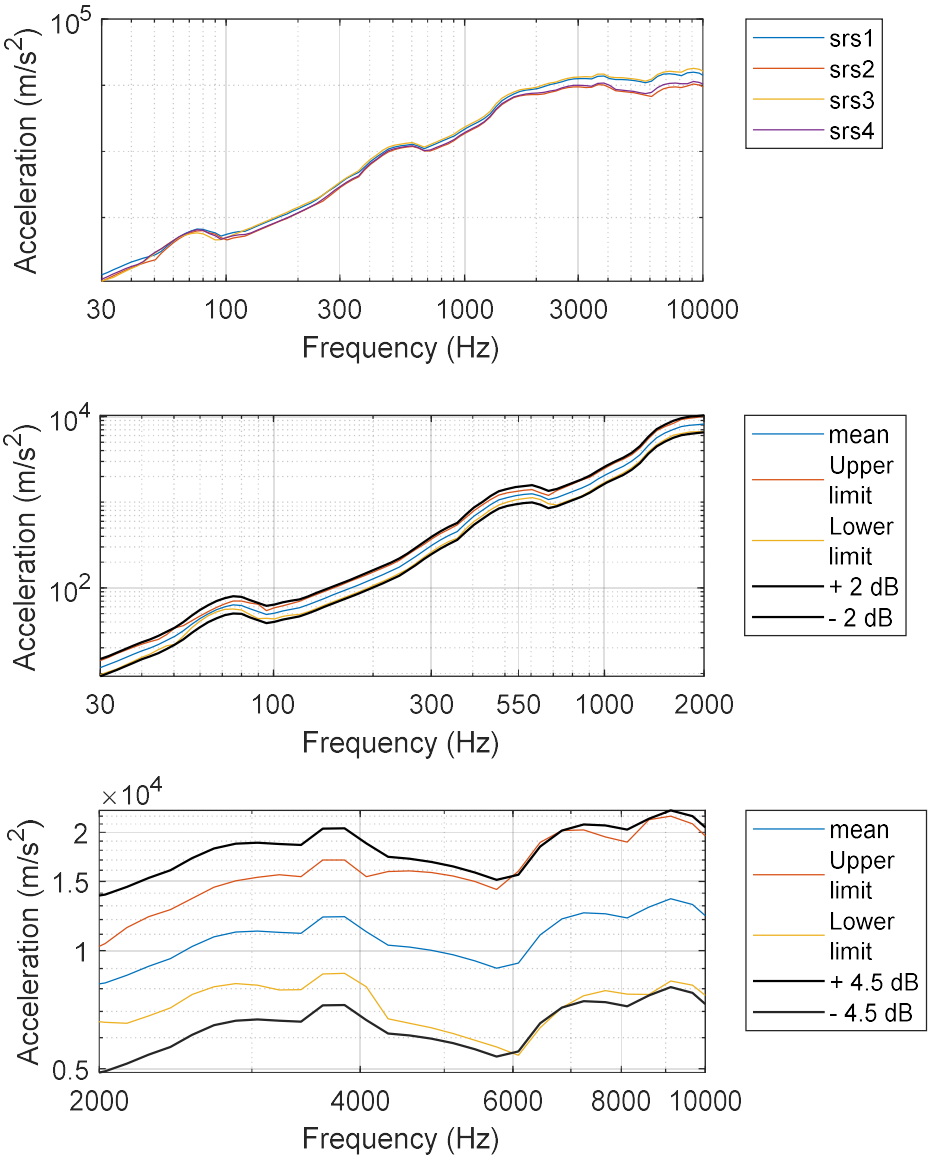

Figure 4-19 Lower and upper tolerance limits for four shocks (0.05 MPa, 3.5mm felt, 2.9 kg Al bullet). The middle plot shows that the variation of the measured data was fully contained within a 2 dB tolerance below 2,000 Hz. The bottom plot shows that the variation increased to 4.5 dB above 2,000 Hz

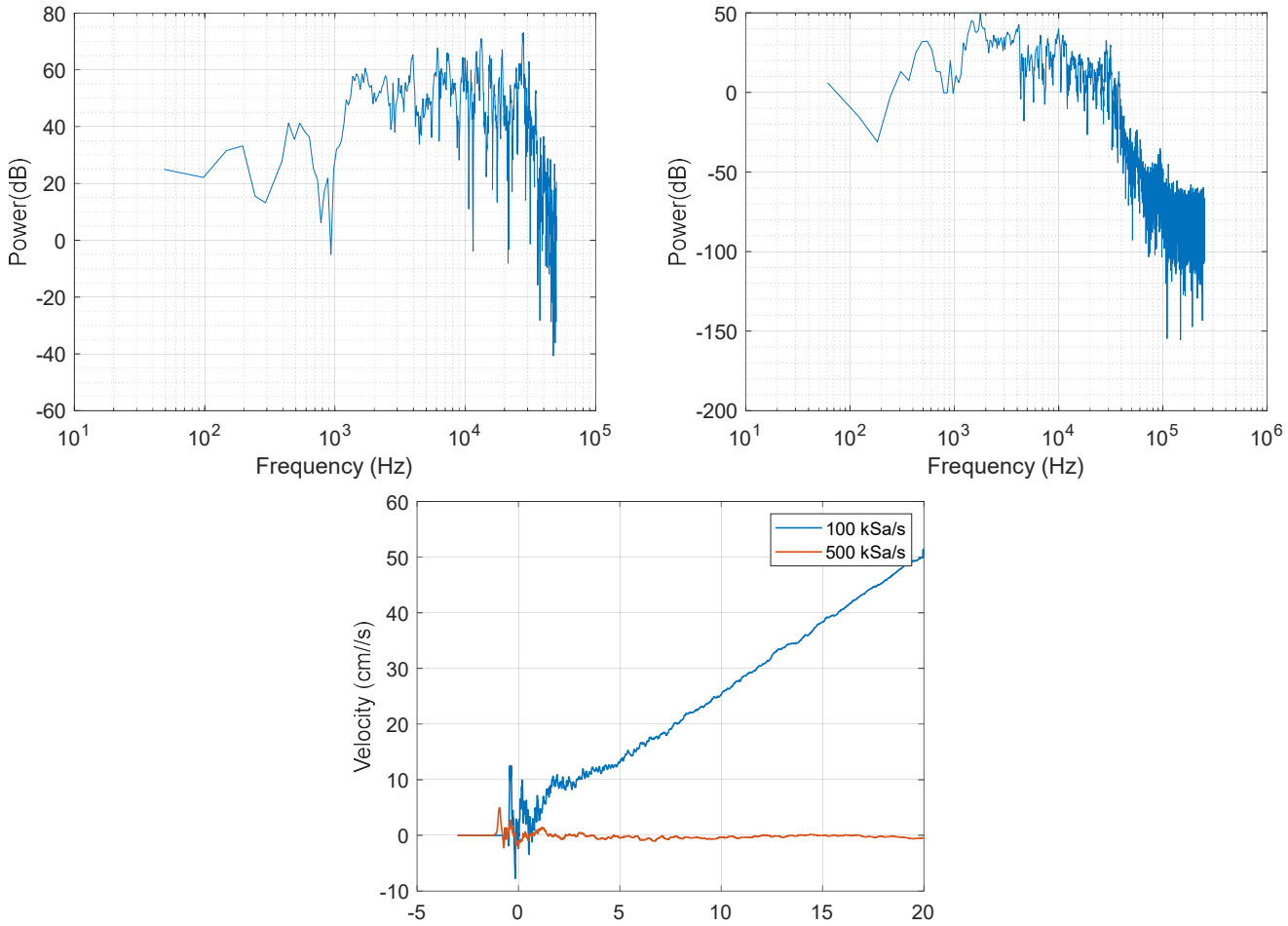

Figure 4-20 Validation of test data with the velocity-time history and the wideband DFT. The top left figure is the wideband DFT when sampling at 100 kSa/s while the top left figure is the DFT for sampling at 500 kSa/s. At the Nyquist frequency, the power should be -80 dB or greater for high resolution systems. The bottom plot shows that when sampling at 500 kSa/s, the velocity-time history has a net zero velocity compared to sampling at 100 kSa/s. In both results, a 10 kHz LPF was used.

4.9 Changing the material (absorber) between impacting surfaces

A material placed between two impacting surfaces (a projectile and a target) can affect the shock response measured on the target. Vigness and Clements [62] showed that placing a well-shaped elastic or plastic material between two impacting surfaces may produce sawtooth or half-sine shock pulses. They also showed that the pulse duration of the sawtooth or half-sine pulse may be controlled by stacking the absorbers . Figure 4-21 shows some of the absorber materials frequently used in shock simulation using the air gun shock machine.

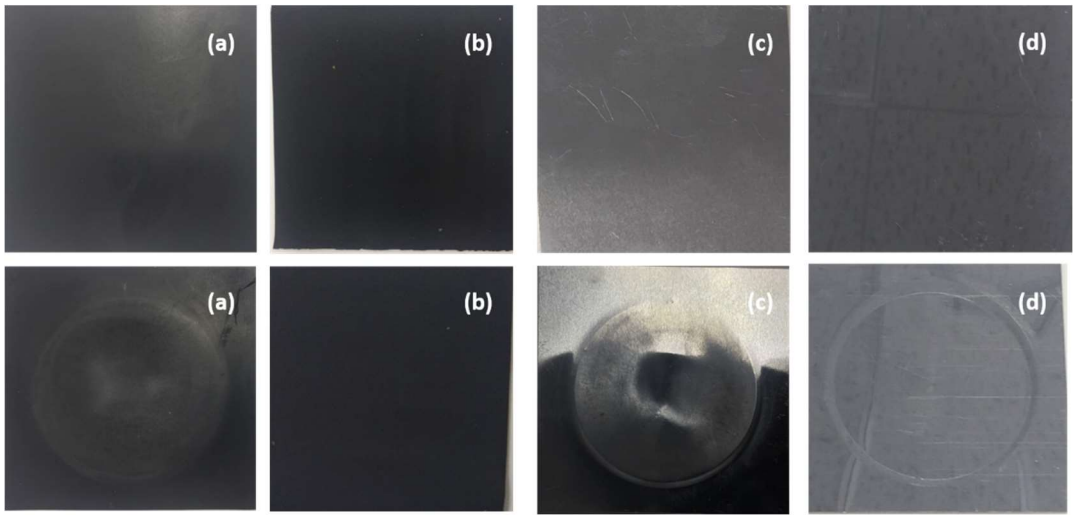

Figure 4-21 Absorbers frequently used in shock simulation (a) Natural rubber (b) Natural rubber type 2 (c) Aluminum (d) Stainless steel. The top figures show the absorber before impact. The bottom figures show the absorbers after impact. The circular pattern is the indentation of the projectile as a result of compression during impact.

Apart from shaping the input shock, elastic and semi-elastic materials (like cork, rubber, and felt) are often used in resilient mounts for vibration isolation [63]. Typically, a shock test may be conducted without using absorbers. However, when absorbers are used (individually or stacked), the goal is to raise or lower the measured SRS. Figure 4-22 shows the effect of using a felt absorber in a test at an driving pressure of 0.05 MPa using a nylon projectile. The SRS amplitude reduces across the spectrum. The SRS

accelerations reduced in magnitude beyond the knee frequency when a 3.5 mm felt material is placed between the impacting surfaces. The amplitude reduction is more pronounced above the knee frequency (2000 Hz).

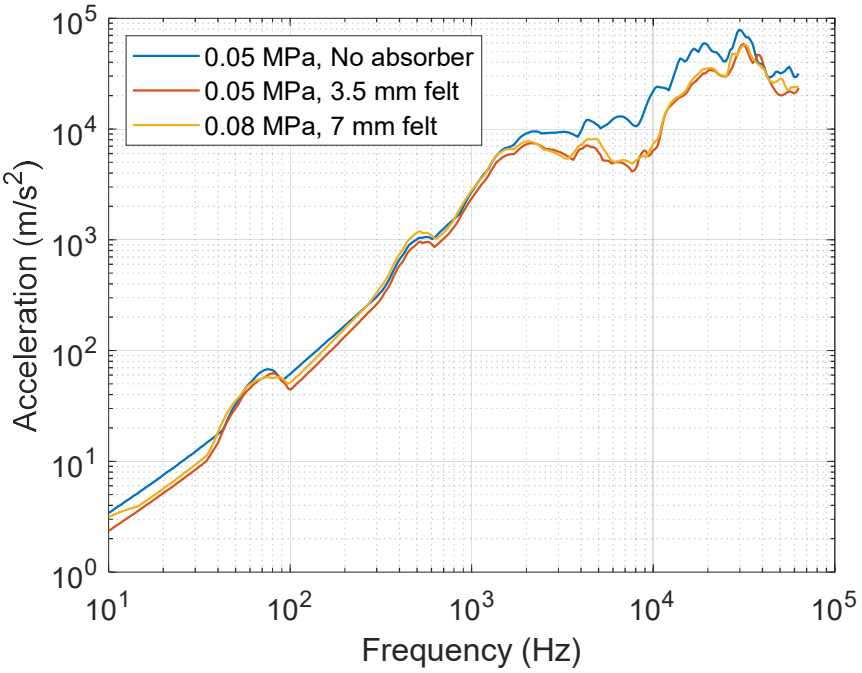

Figure 4-22 Effect of absorber on SRS in an impact with a Nylon (1.3 kg) projectile

The shock amplitude reduction can be explained roughly with the concept of vibration transmissibility. The acceleration transmissibility function (equation 4.1) defines the steady state response of a single-degree-of-freedom system to sinusoidal base excitation.

$$Transmissibility = \sqrt{\frac{1 + \left(2\xi \frac{f}{f_n}\right)^2}{\left(1 - \left(\frac{f}{f_n}\right)^2\right)^2 + \left(2\xi \frac{f}{f_n}\right)^2}} \tag{4.1}$$

Where ξ = damping ratio, f = base excitation frequency, and f_n = natural frequency. Q is the quality factor, and it is defined mathematically as $Q = \frac{1}{2\xi}$. The peak transmissibility

occurs when Q ≥ 2 and the base excitation frequency is equal to the system resonance frequency. Vibration isolation is achieved when $f \gg f_n$.

The knee frequency is the dominant response mode (resonant frequency) in a shock environment. Beyond the knee frequency, the shock amplitude attenuates. The damping loss (1/Q) of a felt material increases with vibration amplitude[63]. At the knee frequency (resonance), the vibration amplitude increases, and so does the damping. The region immediately after the resonant frequency (knee frequency) experiences lower acceleration amplitude because the damping loss of felt increases at resonance.

In Figure 4-22, the higher magnitude of the acceleration response beyond 10 kHz is due to the resonance of the accelerometer's sensing element. The resonance of an accelerometer's sensing element can compromise the measurement's accuracy.[5] An analog low-pass (anti-alias) filter with a sharp roll-off at least once octave below the sensor's resonant frequency can remove the unwanted signal (above 10 kHz) prior to digitization [44]. Figure 4-23 shows the experimental setup to verify the influence of the in-built 10 kHz low pass filter in the signal conditioner described in section 4.5. Figure 4-24 shows the SRS of a 0.05 MPa impact using a 4.1 kg stainless (SUS) projectile on the interface jig in Figure 4-23. First, the shock is measured without a low-pass filter. In a second impact, the signal conditioner's 10kHz low-pass filter (LPF) was used to set the cutoff frequency at 10 kHz, and the sampling rate was 500 kSa/s. It is immediately apparent that the LPF reduced the acceleration magnitude between 10 kHz and 50 kHz.

[5] The usable range of a resonating accelerometer's measurement is 1/3 of the resonant frequency, and conservatively 1/5 of the resonant frequency when using an unisolated PE accelerometer [11].

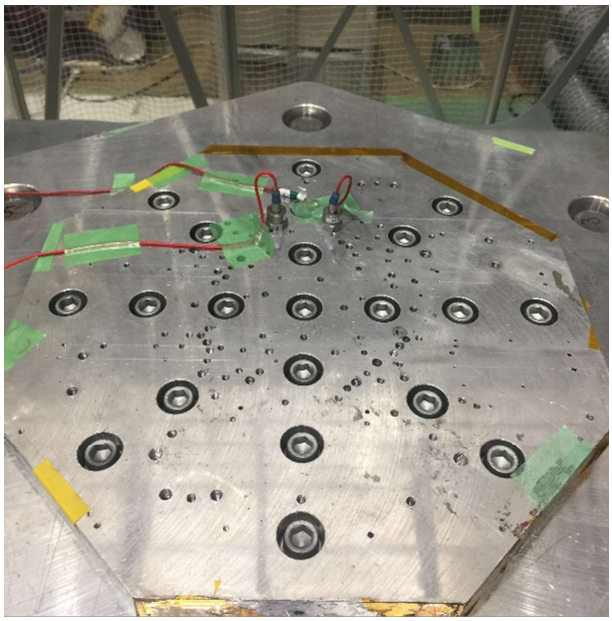

Figure 4-23 Measurement positions on IF Jig C-2

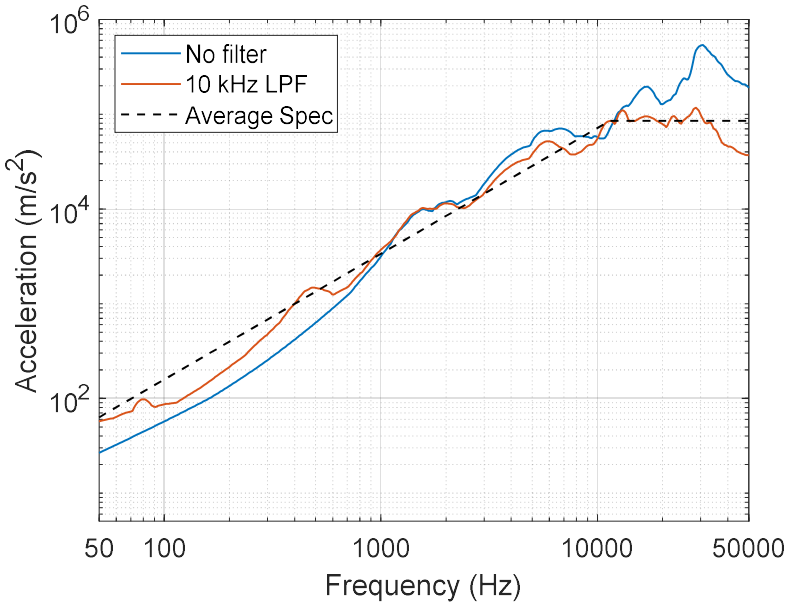

Figure 4-24 Effect of low pass filter on SRS measurement. A 10 kHz low pass filter attenuates the resonance of the accelerometer at 30 kHz.

4.10 Adjusting the knee frequency

Section 4.8 showed the relationship between the driving pressure and a projectile's exit velocity for an air gun. At the same pressure level, two projectiles of different masses will have different exit velocity (Figure 4-6). For example, at 0.05 MPa, the exit velocity for a 4 kg projectile is about 8 m/s and 14.5 m/s for a 1.25 kg projectile. Assuming that the acceleration pulse at impact has a simple saw-tooth profile, the peak acceleration of the of the input pulse is proportional to the impact velocity and inversely proportional to the pulse duration, as shown in equation 4.2 [62].[6]

$$G = \frac{2M_p V_i}{(M_T + M_p) g \tau} \qquad 4.2$$

Where G is the peak acceleration of the input pulse expressed in units of gravity, M_p is the mass of the projectile, V_i is the impact velocity, M_T is the mass of the shock table, g is the acceleration due to gravity, and τ is the pulse duration. The duration in non-penetrating impacts can range from $10^{-2}\ to\ 10^{-6}$ seconds [42]. To excite a natural frequency, the duration of a shock pulse should be at least half the period of the target natural frequency [7]. A soft material impacting a rigid target (such as nylon on steel or aluminum) will have a longer duration than an impact between two aluminum bars. The momentum of the projectile ($M_p V_i$) determines the peak acceleration of the input pulse. The pseudo velocity shock response in Figure 4-25 shows that the peak velocity change occurs at a frequency that corresponds to the knee frequency on the SRS.

Figure 4-25 also shows that varying the projectile's mass (and material) could lower the measured SRS's knee frequency when the SRS measurement is along the impact

[6] Equation 4.2 gives the relationship between the peak acceleration of a shock table under a hammer impact based on the principle of conservation of momentum and holds for very small impacts. At very high impacts, the relationship is non-linear, and the acceleration is greater than can be derived using this equation.

direction. Considering that the usable bandwidth of an unisolated PE accelerometer is 1/5 to 1/3 times the mounted resonant frequency [11], we ignore the SRS above 10 kHz. In Figure 4-25 (a), the two SRS measurements using two different projectiles of different materials have a different knee frequency. The knee frequency corresponds to the frequency with the peak velocity on a pseudo velocity shock response plot as shown in Figure 4-25 (b). An average SRS profile showing a straight acceleration ramp and constant peak acceleration value above the knee frequency can be drawn by curve fitting the linear portion of the ramp and making the acceleration magnitude above the knee frequency equal to the acceleration at the knee frequency Figure 4-25 (c). This peak pseudo velocity value occurs at the same frequency within the data acquisition bandwidth even after filtering out the spectral response above 10 kHz (Figure 4-25 (d)).

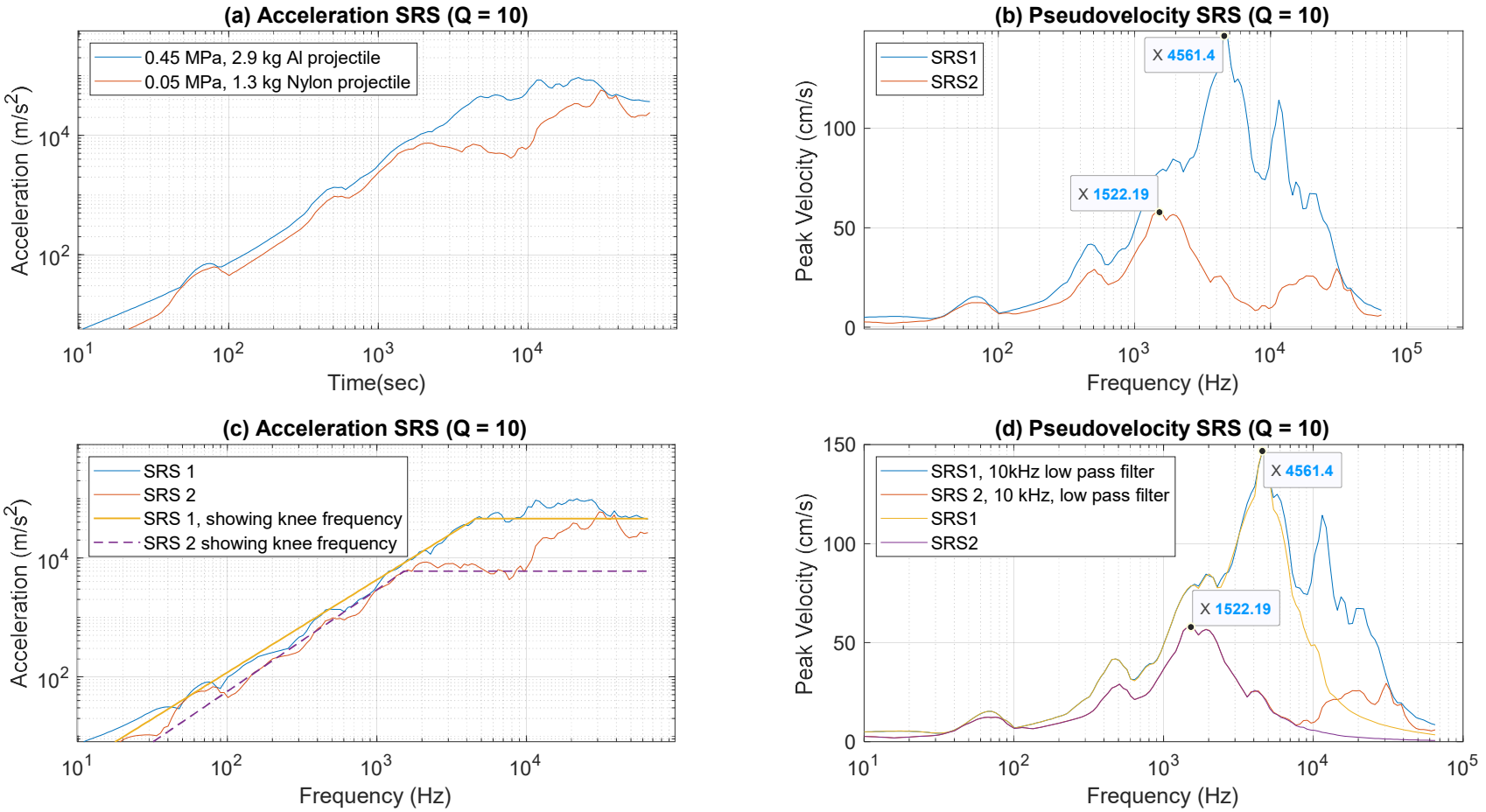

Figure 4-25 Shift in Knee frequency with projectile mass and material using C-3 IF jig (a). The knee frequency was identified as the frequency with the peak pseudo velocity (b). If we ignore the spectral response above 10 kHz, the acceleration magnitude above the knee frequency is approximately constant. The peak pseudo velocity was the same with or without a low pass filter, assuming there is no significant sensor resonance in the bandwidth of interest (d)

5. Retrieving an SRS from a database for Rapid Qualification Testing

The complete set of SRS measurements for a shock test comprises measurements in the X, Y, and Z axes when the shock impact is along the Z-axis. This chapter discusses the result of using the wRMSE to retrieve the most similar SRS to the target SRS for each axis. The purpose of this section is to show the potential time savings possible by using the wRMSE for database SRS retrieval.

When, we split the database into SRS accelerations measured in the X, Y, and Z axes. Three-axis acceleration measurements may be taken using a triaxial accelerometer (that measures the three acceleration components at a single point) or three independent single-axis accelerometers. This section refers to the latter case where three independent single-axis accelerometers are used. If an SRS database comprises 108 shocks (N) and each shock has SRS three measurements corresponding to X, Y, and Z axes (324 channels), the weighted RMSE for each test is the average weighted RMSE over the three axes. Equation 5.1 calculates the average weighted distance for each test in an SRS database with N shocks.

$$\Delta_j = \frac{1}{3}\sum_{i=1}^{3} \Delta_{ji}\,, \quad j = 1,2 \ldots N \tag{5.1}$$

Table 5-1 shows the shock test requirements in a spacecraft qualification test. Using the test specifications as reference, the top three conditions matching the SRS specification were retrieved using the wRMSE (Equation 5.1) and shown in Table 5-2. The SRS corresponding to TN48 (the most similar SRS to the shock specification) is

shown in Figure 5-1. Only the shock absorber was different in the actual test result (determined after 18 trials without using the wRMSE).

Table 5-1 SRS test specification

Frequency (Hz)	SRS spec (m/s^2)	Lower spec limit
100	260.8	130.4
1000	5227.3	2613.7
10000	5227.3	2613.7

Table 5-2 Tuning parameters for retrieved SRS

TN	Pressure (MPa)	Absorber	Thickness (mm)	Projectile
48	0.150	Aluminum	0.3	Aluminum (2.9 kg)
		N. rubber	1	
28	0.090	Aluminum	0.3	Aluminum (2.9 kg)
		Aluminum	0.3	
29	0.100	Aluminum	0.3	Aluminum (2.9 kg)
Actual	**0.150**	**N. rubber**	**1**	**Aluminum (2.9 kg)**

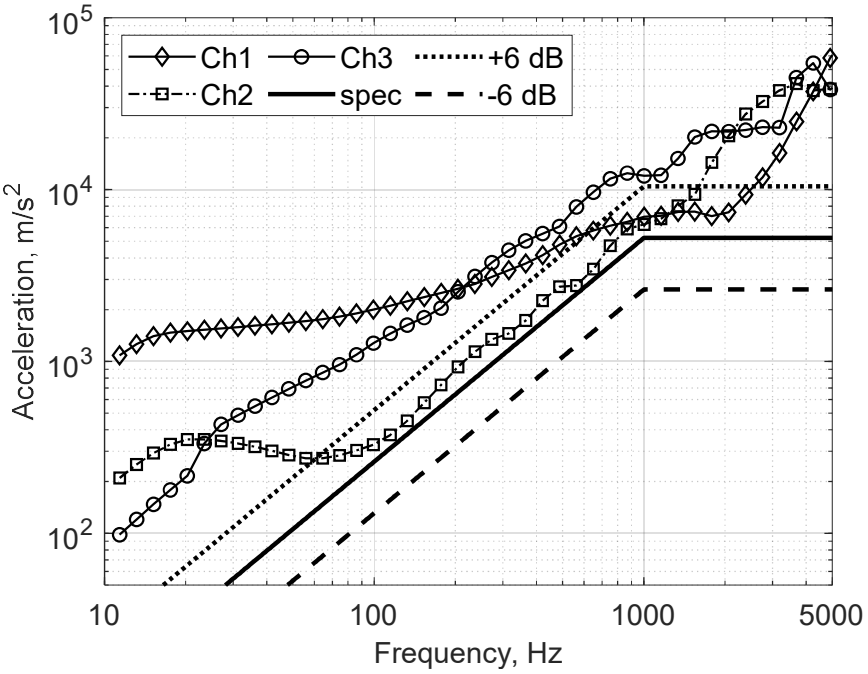

Figure 5-1 Database SRS most similar to the shock specification (TN48)

The tuning conditions retrieved using the wRMSE were used in conducting a shock test for the specifications in Table 5-3. The top two most similar SRS to the specification is the same as in Table 5-2 (TN48 and TN28). Figure 5-2 shows the SRS from a shock test using the retrieved conditions. After testing with the retrieved conditions, the SRS did not satisfy the SRS specifications, especially in Ch2 (lateral axis). The measured SRS in the impact direction just falls below the specification for the top two retrieved conditions. The SRS conditions stored in the database were for tests sampled at 100 kSa/s. As discussed in section 4.7 and 4.8, SRS measurements sampled at 100 kSa/s vary from test-to-test under the same experimental setup by as much as ± 6 to ± 8 dB.

Figure 5-3 shows selected SRS from the results in Figure 4-17 and Figure 4-18. SRS3 (sampled at 100 kSa/s) has a similar profile to SRS 4 -6 sampled at 500 kSa/s. However, SRS1 and SRS2 differ from the rest of the data, especially below 2000 Hz. If the results of SRS1 are stored in a database, for the same set of conditions, the results in SRS4 to 6 are plausible. Therefore, we can conclude that the current database should not be used for SRS retrieval since it is based on data sampled at 100 kSa/s that has wide tolerance limits not suitable for experiments based on similarity.

Moreover, considering that the SRS for TN48 and TN28 are nearly overlapping in Figure 5-2, we can assume that there is an equivalence in the conditions (that is, an impact of 0.15 MPa using a 0.3 mm aluminum plate and 1 mm natural rubber as absorber is equivalent to an impact of 0.09 MPa using two 0.3 mm aluminum plates as absorbers) when the same projectile is used. This equivalence can be used to select alternate absorber and pressure conditions if the regularly used absorber is not in stock.

Table 5-3 Shock test specifications 2

Frequency (Hz)	SRS specifications (m/s^2)	Lower Spec limit
100	250.84	125.42
1000	4954.1	2477.01
4000	4954.1	2477.01

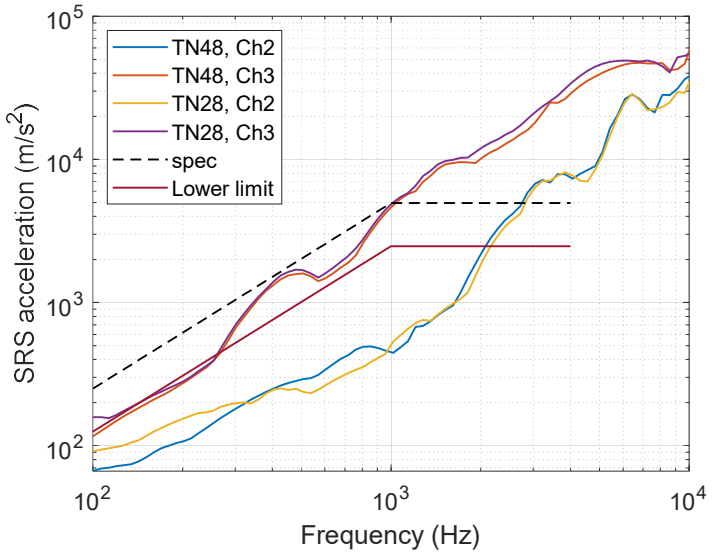

Figure 5-2 Shock test using retrieved conditions (Sampling speed = 500 kSa/s). Ch1 data is not shown because it is corrupted.

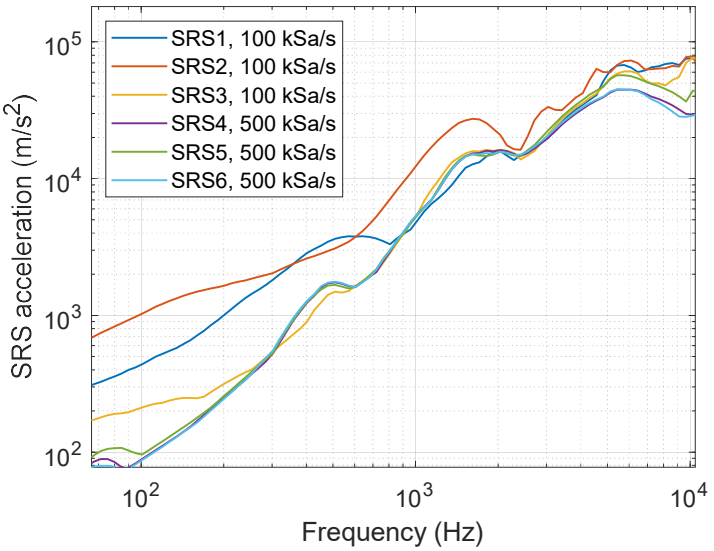

Figure 5-3 SRS at different sampling rates. This figure shows that sometimes when sampling at 100 kSa/s, the SRS may be similar to the SRS when sampling at 500 kSa/s.

The lateral axis (Ch 2 of Figure 5-2) is much lower than the shock test specification. Since the measurement point is on the edge (side) of the interface jig, it is clear that the shock will take more time to propagate compared to the impact direction, and the farther from the shock source, the lower the shock level. The lateral shock will be higher if a jig with a smaller width is used, or if the shock propagation is faster. Changing the projectile to a stainless projectile (mass 4.1 kg) will increase the impact momentum, raise the SRS amplitude, and cause the lateral shock to propagate faster (section 4.10).

Figure 5-4 shows that changing the aluminum projectile (2.9 kg) to stainless steel (4.1 kg) raises the SRS level in the impact direction as well as in the lateral direction compared to the SRS shown in Figure 5-2. Also, after changing the interface jig to another interface jig (from B-1 to C-3, *see section 4.2*) of smaller width and thickness, and raising the driving pressure, the impact direction shock level increased as expected. This result is shown in Figure 5-5. However, the lateral axis shock level did not increase as expected. This could be due to the similarity in clamping conditions for both jigs.

Moreover, there is an uncertainty regarding the actual IF jig used in acquiring the database SRS retrieved as the most similar SRS to the shock test specification. The information regarding the IF jig could not be captured in the database because it is not usually logged during testing. However, the shock response in the impact direction could be predicted reasonably. In all instances, the measured SRS and retrieved SRS both exceed the target SRS, and the deviation increases as the frequency tend to 10,000 Hz.

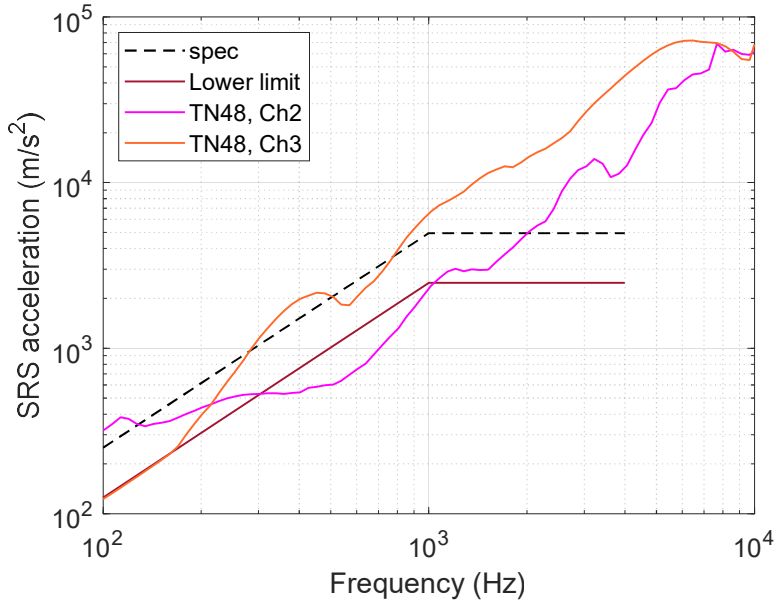

Figure 5-4 Increasing the projectile mass and maintaining other conditions (TN28) raises the SRS level.

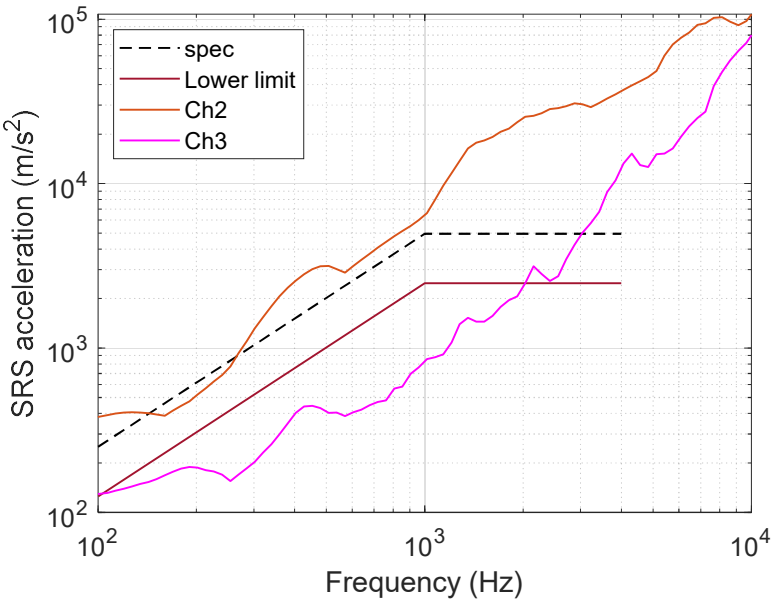

Figure 5-5 Using a smaller interface jig and an aluminum projectile, the impact direction shock is higher, but lower in the lateral axis.

The reason is that in the test configuration, the shock machine simulates a near-field pyroshock. As explained in section 4.10, at the peak velocity of the pseudo velocity response spectrum occurs at the dominant (knee) frequency of the shock environment.

The spectrum response reduces in magnitude only after the knee frequency. Figure 5-6 shows the pseudo velocity response of the Ch2 SRS in Figure 5-4. The peak pseudo velocity occurs at 5400 Hz. In this case, the knee frequency of the shock is above the upper frequency limit of the test specification Table 5-3, meaning that the shock amplitude below the knee frequency will continue to rise. Changing the projectile to a soft projectile (like nylon) may lower the knee frequency, however, the acceleration amplitude below the knee frequency will be lower. It is difficult to raise the acceleration amplitude and lower the knee frequency at the same time.

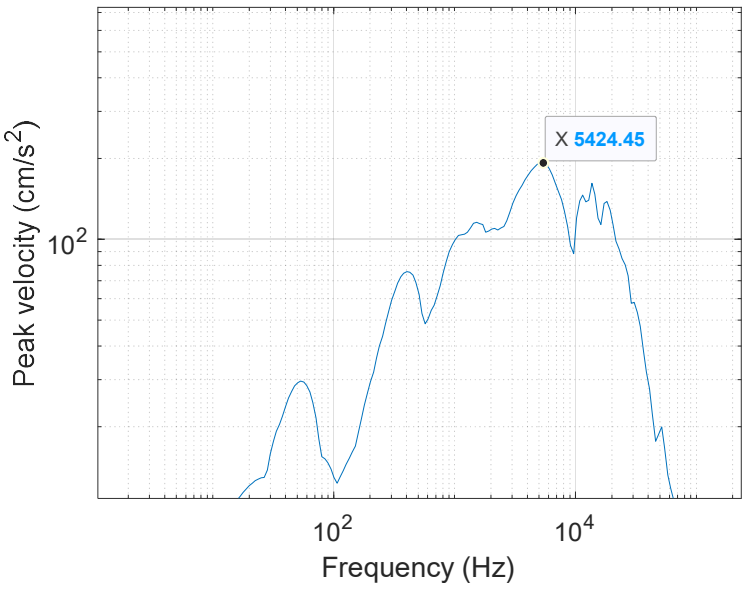

Figure 5-6 Pseudo velocity spectrum showing peak velocity at the knee frequency of Ch2 SRS shown in Figure 5-4.

6. Conclusion and Future Work

This thesis researched on the problem of too many trial-and-errors in the qualification tests of spacecrafts (components) for the mechanical shock environment. The shock tests were done on an air gun shock machine. The shock response spectrum measured on the machine under successive tests were evaluated for repeatability. A novel method to quantify SRS similarity was introduced to facilitate rapid qualification testing by retrieving the experimental conditions for a test from a database of previous test conditions. In the build up to developing the similarity metric, five SRS similarity metrics were evaluated for suitability in retrieving an SRS with a similar profile to a target SRS specification from a shock test database. All evaluated metrics are calculated from the absolute deviation between the SRS magnitudes. The SRS's absolute deviation does not account for the sign of the deviations of the database SRS from the target SRS.

The weighted RMSE proposed as a metric in this work solves the limitation of the RMSE in retrieving a similar SRS to a shock specification from a database. The conditions of the SRS retrieved from the database in one instance matches the final tuning conditions of an actual shock test determined after 18 trials. In an experiment to demonstrate the SRS retrieval using the wRMSE, the SRS measured in a test using the retrieved conditions was below the required shock level. The reason is because the SRS database comprises data acquired with a wide variation in the measured SRS (± 8 dB). When applying the methods learned in the characterization experiments to modify the SRS, the behavior of the measured SRS in the shock impact direction could be predicted easily. However, the lateral shock response did not behave as expected. The difficulty in

predicting the lateral shock response can be attributed to the uncertainty in determining the actual interface jig on which the database SRS was measured. Moreover, the database retrieval method depends highly on the quality of the SRS data in the database. If corrupted data is stored in the database, the quality of future SRS retrievals will be bad. Generally, this method is appropriate for retrieving shocks in the impact direction.

The SRS repeatability analysis revealed that successive SRS measurements under controlled condition varied by as much as 16 dB between the two limits of plausible measurement values (mean ± 8 dB) when resonant frequencies above 1000 Hz are excited. This variation is too wide and impractical for QTs that require only a variation of ± 6 dB from the shock test specification on average. In order to reduce the variations in the measured SRS especially in the lower resonant frequencies (below 500 Hz), the sampling rate of the data acquisition system was increased. Using the maximum sampling speed of the DAQ system reduced the SRS variations two within ± 2 dB. This result suggests the presence of aliased signals in the data acquired due to inadequate sampling. To further reduce aliasing and filter out-of-band resonance noise from the acquired signal, an in-built low pass filter was used to implement a delta-sigma DAQ architecture, as recommended in data acquisition literature. The measured SRS data were subsequently validated using a wideband discrete Fourier transform and the velocity-time history.

The effect of changing various tuning parameters on the measured SRS were also investigated and the following observations were made.

1. A felt absorber is effective for damping out excessive vibration in the high frequencies of the SRS.

2. More consistent and repeatable SRS measurements were obtained at a sampling rate of 500 kSa/s compared to 100 kSa/s while using a felt absorber and a low-pass filter.
3. The knee frequency corresponds to the peak velocity of the pseudo velocity response spectrum.
4. The knee frequency occurred reduced when changing between a more massive projectile (aluminum) to a less massive projectile of different material (nylon).
5. Shock amplitude increased with an increase in the driving pressure. Variation in the measured SRS was most pronounced below 500 Hz.

Trying to simultaneously satisfy the shock test requirements on the lateral axis contributes to the high level of trial-and-error in shock testing. As a future work, the SRS database should be expanded to include data sampled at a minimum sampling rate of 500 kSa/s. Moreover, changing the mounting of the test item so that the impact can be delivered directly to each axis will significantly reduce the number of trials. The reason is because shocks in the impact direction can be predicted with more accuracy. Also, it may be possible in the future to utilize a deep learning framework to extract features for similarity estimation between two or more shock transients. In the current database retrieval scheme, the acceleration time history, SRS, and experimental conditions of past shock tests are always available ahead of time. Deep learning algorithms have been demonstrated for similarity estimation in other fields such as facial recognition and fingerprint matching. Similar techniques may be useful in the future for shock response similarity estimation utilizing unique features such as the slope or knee frequency of the

SRS. A deep learning method could help determine the experimental conditions for a given shock transient if the experimental conditions are unknown or if the record is lost.

REFERENCES

[1] J.R. Wertz, D.F. Everett, J.J. Puschell, eds., Spacecraft Subsystems V - Structures and Thermal, in: Space Mission Engineering: The New SMAD, Microcosm Press, 2011: pp. 674–675.

[2] C. Sisemore, V. Babuška, The Science and Engineering of Mechanical Shock, Springer International Publishing, Cham, 2020. https://doi.org/10.1007/978-3-030-12103-7.

[3] Orbital Launches of 2019 - Gunter's Space Page, (n.d.). https://space.skyrocket.de/doc_chr/lau2019.htm (accessed February 3, 2021).

[4] H-IIA User's Manual, MHI Launch Services, Japan, 2015.

[5] NASA -8056 Flight Separation Mechanisms, National Aeronautics and Space Administration, USA, 1970. https://ntrs.nasa.gov/archive/nasa/casi.ntrs.nasa.gov/19710019510.pdf (accessed April 20, 2020).

[6] First flight for microsatellite separation system by RUAG Space on Electron rocket, Space Newsfeed. (n.d.). https://www.spacenewsfeed.com/index.php/news/3096-first-flight-for-microsatellite-separation-system-by-ruag-space-on-electron-rocket (accessed February 1, 2021).

[7] N.T. Davie, V.I. Bateman, Pyroshock Testing, in: C.M. Harris, A.G. Piersol (Eds.), Harris' Shock and Vibration Handbook, 5th ed, McGraw-Hill, New York, 2002: p. 810.

[8] NASA-STD-7003A: Pyroshock Test Criteria, NASA Washington, DC 20546-0001, 2011. https://standards.nasa.gov/standard/nasa/nasa-std-7003 (accessed March 6, 2020).

[9] J.-R. Lee, J.-K. Jang, M. Choi, C.-W. Kong, Visualization and simulation of a linear explosive-induced pyroshock wave using Q-switched laser and phased array transducers in a space launcher composite structure, Optics & Laser Technology. 67 (2015) 12–19. https://doi.org/10.1016/j.optlastec.2014.09.005.

[10] J.S. Cap, A study of the test-to-test variability in pyroshock data, Sandia National Laboratories, n.d. https://www.osti.gov/servlets/purl/1124362 (accessed June 17, 2020).

[11] A. Chu, Problems in high-shock measurement, 2019. https://endevco.com/contentStore/mktgContent/endevco/dlm_uploads/2019/02/TP308.pdf (accessed January 8, 2021).

[12] R.C. Ferebee, J. Clayton, D. Alldredge, T. Irvine, An Alternative Method of Specifying Shock Test Criteria, (n.d.) 48.

[13] V.I. Bateman, N.T. Davie, Pyroshock Simulation for Satellite Components Using a Tunable Resonant Fixture - Phase 2, 1997. https://www.osti.gov/servlets/purl/469143 (accessed March 3, 2020).

[14] H. Masui, Report of results of environmental testing in CeNT and future strategy for mass producing of Lean satellines, (2018). https://lean-sat.org/nsat/2018_kitakyushu/pdf/day1-8-presentation.pdf (accessed January 21, 2021).

[15] T. Hatamura, Development of a Shock Test Method Suitable for Nano Satellites, Kyushu Institute of Technology, 2015. http://hdl.handle.net/10228/5449 (accessed January 29, 2021).

[16] J.E. Alexander, Shock Response Spectrum – A Primer, Sound and Vibration Magazine. 43 (2009) 9.
[17] I. Vigness, NAVY High-Impact Shock Machines for Lightweight and Mediumweight Equipment, Defense Technical Information Center, Fort Belvoir, VA, 1961. https://doi.org/10.21236/AD0260008.
[18] J. Dwyer, S. Moul, Pyro Shock Simulation: Experience with the MIPS Simulator, in: Support the Highway to Space Through Testing, Williamsburg, VA, 1988: pp. 125–138. https://ntrs.nasa.gov/archive/nasa/casi.ntrs.nasa.gov/19890003222.pdf.
[19] T. Hatamura, H. Masui, M. Cho, K. Maeno, The Simulation about Adjustment Method of Shock Level of Nano Satellites, Journal of the Japan Society for Aeronautical and Space Sciences. 63 (2015) 117–119. https://doi.org/10.2322/jjsass.63.117.
[20] V.I. Bateman, The Latest in Pyroshock Testing Techniques, (2020). https://www.iest.org/Standards-RPs/Recommended-Practices/Pyroshock-Testing-Techniques (accessed January 27, 2020).
[21] Falcon User's Guide, SpaceX, 2020. https://www.spacex.com/media/falcon_users_guide_042020.pdf (accessed February 4, 2021).
[22] LM - 3A Series Launch Vehicle User's Manual, China Aerospace Science and Technology Corporation, China, 2011. http://www.cgwic.com/launchservices/download/manual/LM-3A%20Series%20Launch%20Vehicles%20User's%20Manual%20Issue%202011.pdf (accessed February 4, 2021).
[23] R. Lagier, Soyuz CSG User's Manual, Arianespace, 2018. https://www.arianespace.com/wp-content/uploads/2015/10/Soyuz-UsersManuel-issue2-Revision1-May18.pdf (accessed February 4, 2021).
[24] Launch: Payload User's Guide, Rocket Lab, USA, 2020.
[25] Proton Launch System Mission Planner's Guide, International Launch Services (ILS), 2009. https://mk0ilslaunchupbj5chy.kinstacdn.com/wp-content/uploads/pdf/PMPG%20Section%203.pdf (accessed February 4, 2021).
[26] KZ-1A Solid Launch Vehicle User's <amia;, ExPace, Wuhan, China, 2016. https://forum.nasaspaceflight.com/index.php?action=dlattach;topic=23525.0;attach=1397368.
[27] Epsilon Launch Vehicle User's Manual, Japan Aerospace Exploration Agency (JAXA), Japan, 2018.
[28] 2003336 Advanced Lightband User's Manual, Planetary Systems Corporation, 2019.
[29] J.M. Newell, Mechanical Impulse Pyro Shock (MIPS) Simulation, in: Boston, MA, United States, 1999. https://trs.jpl.nasa.gov/bitstream/handle/2014/18340/991815.pdf?sequence=1 (accessed March 25, 2019).
[30] M. Jonsson, Development of a Shock Test Facility for Qualification of Space Equipment, Master's Thesis, Chalmers University of Technology, 2012. publications.lib.chalmers.se/records/fulltext/167112.pdf (accessed June 19, 2020).
[31] E. Filippi, H. Attouoman, Pyroshock Simulation Using The Alcatel Etca Test Facility, in: Launch Vehicle Vibrations, Toulouse, 1999.

[32] J. Markl, ANALYSIS OF A CIRCULAR RESONANT PLATE FOR SHOCK TESTING, Master of Science in Mechanical Engineering, Michigan Technological University, 2020. https://doi.org/10.37099/mtu.dc.etdr/1083.
[33] Y. Narita, Free Vibration of Elastic Plates with Various Shapes and Boundary Conditions, Doctoral Dissertation, Hokkaido University, 1979.
[34] C. Sisemore, M. Spletzer, Design of a Resonant Plate Shock Fixture to Attenuate Excessive High-Frequency Energy Inputs, in: Shock and Vibration Exchange, Jacksonville, Florida, n.d.: p. 14. https://www.osti.gov/servlets/purl/1455321.
[35] S.-J. Lee, D.-H. Hwang, J.-H. Han, Development of Pyroshock Simulator for Shock Propagation Test, Shock and Vibration. 2018 (2018) 1–13. https://doi.org/10.1155/2018/9753793.
[36] I.O. Adebolu, H. Masui, I. Inoue, M. Cho, Improving the tuning efficiency of an air pressure based shock machine, in: Fly like a Phoenix to Space: 32nd International Symposium on Space Technology and Science, Fukui, Japan, 2019: p. 6. https://archive.ists.or.jp/upload_pdf/2019-c-24.pdf.
[37] A. García-Pérez, F. Sorribes-Palmer, G. Alonso, A. Ravanbakhsh, FEM simulation of space instruments subjected to shock tests by mechanical impact, International Journal of Impact Engineering. 126 (2019) 11–26. https://doi.org/10.1016/j.ijimpeng.2018.12.008.
[38] E. Bodin, B. Brévart, P. Wagstaff, G. Borello, Pyrotechnic shock response predictions combining statistical energy analysis and local random phase reconstruction, The Journal of the Acoustical Society of America. 112 (2002) 156–163. https://doi.org/10.1121/1.1446050.
[39] H. Zhao, W. Liu, J. Ding, Y. Sun, X. Li, Y. Liu, Numerical study on separation shock characteristics of pyrotechnic separation nuts, Acta Astronautica. 151 (2018) 893–903. https://doi.org/10.1016/j.actaastro.2018.07.040.
[40] J. Ding, H. Zhao, J. Wang, Y. Sun, Z. Chen, Numerical and experimental investigation on the shock mitigation of satellite-rocket separation, Aerospace Science and Technology. 96 (2020) 105538. https://doi.org/10.1016/j.ast.2019.105538.
[41] T. Iwasa, Q. Shi, Simplified Estimating Method for Shock Response Spectrum Envelope of V-Band Clamp Separation Shock, Journal of Space Engineering. 1 (2008) 46–57.
[42] J.A. Zukas, ed., Introduction to Hydrocodes, 1st ed., Elsevier, 2004.
[43] J. Wen, C. Liu, H. Yao, B. Wu, A nonlinear dynamic model and parameters identification method for predicting the shock pulse of rubber waveform generator, International Journal of Impact Engineering. 120 (2018) 1–15. https://doi.org/10.1016/j.ijimpeng.2018.05.009.
[44] V. Bateman, R. Merritt, Validation of Pyroshock Data, Journal of the IEST. 55 (2012) 40–56. https://doi.org/10.17764/jiet.55.1.2q4650xqt7j0k506.
[45] A. Chu, A shock amplifier evaluation, 1989. https://endevco.com/contentStore/mktgContent/endevco/dlm_uploads/2019/02/TP293.pdf.
[46] A. Maskey, Convolutional Neural Network Designed for On-orbit Binary Image Classification on a 1U Cubesat, PhD Disssertation, Kyushu Institute of Technology, 2020.

[47] 7 Types of Activation Functions in Neural Networks: How to Choose?, MissingLink.Ai. (n.d.). https://missinglink.ai/guides/neural-network-concepts/7-types-neural-network-activation-functions-right/ (accessed March 14, 2021).
[48] D.O. Smallwood, Characterization and Simulation of Transient Vibrations Using Band Limited Temporal Moments, Shock and Vibration. 1 (1994) 507–527. https://doi.org/10.1155/1994/940635.
[49] P. Perner, Case-Based Reasoning and the Statistical Challenges II, in: Dr.A. Gruca, T. Czachórski, S. Kozielski (Eds.), Man-Machine Interactions 3, Springer International Publishing, Cham, 2014: pp. 17–38. https://doi.org/10.1007/978-3-319-02309-0_2.
[50] E. Hullermeier, Similarity and Case-Based Inference, in: Case-Based Approximate Reasoning, Springer, Dordrecht, Netherlands, 2007: pp. 17–53.
[51] J.L. Kolodner, An introduction to case-based reasoning, (n.d.) 32.
[52] H.-S. Park, D.-H. Hwang, J.-H. Han, J. Yang, Development of shock-absorbing insert for honeycomb sandwich panel, Aerospace Science and Technology. 104 (2020) 105930. https://doi.org/10.1016/j.ast.2020.105930.
[53] Y. Yan, Q.M. Li, A general shock waveform and characterization method, Mechanical Systems and Signal Processing. 136 (2020) 106508. https://doi.org/10.1016/j.ymssp.2019.106508.
[54] J. Lee, D.-H. Hwang, J.-H. Han, Study on pyroshock propagation through plates with joints and washers, Aerospace Science and Technology. 79 (2018) 441–458. https://doi.org/10.1016/j.ast.2018.05.057.
[55] X. Wang, Z. Qin, J. Ding, F. Chu, Finite element modeling and pyroshock response analysis of separation nuts, Aerospace Science and Technology. 68 (2017) 380–390. https://doi.org/10.1016/j.ast.2017.05.028.
[56] X. Wang, T. Yu, H. Yan, J. Ding, Z. Li, Z. Qin, F. Chu, Application of stress wave theory for pyroshock isolation at the spacecraft-rocket interface, Chinese Journal of Aeronautics. (2020) S100093612030128X. https://doi.org/10.1016/j.cja.2020.04.005.
[57] MIL-STD-810H: Environmental Engineering Considerations and Laboratory Tests, DoD, 2019.
[58] ISO-19683:2017 Space systems — Design qualification and acceptance tests of small spacecraft and units, (2017).
[59] Q. Shi, A. Shigemasa, JAXA-RR-04-020: Removing the Zero shift of Pyroshock Measurement Data by Wavelet Technique and its Verification, Japan Aerospace Exploration Agency (JAXA), Japan, 2005. https://repository.exst.jaxa.jp/dspace/bitstream/a-is/50174/1/48059000.pdf.
[60] H.J. Davis, Impact Testing Using A Four-Inch Air Gun and Lead Targets, Washington DC, 1968. https://https://apps.dtic.mil/dtic/tr/fulltext/u2/671616.pdf.
[61] M.A. Underwood, Application of Digital Computers, in: Harris' Shock and Vibration Handbook, 5th ed., McGraw-Hill, n.d.: pp. 832–834.
[62] I. Vigness, E.W. Clements, Sawtooth and Half-Sine Shock Impulses from The Navy Shock Machine for Mediumweight Equipment, Naval Research Laboratory, 1963.
[63] J.I. Dunlop, Felt pad vibration properties and design criteria, The Journal of the Acoustical Society of America. 91 (1992) 2696–2702. https://doi.org/10.1121/1.402977.

[64] A.G. Piersol, Procedures to Compute Maximum Structural Responses from Predictions or Measurements at Selected Points, Shock and Vibration. 3 (1996) 211–221. https://doi.org/10.1155/1996/907854.

7. Appendices

7.1 Statistical SRS limits

SRS estimates at a single location on a test article (or interface jig) obtained from repeated testing under identical experimental conditions have an unknown probabilistic structure [57,64]. We can establish statistical lower and upper SRS limits if we assume SRS similarity and insignificant individual SRS error. Moreover, the individual estimates in the given measurements must be uncorrelated to the independent variable. We follow Piersol's recommendation [64] establish statistical limits for $\boldsymbol{n}$ estimates covering $\boldsymbol{m}$ natural frequencies:

i. Logarithmic transformation of each SRS estimate;

ii. Normality (Chi-square) test to see if the estimates fit a Normal (log-normal) distribution. The SRS acceleration values corresponding to a given natural frequency form a set of estimates;

iii. Calculating the mean ($\boldsymbol{\bar{y}_j}$) and standard deviation ($\boldsymbol{s_{y_j}}$) for each set of estimates;

iv. Calculating the Normal Tolerance Limit, $\boldsymbol{NTL_y(n,\beta,\gamma)}$, using equations (7-1). $\boldsymbol{NTL_y(n,\beta,\gamma)}$ is the value of y that will exceed at least the β portion of all possible values of y_j with a confidence coefficient of γ. $k_{(n,\beta,\gamma)}$ is the normal tolerance factor

v. Use equation (7-2) to transform the Normal Tolerance Limit back to its original engineering units.

$$NTL_y(n,\beta,\gamma) = \bar{y}_j + k_{(n,\beta,\gamma)} s_{y_j} \qquad j = 1.2, \ldots, m \tag{7-1}$$

$$NTL_x(n,\beta,\gamma) = 10^{NTL_y(n,\beta,\gamma)} \tag{7-2}$$

7.2 Normal Tolerance Factor for different confidence intervals

N	γ = 0.50			γ = 0.90			γ = 0.95		
	β = 0.90	β = 0.95	β = 0.99	β = 0.90	β = 0.95	β = 0.99	β = 0.90	β = 0.95	β = 0.99
3	1.50	1.94	2.76	4.26	5.31	7.34	6.16	7.66	10.55
4	1.42	1.83	2.60	3.19	3.96	5.44	4.16	5.14	7.04
5	1.38	1.78	2.53	2.74	3.40	4.67	3.41	4.20	5.74
6	1.36	1.75	2.48	2.49	3.09	4.24	3.01	3.71	5.06
7	1.35	1.73	2.46	2.33	2.89	3.97	2.76	3.40	4.64
8	1.34	1.72	2.44	2.22	2.75	3.78	2.58	3.19	4.35
9	1.33	1.71	2.42	2.13	2.65	3.64	2.45	3.03	4.14
10	1.32	1.70	2.41	2.07	2.57	3.53	2.35	2.91	3.98
11	1.32	1.70	2.40	2.01	2.50	3.44	2.28	2.82	3.85
12	1.32	1.69	2.39	1.97	2.45	3.37	2.21	2.74	3.75
13	1.31	1.69	2.39	1.93	2.40	3.31	2.16	2.67	3.66
14	1.31	1.68	2.38	1.90	2.36	3.26	2.11	2.61	3.58
15	1.31	1.68	2.38	1.87	2.33	3.21	2.07	2.57	3.52
16	1.31	1.68	2.38	1.84	2.30	3.17	2.03	2.52	3.46
17	1.31	1.68	2.37	1.82	2.27	3.14	2.00	2.49	3.41
18	1.30	1.67	2.37	1.80	2.25	3.11	1.97	2.45	3.37
19	1.30	1.67	2.37	1.78	2.23	3.08	1.95	2.42	3.33
20	1.30	1.67	2.37	1.77	2.21	3.05	1.93	2.40	3.30

7.3 Comparison of different SRS retrieval methods (octave spacing = 1/12)

SRS no	Data above Spec (%)	MAD (%)	ASR	E_R	M_R	RMSE(dB)	Δ_j
3	100	159.7	2.6	2.7	6.4	8.3	0.093
5	91	83.0	2.7	2.3	3.8	5.8	0.088
8	68	50.0	1.8	1.7	3.3	4.1	0.103
1	51	40.3	1.7	1.5	3.7	3.6	0.120
6	33	45.6	1.5	1.3	4.1	5.0	0.201
4	32	52.9	1.7	1.5	4.5	4.7	0.195
7	6	66.6	0.6	0.5	1.5	11.6	0.615
2	0	55.6	0.5	0.5	0.9	7.4	0.411

7.4 Code: Retrieving similar SRS from an SRS database

```
%%% RMSE ALGORITHM DECEMBER 1 2019
%%% COMPILED BY IBUKUN O. ADEBOLU

%%% This program computes the weighted RMSE between a target SRS and
%%% database SRS. The computation is in the logarithmic space, to scale
the
%%% distance between the SRS below and under the target as a metric for
%%% selecting most similar data from the database.
```

INPUT THE TARGET SRS FREQUENCY AND ACCELERATION VALUES

```
clc
% clearvars
close all

out1 = sprintf('Input the number of breakpoints (>2) target SRS');
disp (out1)
n = 0;
while (n<2)
    %input number of frequency and acceleration combinations
    n = input (' ');
    if (n<=2)
        n=3;
    end
end

f=zeros(n,1);
a=zeros(n,1);
for i  = 1:n
    out2 = sprintf(' input frequency(Hz) %d:' ,i );
    disp(out2)
    f(i) = input (' ');
    out3 = sprintf(' input acceleration(m/s^2) %d: ',i );
    disp (out3)
    a(i) = input (' ');
end
%calculate the slope(s) of the input SRS
num = size(f);
freq = f;
r= a;
```

```
for j = 1:num-1
    x = log10(f(j+1))-log10(f(j));
    y = log10(a(j+1))- log10(a(j));
    s(j)= y/x;
end
tic
```

EXTRAPOLATE THE DATA TO AN INDICATED LOWER FREQUENCY,

RECOMMEND 10 HZ

```
out4 = sprintf('Do you want to extrapolate to a lower frequency?');
disp(out4)
disp('1. Yes 2. No');
```

```
1. Yes 2. No
```

```
fmore = input(' ');
if (fmore ==1)
    out5 = sprintf('input the lowest frequency');
    disp(out5)
    f(4) = input(' ');
    %% calculate a(4) for f(4) and re-sort the data in ascending order
    % recall the formula for slope
    ja = log10(f(2))-log10(f(4))
    p = log10(a(2))-(s(1)*ja)
    a(4) = 10.^p;
    a= sort(a);
    f = sort (f);
else
end
if (f(end) <=10000)
    f(end) = 10000;
else
    f(end)= f(end);
end
a(2)= [];
f(2)=[];
n = length(f);

srs = [f,a];
%% recalculate slope?
for j = 1:n-1
    x = log10(f(j+1))-log10(f(j));
    y = log10(a(j+1))- log10(a(j));
    s(j)= y/x;
end
```

```
 %% create same number of points (480) as recorded SRS as the input SRS
using the slope equation from Taylor’s series.
 %% oct = octave spacing, spec = acceleration

 fb = f(1);
 spec(1) = a(1);
 % oct = 1.01455;
 oct = 2^(1/48);
 ff(1) = f(1);
 fr= f;
 i = 2;
 num = length(fr);

 clear f
 clear spec
 f(1) = fr(1);
 while (1)
     ff = oct * fb;
     fb = ff;
     if (ff> fr(num))
         break;
     end
     if ( ff >= fr(1))
         for j = 1: num

             if (ff == fr(j))
                 f(i) = ff;
                 spec (i) = r(j);
                 nspec =i;
                 i = i+1;
                 break;
             end

             if (ff < fr(j) && j>1)
                 f(1) = fr(1);
                 spec(1)= a(1);
                 f(i) = ff;
                 az = log10(a(j-1));
                 az = az +(s(j-1)*(log10(ff)-log10(fr(j-1))));
                 spec (i) = 10.^az;
                 nspec = i;

                 while (f(i)<freq(1))
                     k1 = i;
                     break
                     if (f(k1)< freq(1))
```

```
                        k1 = k1+1;
                    end
                end
                while (f(i)<freq(3))
                    k3 = i;
                    break
                    if (f(k3)< freq(3))
                        k3 = k3+1;
                    end
                end
                while (f(i)<1000)
                    k1k = i;
                    break
                    if (f(k1k)< 1000)
                        k1k = k1k+1;
                    end
                end

                while (f(i)<fr(2))
                    kn = i;
                    break
                    if (f(kn)< fr(2))
                        kn = kn+1;
                    end
                end
                i = i+1;
                break
            end
        end
    end
end

if (f(nspec) < fr(end))
    nspec = nspec +1;
    f(nspec)= fr(end);
    spec(nspec)=a(end);
end
srss = [f;spec]';
```

LOAD THE DATABASE (FOR EXAMPLE ACC)

```
sspec = spec';
load 'ACCLSMLPR2.mat'
% ACC = ACCLPRLSMTune1{:,:};
```

```
 % load 'one12.mat'                %axel.mat is reduced database having
10 elements
 % load 'ACCLSMLPRZ.mat'

 ACC = ACCLSMLPR{:,:};
 % ACC = ex;

 % clear ACC
 % ACC = one12;

 [h,q]=size(ACC);
 ACCe = ACC;
 ACCe(:,1)=[];
 err1 = zeros(h,q-1);

 err2 = zeros(kn,q-1);
 %
```

APPLY WEIGHTS, W_I TO ALL FREQUENCIES AND CALCULATE THE WEIGHTED RMSE FOR ALL DATA

```
 % Weights for frequencies from 10 Hz to original test f1, c
 % Weights for frequencies from f1 to kf (f2), g
 % Weights for frequencies from kf to (Kf+3000), e
 % Weights for frequencies from (Kf+3000) to f2,



 w = zeros(length(f),1);
 fw = freq(2) + 3000; % originally plus 1000
 % up to the knee frequency, the weight = 1 and decreases afterwards to
 % minimize the big deviations of the upper frequencies.
 % find all freq less than first frequency of srs(g),
 % find all extrapolated spectrum(c), then find all f greater than set
threshold
 % fw as (e)
 g = find (f(freq(1)>=f));
 c = find (f(fr(2)>=f));
 e = find (f>fw);
 % Double alphabeth correspond to index positions in the
 % range g c and e

 cc = c(end);
 ee = e(1);
```

```
 for d = 1:g(end) % from 10 Hz to f1
     w(d) = 1;

     %                      w(d) = 0.05;     default for w(d) = 5
 end


 for d = (g(end)+1:cc+1) % from f1(100 Hz) to 1 index before knee
frequency, f(2)
     w(d) = 1;
 end


 for (d = cc+2:ee-1) % from knee frequency to certain value before zero
 weighting starts

     w(d) = 0.5;
 end


 for d = (e(1):e(end)) % beyond knee frequency + X
     w(d) = 0.05;
 end
```

CALCULATE THE DEVIATION (ERROR), Q IS THE NUMBER OF COLUMNS

(INCLUDING THE COLUMN FOR FREQUENCY%

```
 % ... and the acceleration data for each XYZ channel per test
 % The number of tests = (q-1)/3, err = error, S_err = squared error.
 % Resolve error computation in vector space to solve scaling problem.
 % weight at all frequencies w_i = 1

 for i = 1:(q-1)
 % %     mad(:,i) = (abs(ACCe(:,i)-sspec(:,1))./sspec(:,1))*100;
 % %     mad2(:,i) = (abs(ACCe(k1:k3,i)-
sspec(k1:k3,1))./sspec(k1:k3,1))*100;
 % %     mad3 = mean(mad2);
 % %     SRS_ratio(:,i) = (ACCe(:,i)./sspec(:,1));
 % %     SRS_ratio2 = mean(SRS_ratio(k1k:k3,:));
 % %     %asr = SRS_ratio2;
 %     %Asr = find(asr>1);
 %     %Asr(:,2) = SRS_ratio2(Asr);
 %     %ASr = sortrows(Asr,2);
```

```
 %     Er(:,i) = (sum(ACCe(:,i))/(sum(sspec(:,1))));
 %     for k = 1:(q-1)

 %         Er2(:,k) = (sum(ACCe(k1:k3,k))/(sum(sspec(k1:k3,1))));
 %         if k==k3

 %         end
 %     end
     %her = Er2;
     %Her = find(her>1);
     %Her(:,2) = Er2(Her);

     %HEr = sortrows(Her,2, 'ascend');
     Mr(:,i) = max(ACCe(:,i))/max(sspec(:,1));

     Mr2(:,i) = max(ACCe(k1:k3,i))/max(sspec(k1:k3,1));
 %     mer = Mr2';
 %     Mer = find(mer>=1);
 %     Mer(:,2) = Mr2(Mer);
 %     MEr = sortrows(Mer,2,'ascend');
     err(:,i)= ((20*(log10(ACCe(:,i))-log10(sspec(:,1)))));
     err1(:,i)= ((20*(log10(ACCe(:,i))-log10(sspec(:,1)))).^2); % whole
spectrum

     %                          err2 = err1
     %                          err2(kn+1:end,:)=[]%knee frequency only

     %                          err3(:,i)=w'*(20*((log10(ACCe(:,i))-
log10(sspec(:,1)))).^2); %weighted root mean square error

     % calculate the mean square error and the root mean square error for
all the data
     MSE1 = mean(err1);
     RMSE = sqrt(mean(err1));

     % calculate the mean of the square error (MSE) and root mean square
error up to the knee frequency

     err3(:,i) = w .* err1(:,i);
     err2 = err3;
     err2(kn+1:end,:)=[];
     err4 = err1(k1:k3,:);
     MSE2 = sqrt(mean(err1(k1:k3,:)));
     % calculate the mean of the square error (MSE) and root mean square
error up to the knee frequency
```

```
    %                          MSE2 = mean(err2);
    RMSE_star = sqrt(mean(err2));
end
```

```
wMSE= (sum(err3));
que = sum(w);
wRMSE = wMSE/que;
```

FIND THE CUMULATIVE RMSE THAT ADDS THE RESULTS FOR ALL THREE CHANNELS

```
% find the cumulative wRMSE that adds the results for the channels ; one
reason to not use RMSE as an index is that it is heavily
% biased by frequency deviations in the high frequency(0 slope) srs
region, so it is better to use only the straight portion of the graph

clear n

while (1)
    [b m]= size(RMSE);

%     n = m/3

    if rem(m,3)==0
         n = m/3
    else

         n = (m-1)/3
    end
     qq = n;


    CH = zeros(1,n)
    g = numel(CH);
    k = numel(CH);
    j = 1
    alpha = 1.0

    for v = 1:n

        k(v) = (RMSE(j)) + RMSE(j+1) + ((alpha).*RMSE(j+2));
        t(v) = (RMSE_star(j)) + RMSE_star(j+1) +
(alpha.*RMSE_star(j+2));
        z(v) = (wRMSE(j)) + wRMSE(j+1) + (0.05*wRMSE(j+2));
```

```
        ty(v)= (MSE2(j)) + MSE2(j+1) + ((alpha).*MSE2(j+2));
        j = j+3;
    end
    if j >=q-3
        break
    end


end
%  CH = g;
```

SORT THE RESULT

```
 [pp kk] = sort (k);
 [pp tt] = sort (t);
 [pp gg] = sort (z);
 [pp yy] = sort (ty);
```

FIND THE PERCENTAGE POSITIVE ERROR

```
clear y

[x l] = size (ACCe);
percposit = zeros(1,l);
percplus = zeros(1,l);
for i = 1:l
    u = find(err(err(k1:k3,i)>0));
    y = find(err(err(:,i)>0));
    percposit(i)= 100.*(length(y)/(480)); %percentage positive error
    percplus(i)= 100.*(length(u)/(k3-k1+1));
    i = i+1
    if i>l
    end
end
[i pec]=sort(percposit','descend');
[i peck]=sort(percplus','descend');

clear jo
jo = 0.01; % scalar multiplier

me = [pec i];
me(:,3 )= RMSE (pec);%(to undo sort before assigning RMSE)
% sort before doing (be careful to check raw code)
me(:,4) = 0.01.*(100-me(:,2));%percentage negative error
me(:,5) = me(:,3)/(max(RMSE)-min(RMSE))
```

```
 me(:,6) = 100*(me(:,3)/sum(RMSE))
 me(:,7)= me(:,5).*me(:,4);
 % me(:,7)= 1-(me(:,3)/max(RMSE))
 % me(:,7)=me(:,6).*me(:,5)

 % me(:,7)=0.2*((4.*me(:,6))+(1.*(me(:,5))))
 me(:,8)=me(:,5).*(me(:,4)+ jo*me(:,6))
 sortrows(me2,[8,6]);
 while(1)
     rk_fact = sortrows (me);
     rk_fact2 = rk_fact(:,8);
     n = length(rk_fact2);
 %     aa= zeros(1,(n)/3);
     aa= zeros(1,qq);
     alpha = 1;
     j = 1;
     for v = 1:(n-1)/3 % for database size = 10, change n to n-1

         aa(v) =(rk_fact2(j) + rk_fact2(j+1) +
((alpha).*rk_fact2(j+2)))/3;
         j = j+3;
     end
     if j >=n-3

         break
     end
 end

 [bb cc]=sort(aa);
 % me2 is wRMSE calculation between 100 Hz and upper frequeny limit of
spec

 me2 = [peck i];
 me3 = sortrows(me2);
 me2 = me3;
 clear me3
 % me2(:,3 )= 1-((MSE2/max(MSE2)));
 % me2(:,3 )= (MSE2/sum(MSE2))*100;
 me2(:,3)= MSE2/(max(MSE2))%-min(MSE2));
 % me2(:,3)= MSE2/(max(MSE2)-min(MSE2))
 me2(:,4) = (100-me2(:,2))*jo;%percentage negative error
 % me2(:,5) = ((me2(:,3)).*(me2(:,4).*4)+(1.*me2(:,3)))/5
 me2(:,5) = (me2(:,3)).*(me2(:,4))
 me2(:,6)= MSE2(:,:);
 me2(:,7 )= (MSE2/sum(MSE2))*100;
 me2(:,8) = (me2(:,3).*me2(:,4))+jo*me2(:,7)
```

```
while(1)
    r_fact = sortrows (me2);

    r_fact2 = r_fact(:,8);
    m = length(r_fact2);

    dd= zeros(1,qq); %for database size = 10, change m to m-1
    alpha = 1;
    j = 1;
    for v = 1:n/3
        dd(v) =( r_fact2(j) + r_fact2(j+1) + ((alpha).*r_fact2(j+2)))/3;

        j = j+3;
    end

    if j >=n-3
        break

    end

end
[ee, ff]= sort(dd,'ascend');
```

READ THE TUNING CONDITIONS

```
dayta = readtable ('Tuning2.xlsx','ReadRowNames',true);
dayta(ff(1:10),:)
toc
```

7.4.1 Tuning conditions for all tests in the SRS database

TN#	Pressure	C1	QC1	C2	QC2	Remark	Projectile
1	0.05	Al	1	NR	1	Natural rubber thickness = 0.3 mm	SUS2.9
TN2	0.05	NONE	0	NONE	1		SUS2.9
TN3	0.05	NONE	0	NONE	1		SUS2.9
TN4	0.06	Al	1	NR	1	Natural rubber thickness = 0.3 mm	SUS2.9
TN5	0.05	NONE	0	0	0	No Center Bolt	SUS2.9
TN6	0.05	NONE	0	0	0	Fixing torque change (20 Nm)	SUS2.9
TN7	0.05	NONE	0	0	0	Fixing torque (20 Nm)	SUS2.9
TN8	0.05	NONE	0	0	0	Fixing torque (20 Nm) + center bolt	SUS2.9
TN9	0.05	NONE	0	0	0	Torque change (30 Nm)	SUS2.9
TN10	0.05	NONE	0	0	0		SUS2.9
TN11	0.052	NONE	0	0	0	Torque change (15 Nm), No center bolt	SUS2.9
TN12	0.052	NONE	0	0	0		SUS2.9
TN13	0.035	NONE	0	0	0		SUS2.9
TN14	0.035	Al	1	NR	1		SUS2.9
TN15	0.035	Al	1	NR	1		SUS2.9
TN16	0.035	Al	1	NR	2		SUS2.9
TN17	0.035	Al	1	NR	2		SUS2.9
TN18	0.04	Al	1	NR	2		SUS2.9
TN19	0.05	Al	1	NR	2		SUS2.9
TN20	0.05	Al	1	NR	2	Projectile is changed (from SUS to PL)	PN
TN21	0.05	Al	1	NR	2		PN

TN22	0.04	Al	1	NR	2		PN
TN23	0.05	Al	1	NR	3		PN
TN24	0.045	Al	1	NR	3		PN
TN25	0.05	Al	1	NR	4		PN
TN26	0.05	Al	1	NR	4		PN
TN27	0.05	Al	1	NR	4		PN
TN28	0.09	Al	2	NONE	0		Al2.5
TN29	0.1	Al	1	NONE	0		Al2.5
TN30	0.1	Al	2	NONE	0		Al2.5
TN31	0.1	F	1	NONE	0	200123	Al2.5
TN32	0.1	F	1	NONE	0		Al2.5
TN33	0.1	NR	1	NONE	0		Al2.5
TN34	0.12	NR	1	NONE	0		Al2.5
TN35	0.12	NR	1	NONE	0		Al2.5
TN36	0.123	NR	1	NONE	0		Al2.5
TN37	0.13	NR	1	NONE	0		Al2.5
TN38	0.08	NONE	0	NONE	0		Al2.5
TN39	0.075	NONE	0	NONE	0		Al2.5
TN40	0.075	NONE	0	NONE	0		Al2.5
TN41	0.08	NONE	0	NONE	0		Al2.5
TN42	0.09	NONE	0	NONE	0		Al2.5
TN43	0.1	NONE	0	NONE	0		Al2.5
TN44	0.11	NONE	0	NONE	0		Al2.5
TN45	0.145	Al	1	NR	1	200121	Al2.5
TN46	0.145	Al	1	NR	1		Al2.5
TN47	0.145	Al	1	NR	1		Al2.5
TN48	0.15	Al	1	NR	1		Al2.5
TN49	0.15	Al	1	NR	1		Al2.5
TN50	0.155	Al	1	NR	1		Al2.5
TN51	0.175	Al	1	NR	1		Al2.5
TN52	0.185	Al	1	NR	1		Al2.5
TN53	0.2	Al	1	NR	1		Al2.5
TN54	0.2	Al	1	NR	1		Al2.5
TN55	0.2	Al	1	NR	1	Torque changed to 25 Nm	Al2.5

TN56	0.2	Al	1	NR	1		Al2.5
TN57	0.2	Al	1	NR	1		Al2.5
TN58	0.145	Al	1	NR	1		Al2.5
TN59	0.12	Al	1	NR	1		Al2.5
TN60	0.12	NONE	0	NONE	0		Al2.5
TN61	0.13	NONE	0	NONE	0		Al2.5
TN62	0.13	NONE	0	NONE	0		Al2.5
TN63	0.13	NONE	0	NONE	0		Al2.5
TN64	0.13	NONE	0	NONE	0		Al2.5
TN65	0.051	NONE	0	NONE	0	20191224	PN
TN66	0.08	NONE	0	NONE	0		PN
TN67	0.08	NONE	0	NONE	0		PN
TN68	0.081	NONE	0	NONE	0		PN
TN69	0.08	NONE	0	NONE	0		PN
TN70	0.084	NONE	0	NONE	0		PN
TN71	0.084	Al	1	NONE	0		PN
TN72	0.09	NONE	0	NONE	0		Al2.5
TN73	0.12	NONE	0	NONE	0		Al2.5
TN74	0.09	NONE	0	NONE	0		Al2.5
TN75	0.08	NONE	0	NONE	0		Al2.5
TN76	0.08	NONE	0	NONE	0		Al2.5
TN77	0.08	NONE	0	NONE	0		Al2.5
TN78	0.075	NONE	0	NONE	0		Al2.5
TN79	0.083	Al	1	NR	1		Al2.5
TN80	0.066	Al	1	NR	1		Al2.5
TN81	0.065	Al	1	NR	1		Al2.5
TN82	0.065	Al	1	NR	1		Al2.5
TN83	0.065	Al	1	NR	1		Al2.5
TN84	0.065	Al	1	NR	1		Al2.5
TN85	0.065	Al	1	NR	1		Al2.5
TN86	0.1	SUS0.3	1	NR	1	20180503	SUS4.2
TN87	0.2	SUS0.5	1	NR	1		SUS4.2
TN88	0.2	SUS0.5	1	NR	1		SUS4.2
TN89	0.23	SUS0.3	1	NR	1		SUS4.2
TN90	0.23	SUS0.3	1	NONE	0		SUS4.2

TN91	0.23	Al	1	NONE	0		SUS4.2
TN92	0.232	Al	1	NR	1		SUS4.2
TN93	0.229	Al	2	NONE	0		SUS4.2
TN94	0.229	Al	2	NR	1		SUS4.2
TN95	0.229	Al	2	NONE	0		SUS4.2
TN96	0.23	Al	2	NONE	0	20180511	SUS4.2
TN97	0.22	Al	2	NONE	0		SUS4.2
TN98	0.2	Al	2	NONE	0		SUS4.2
TN99	0.22	Al	2	NONE	0		SUS4.2
TN100	0.23	Al	2	NONE	0		SUS4.2
TN101	0.08	NONE	0	NONE	0	200129	Al2.5
TN102	0.08	NONE	0	NONE	0		Al2.5
TN103	0.08	Al	1	NONE	0		Al2.5
TN104	0.08	Al	1	NONE	0		Al2.5
TN105	0.08	Al	2	NONE	0		Al2.5
TN106	0.08	Al	2	NONE	0		Al2.5
TN107	0.08	NR	1	NONE	0		Al2.5
TN108	0.08	NR	1	NONE	0		Al2.5